1985

Progress Report No. 21

Biomedical Computer Laboratory

PROGRESS REPORT

No. 21

1 July 1984 - 30 June 1985

Biomedical Computer Laboratory

Institute for Biomedical Computing

Washington University

700 South Euclid Ave.

St. Louis, Missouri 63110

BIOMEDICAL COMPUTER LABORATORY

INSTITUTE FOR BIOMEDICAL COMPUTING

WASHINGTON UNIVERSITY

PROGRESS REPORT NO. 21

JULY 1, 1984 - JUNE 30, 1985

TABLE OF CONTENTS

I. INTRODUCTION

This progress report from the Biomedical Computer Laboratory (BCL) summarizes activities during the period from July 1, 1984 through June 30, 1985. The Biomedical Computer Laboratory collaborates with research investigators throughout the Washington University School of Medicine and its affiliated hospitals in the application of advanced computer techniques to problems in biology and medicine. This often requires work in areas stretching from basic physiology through mathematical models to equipment design. Our orientation is interdisciplinary with the recognition that effective communication for workers with differing backgrounds comes only through extended collaboration and mutual respect.

The vigorous development and evolution of specialized computer systems for use in the solution of research and clinical problems has continued to be the central focus of BCL activities. Several systems now in clinical use have seen a progression from exploratory pilot studies, to major developmental project, to local clinical trial, to clinical trials in multiple locations, to public availability through commercial manufacture. Perseverance in this sometimes tedious chain of development has found reward in the effective fielding of specialized computer systems to the medical community.

One class of computer applications requires strong coupling of the computer to its environment for digital signal processing. These applications typically involve the use of commercially available minicomputers and microprocessors in conjunction with specialized hardware designed and built locally. We have pursued many such applications by bringing signals from hospital wards and research laboratories to BCL by means of either analog or digital tape recordings or telephone lines and, more frequently, by taking the computers to the investigator's laboratory or the patient's bedside. More recently, an emphasis at BCL has been on the development of a flexible digital communication capability for linking data sources and information destinations with research-oriented computational resources at BCL as well as at collaborators' sites.

Of particular importance to current and future BCL projects is the development, in a closely related sister lab (Computer Systems Laboratory, or CSL), of a capability for the design and fabrication of custom very-large-scale integrated (VLSI) circuits. The realization of such circuits through collaboration with CSL is already opening up new opportunities for solving problems intractable with conventional computing devices.The CSL has as its goal the development of innovative approaches to computing that will have important implications for medicine and biology in the future.

For those classes of applications dominated by information processing requirements, provisions have matured from telephone lines linking our minicomputers to the large IBM Systems at the Washington University Computing Facilities, through development and support of a minicomputer based MUMPS system, to the establishment of independent groups such as the Medical Computing Facility and the Medical Computing Service Group which serve the local medical complex. Diverse needs continue to be met by these various options as well as by an increasing number of independent computing facilities within medical school departments.

Still another class of applications requires extensive use of large-scale computational services. Many investigators are assisted in their research through the use of generalized numerical, non-numerical, and statistical routines. Such work is sometimes carried out by staff members of BCL, but primarily by members of the Division of Biostatistics under the direction of Dr. Dabeeru C. Rao, and the University Computing Facilities whose director is Robert J. Benson.

Over the years, the BCL has enjoyed collaborations with most departmental divisions within the medical school but has also found support and enrichment through close ties with other facilities throughout the University. These arrangements are of benefit both to the BCL and to graduate students who find projects and employment among the activities in the laboratory. The Department of Computer Science is under the direction of Dr. Jerome R. Cox, Jr., past Director of the BCL. Strong ties with the Department of Electrical Engineering are sustained through the Engineering School's Biomedical Engineering Program and common interests in digital signal processing techniques. The Department of Electrical Engineering is chaired by Dr. Donald L. Snyder, past Associate Director of BCL.

Two years ago, Washington University established an interschool Institute for Biomedical Computing. The new Institute encompasses the Biomedical Computer Laboratory and the Computer Systems Laboratory in an organizational setting designed to recognize and foster the joint interests in biomedical computing of the School of Medicine and the School of Engineering and Applied Science. The purpose of the reorganization is to recognize that the development and application of advanced computing and engineering technology to problems in biomedical science are essential components of the research and teaching activities of Washington University. Accordingly, attention has been given to the development of a stable organizational structure that will 1) provide a means by which the primary academic affiliations of its faculty can be in an organizational setting with an adequately broad commitment to research and teaching in biomedical computing; 2) establish a formal administrative connection to the School of Engineering and Applied Science that will facilitate the involvement of its students and faculty in research and instructional activities in biomedical computing; 3) establish mechanisms for adminstration, funding, and review of appointments, promotion, and tenure for the academic staff of this activity; 4) foster organizational and procedural coherence between the Biomedical Computer Laboratory and the Computer Systems Laboratory by placing them within a common administrative structure; 5) create a focal point for interdisciplinary teaching and student research, both in the School of Medicine and the School of Engineering and Applied Science, in areas that do not fit comfortably into existing departments; and 6) encourage a scholarly environment for the activities of the two computer laboratories that will promote and encourage teaching, research, and publication as vehicles for personal development and academic contribution.

In addition to current BCL and CSL space on the Medical School campus, space for part of the activities of the Institute has been provided on the Engineering School campus by completion of a fifth-floor addition to Lopata Hall in December of 1983. This new space (about 6000 square feet), called the Edward L. Bowles Laboratory, is immediately adjacent to the Departments of Computer Science and Electrical Engineering.

The Institute for Biomedical Computing (IBC) has replaced the former Washington University Computer Laboratories (WUCL) which was a less formal federation of BCL and CSL plus working groups within the Departments of Computer Science and Electrical Engineering. Dr. Charles E. Molnar, Director of the Computer Systems Laboratory, and Dr. Lewis J. Thomas, Jr., Director of the Biomedical Computer Laboratory, have been appointed as respective Director and Associate Director of the Institute. Both BCL and CSL continue to retain their identities and internal organizations. Accordingly, this Progress Report addresses activities centered primarily within BCL.

Planning and policy development of the Institute are overseen by a Governing Board, the membership of which is drawn from both Schools. The present composition of the Governing Board is:

J. R. Cox, Jr., Chairman, Department of Computer Science
N. Daw, Professor, Department of Cell Biology and Physiology and Department of Ophthalmology
R. G. Evens, Head, Department of Radiology
M. K. King, Dean, School of Medicine
D. M. Kipnis, Chairman, Department of Internal Medicine
E. L. MacCordy, Associate Vice-Chancellor for Research
J. M. McKelvey, Dean, School of Engineering and Applied Science
C. E. Molnar, Director, Computer Systems Laboratory
P. Needleman, Head, Department of Pharmacology
D. L. Snyder, Chairman, Department of Electrical Engineering
L. J. Thomas, Jr., Director, Biomedical Computer Laboratory

To aid in long-range planning of the health-related activities of the Institute, a National Advisory Panel is convened periodically. Particular attention is given to the confluence of important needs in biology and medicine with the technical advances capable of meeting these needs. Successful development may suggest implementation on a larger, perhaps national scale. The present composition of the National Advisory Panel is:

Peter H. Abbrecht, M.D., Ph.D., Professor of Physiology and Medicine, Uniformed Services University of the Health Sciences, Bethesda, Maryland

Howard L. Bleich, M.D., Associate Professor, Beth Israel Hospital, Harvard Medical School

Wesley A. Clark, A.B., Consultant, Sutherland & Sproull Associates, New York, New York,

James N. Gray, Ph.D., Tandem Computer Company, Cupertino, California

Frank E. Heart, M.S.E.E., Vice President and Director, Computer Systems Division, Bolt, Beranek & Newman, Cambridge, Massachusetts

David M. Kipnis, Professor and Chairman, Department of Internal Medicine, Washington University

Brian W. Matthews, Ph.D., Professor, Institute of Molecular Biology, University of Oregon

John M. Smith, Director, Sponsored Research Division, Computer Corporation of America, Cambridge, Massachusetts

Eugene A. Stead, Jr., M.D., Florence McAlister Professor of Medicine, Department of Medicine, Duke University

Carlos Vallbona, M.D., Chairman, Department of Community Medicine, Baylor College of Medicine

II. SOURCES OF SUPPORT

During the period covered by this report the primary source of support for the Biomedical Computer Laboratory was from two grants from the National Institutes of Health, Division of Research Resources.

RR 01380	A Resource for Biomedical Computing.
RR 01362	Tissue Characterization via Ultrasonic Imaging.

NHLBI contract NO1 HV 72941 continues to fund a Holter Monitoring Core Laboratory to support a Multicenter Investigation of Limitation of Infarct Size.

Collaboration with other investigators often involved work already supported by other grants and contracts.

Public Health Services.

AM 07296	Cell Biological Approaches to Diabetes Research,
CM 47696	Evaluation of High Energy Photon External Beam Treatment Planning,
EY 03703	Chromatic Static Perimetry in the Diagnosis of Glaucoma,
GM 28232	Physical Mapping of Yeast Chromosomal DNA,
HL 12839	Erythrocyte Deformability and Vascular Pathophysiology,
HL 13851	Cyclotron Produced Isotopes in Biology and Medicine,
HL 17646	Study of Ischemic Heart Disease,
HL 25430	Characterization of Left Ventricular Diastolic Function,
HL 25944	Time-of-Flight Positron Tomography for Cardiac Imaging,
HL 28995	Adrenergic Factors and Arrhythmogenic Metabolites,
HL 28998	Tissue Characterization with Ultrasound,
NS 06833	An Interdisciplinary Stroke Program,
RR 01379	Research in VLSI Systems for Biomedical Applications.

National Science Foundation Grant.

ECS-82-15181 Study of Time-of-Flight Tomography

Research support was also received from the following industrial collaborators.

Biosensor Corporation, Brooklyn Center, Minnesota,
Computer Services Corporation (CSK), Tokyo, Japan,
Mead Johnson, Evansville, Indiana.

III. PERSONNEL

EMPLOYEES

Personnel employed by the Biomedical Computer Laboratory during the period covered by this report were:

Director

Lewis J. Thomas, Jr., M.D., and Associate Director of Institute for Biomedical Computing, and Associate Professor of Biomedical Computing, Anesthesiology, Physiology and Biophysics, Biomedical Engineering, and Electrical Engineering

Associate Director

G. James Blaine III, D.Sc., and Associate Professor of Biomedical Computing in the Institute for Biomedical Computing, and Affiliate Associate Professor of Electrical Engineering and Computer Science

Senior Research Associates

Jerome R. Cox, Jr., Sc.D., and Professor of Biomedical Computing in the Institute for Biomedical Computing, and Chairman and Professor of Computer Science, and Professor of Electrical Engineering, and Senior Research Associate, Computer Systems Laboratory

Harold W. Shipton, C.Eng., and Professor of Biomedical Engineering in the Institute for Biomedical Computing, and Chairman and Professor of Biomedical Engineering

Donald L. Snyder, Ph.D., and Professor of Biomedical Computing in the Institute for Biomedical Computing, and Chairman and Professor of Electrical Engineering, and Senior Research Associate, Computer Systems Laboratory

Business Manager

Virginia M. Bixon, B.S.

Research Associates

R. Martin Arthur, Ph.D., and Professor of Biomedical Computing in the Institute for Biomedical Computing, and Professor of Electrical Engineering

Kenneth W. Clark, M.S.

Daniel R. Fuhrmann, Ph.D., and Assistant Professor of Electrical Engineering

Robert O. Gregory, D.Sc., and Professor of Electrical Engineering

Kenneth B. Larson, Ph.D.

James G. Miller, Ph.D., and Professor of Physics, and Associate Director for Biomedical Physics, Laboratory for Ultrasonics, and Research Associate Professor of Medicine

Michael I. Miller, Ph.D., and Assistant Professor of Biomedical Computing in the Institute for Biomedical Computing, and Assistant Professor of Electrical Engineering

Frederick U. Rosenberger, D.Sc., and Associate Professor of Biomedical Computing in the Institute for Biomedical Computing

Research Assistants

David E. Beecher, M.S., and Lecturer in Computer Science
Steven R. Broadstone, B.A., B.S.
John C. Chabut, B.S., B.A.
John D. Gorman, B.S.
Russell E. Hermes, M.S.
Patrick H. Johnston, M.A.
Joanne Markham, M.S., and Research Instructor in Medicine
Stephen M. Moore, M.S.
Jack G. Mottley, Ph.D.
John M. Ollinger, M.S.
Kenneth B. Schechtman, Ph.D., and Instructor in Biostatistics in Preventive Medicine, and Research Instructor in Medicine
Tom O. Videen, Ph.D.

Engineering Assistant

Stanley R. Phillips, A.A.S.

Technical Assistant

Alexander W. Stangl

Electronic Technician

Deborah A. Schwab

Librarian

Monica W. Shieh, M.L.S.

Secretaries

Rebecca J. Bozesky
Shirley A. Gonzalez-Rubio
Polly E. Raith

The following members from other departments and divisions have joint appointments with the Biomedical Computer Laboratory to facilitate collaboration and enhance interdisciplinary research:

H. Dieter Ambos, Research Assistant Professor of Medicine (Cardiology)
A. Maynard Engebretson, D.Sc., Associate Professor of Electrical Engineering in the Department of Speech and Hearing, and the Faculty of Arts and Sciences
William M. Hart, Jr., M.D., Ph.D., Associate Professor of Ophthalmology
Rexford L. Hill, III, M.S., Associate Professor of Computer Applications in Radiology
David G. Politte, Research Assistant in Radiology
John W. Wong, Ph.D., Assistant Professor of Radiation Physics in Radiology

In addition, the following people worked at the laboratory for brief periods:

George L. Engel, B.A., B.S.
Abdelkader Gacem, M.S.
Sudjiwo Husodo, B.S.
Rosalie J. Paisley, M.S.
David F. Sandel, B.S.

RESEARCH COLLABORATORS

During the period covered by this report the following investigators from other laboratories, departments, or institutions, collaborated with BCL staff members on problems of joint interest.

D. R. Abendschein, Ph.D., Medicine
H. D. Ambos, Medicine
T. R. Baird, Medicine
D. G. Barr, Radiation Sciences
S. R. Bergmann, M.D., Ph.D., Medicine
D. R. Biello, M.D. Radiology
W. R. Bosch, M.S., Computer Systems Laboratory
T. J. Chaney, M.S., Computer Systems Laboratory
P. B. Corr, Ph.D., Medicine and Pharmacology
M. R. Courtois, M.A., Medicine
S. R. Devries, M.D., Medicine
R. D. Edelman, B.S., Computer Systems Laboratory
J. O. Eichling, Ph.D., Radiology
P. R. Eisenberg, M.D., Medicine
R. G. Evens, M.D., Radiology
D. C. Ficke, B.S., Radiology
L. Fields, M.D. Medicine
K. A. A. Fox, M.B., Ch.B., Medicine
P. T. Fox, M.D., Neurology and Radiology
M. S. Frank, M.D., Genetics
M. H. Gado, M.D. Radiology
E. D. Galie, R.N., Medicine
R. A. Gardner, Ph.D., Mechanical Engineering
E. M. Geltman, M.D., Medicine
R. Genton, M.D., Medicine
W. D. Gillette, Ph.D., Computer Sciences
R. M. Glueck, M.D., Medicine
A. M. Grace, Medicine
R. L. Grubb, Jr., M.D., Neurological Surgery
W. B. Harms, B.S., Radiology
W. M. Hart, Jr., M.D., Ph.D., Ophthalmology
K. H. Haserodt, M.S., Computer Science
P. Herscovitch, M.D., Neurology and Radiology
G. R. Hoffman, B.A., Radiology
T. J. Holmes, D.Sc., Radiology
J. T. Hood, Sr., B.S., Radiology
S. Igielnik, Ph.D., Medical Computing Facilities
A. S. Jaffe, M.D., Medicine
G. C. Johns, B.S., Computer Systems Laboratory
R. G. Jost, M.D., Radiology
M. A. Kass, M.D., Ophthalmology

E. W. Kiebler, M.S., Computer Systems Laboratory
M. R. Kilbourne, Ph.D., Radiology
R. M. Knabbe, Ph.D., Medicine
R. Kopitsky, M.D., Medicine
J. B. Kramer, M.D., Medicine and Surgery
A. Kumar, B. Tech., Radiology
J. L. Lauter, Ph.D., Central Institute for the Deaf
P. A. Ludbrook, M.D., Medicine
E. T. Macke, M.S., Computer Systems Laboratory
J. W. Matthews, D.Sc., Computer Systems Laboratory
T. R. Miller, Radiology
M. A. Mintun, M.D., Neurology
C. E. Molnar, Sc.D., Computer Systems Laboratory
M. V. Olson, Ph.D., Genetics
D. S. Payne, Medicine
C. A. Perez, M.D., Radiology
J. E. Perez, M.D., Medicine
J. L. Perlmutter, M.D., Neurology
S. M. Pogowizd, M.D., Medicine
D. G. Politte, M.S., Radiology
W. J. Powers, M.D., Neurology and Radiology
J. A. Purdy, Ph.D., Radiology
M. E. Raichle, M.D., Neurology and Radiology
D. C. Rao, Ph.D., Biostatistics
M. L. Ridner, M.D., Medicine
T. L. Rosamond, M.D., Medicine
A. P. Rueter, B.S., Radiology
J. E. Saffitz, M.D., Pathology and Medicine
M. L. Sieger, B.S., Electrical Engineering
B. A. Siegel, M.D., Radiology
B. E. Sobel, M.D., Medicine
J. J. Spadero, Jr., M.D., Medicine
A. W. Strauss, M.D., Biochemistry
S. P. Sutera, Ph.D., Mechanical Engineering
A. G. Swift, M.A., Radiology
M. M. Ter-Pogossian, Ph.D., Radiology
A. J. Tiefenbrunn, M.D., Medicine
R. G. Tilton, Ph.D., Pathology
A. W. Toga, Ph.D., Neurology
J. S. Turner, Ph.D., Computer Science
D. F. Wann, D.Sc., Electrical Engineering
M. J. Welch, Ph.D., Radiology
R. A. Wettach, R.N., Medicine
S. Wickline, M.D., Medicine
J. R. Williamson, M.D., Pathology
R. Wolf, M.D., Medicine
K. F. Wong, M.S., Computer Science
J. W. Wong, Ph.D., Radiology
K. A. Yamada, Ph.D., Medicine
A. L. Ysaguirre, Medicine
C. Y. Yu, M.S., Radiology
J. D. Zions, Pathology

Indiana University School of Medicine, Indianapolis, Indiana

C. Fisch, M.D.
S. B. Knoebel, M.D.

Jewish Hospital, St. Louis, Missouri

B. R. Hieb, M.D.
R. E. Kleiger, M.D.
R. J. Krone, M.D.
R. Ruffy, M.D.

Massachusetts General Hospital, Boston, Massachusetts

H. K. Gold, M.D.
H. W. Strauss, M.D.

Pennsylvania State University, University Park, Pennsylvania

D. B. Geselowitz, Ph.D.

Peter Bent Brigham Hospital, Boston, Massachusetts

E. Braunwald, M.D.
P. H. Stone, M.D.,

Research Triangle Institute, Research Triangle Park, North Carolina

W. K. Poole, Ph.D.

Roosevelt Hospital, New York, New York

H. M. Greenberg, M.D.

University of Illinois at Chicago Circle, Chicago, Illinois

R. Langendorf, M.D.

University of Iowa, Iowa City, Iowa

R. C. Arzbaecher, Ph.D.

University of Kentucky College of Medicine, Lexington, Kentucky

B. Surawicz, M.D.

University of Louisville School of Medicine, Louisville, Kentucky

N. C. Flowers, M.D.

University of Texas Health Science Center, Dallas, Texas

J. T. Willerson, M.D.

University of Vermont College of Medicine, Burlington, Vermont

D. S. Raabe, M.D.

As in the past, collaborative efforts with various commercial firms continue (see Section VI). This year projects of joint interest have involved:

Biodata Informatica and Technologica, Ltd., Brazil
Biosensor Corporation, Brooklyn Center, Minnesota,
Computer Services Corporation (CSK), Tokyo, Japan,
Mead Johnson, Pharmaceutical Division, Evansville, Indiana,
Mennen-Medical, Inc., Clarence, New York.

IV. PHYSICAL RESOURCES

The Biomedical Computer Laboratory (BCL) was formed on April 15, 1964 and the original staff moved into 3,800 square feet (net) of laboratory space at 700 South Euclid Avenue in St. Louis. While remaining at this location, adjacent to the Washington University School of Medicine's main building complex, the floor space has been increased to the present 12,000 square feet (net). As a result of the establishment of an interschool Institute for Biomedical Computing at Washington University, space for part of the activities of the Institute (which encompasses both the BCL and the Computer Systems Laboratory (CSL) has been created on the Engineering School campus by completion of a fifth-floor addition to Lopata Hall. This new space (about 6000 square feet), called the Edward L. Bowles Laboratory, is immediately adjacent to the Departments of Computer Science and Electrical Engineering. It became available in December, 1983. In addition to the 700 South Euclid and Bowles Laboratory space, BCL staff members and systems frequently occupy other areas within the Washington University Medical Center at the sites of collaborative project activities.

During the past twenty years BCL has addressed diverse biomedical problems for which digital computing techniques seemed promising and appropriate. A single Laboratory Instrument Computer (LINC) provided the original staff with an opportunity to apply digital computing to a few interesting problems in medicine and biology. Currently BCL has interest and involvement in several specialized instrumentation and computing systems which provide access to diverse image-data sources (modalities) and offer opportunities for collaborative research in biological modeling and algorithm development. BCL has primary responsibility for a complement of computing hardware and software from a variety of system manufacturers. These resources include: Digital Equipment Corporation PDP-11's and LSI-11's, MASSCOMP Corporation MC-500's, California Data Products Model 135's, and Motorola Versamodule M68000's. An MMS-X stroke graphics display system developed by the Computer Systems Laboratory, a Lexidata raster-graphics display system and two MASSCOMP raster-graphic display stations are available for biomedical imaging studies. Personal-class microcomputer systems have been incorporated into the design of biomedical research systems and numerous special-purpose devices have been developed using microprocessor chip-sets and microcomputer board-level assemblies.

A Resource-developed local area network, TERRANET, provides remote terminal-to-computer and inter-computer data communications at rates up to 9600 bps. Two, thirty station networks support terminals and computer systems located throughout the laboratories. Internetwork communication is provided between these networks and others within Washington University, giving access to a broad spectrum of computing equipment and services for use by resource personnel.

A machine shop and reference room are located on the 700 S. Euclid premises and shared with CSL. Other physical resources include a well-stocked electronics shop, a large inventory of electronic and computer test equipment, a variety of digital system modules and both analog and digital recording instruments. Systems for use in developing eight-bit, sixteen-bit and bit-slice microprocessor applications are available.

V. RESEARCH PROJECTS

Introduction

The research program of the Biomedical Computer Laboratory (BCL) is organized into several major project areas with the staff grouped into teams whose interests are focused correspondingly. Because of the growth of the Laboratory's activities in the area of quantitative imaging, that category has been divided into three sections, each dealing with a different imaging modality (ultrasound, radiation-treatment planning, and positron-emission tomography). A total of 50 distinct project activities are grouped into the six project areas briefly summarized below. More complete summaries are given at the beginning of each of the project-report subsections.

Ischemic heart disease and ECG analysis continues to be a major category of research activity, but the development of new algorithms for ECG processing has become less prominent than in the past as a result of a shift in emphasis to exportation of the latest version of our "Argus" algorithm. As that work is being brought to a conclusion, the final evaluation now in progress is showing that the revised algorithm achieves the high level of performance required for real-time, ambulatory ECG-monitoring applications. In the area of ischemic heart disease, more prominent than before are modeling, signal processing, and data analysis work in collaboration with the division of Cardiovascular Medicine as part of their broad program addressed to ischemic heart disease.

Information extraction from quantitative biomedical images continues to increase in prominence within the BCL program. Accordingly, last year's organization of such activities into three categories (by imaging modality) is continued this year. The work in ultrasonic tissue characterization now emphasizes the interpretation of backscattered ultrasonic energy to achieve quantitative estimates of tissue properties, including anisotropy and the state of contraction of cardiac and skeletal muscle, while parallel efforts are directed toward design of a system to employ adaptive beamforming for backscatter measurements.

Work in radiation treatment planning has moved ahead with enhancements and evaluations of our "delta volume" algorithm for three-dimensional absorbed-dose calculations, display experiments employing high-performance stroke graphics (MMS-X system), and the recent completion of two VLSI circuits for expeditious achievement of a demanding kernel of the computations (3-D ray tracing). New work now focuses on the physics of high-energy photon-dose deposition in heterogeneous media.

For positron-emission tomography, work in support of applications and system improvements have continued on several fronts, but the main thrust of BCL activities has been in research on algorithms. Emphasis has been on application of the maximum-likelihood method for improving image quality and for achieving better estimates of physiological parameters through studies of dynamic distributions of tracers. Important new developments include the application of kernel seives to address image artifacts and the formulation of a model for applying the maximum-likelihood method to single-photon emission computed tomography (SPECT).

Systems for Specialized Biomedical Studies embraces a variety of projects that are less broad in scope either because they are in an earlier stage of development or because the nature of the work is necessarily more specialized. The biomedical-imaging theme is well represented in this section as well.

Projects under Resource Development Activities are directed toward improving the Laboratory's capabilities for addressing the needs of multiple research studies involving various facets of biomedical imaging. To that end, a now dominant and integrating activity is the development of a distributed facility for image presentation, analysis and quantification (IPAQ). Components of the IPAQ project include (1) the enhancement of our computational capabilities to support the development of computationally demanding algorithms for information extraction from multi-dimensional measurement data, (2) the establishment of a coherent software environment which incorporates a set of internally consistent software tools, image data formats and display methodologies, (3) the extension of our digital communication capabilities to include the sites of collaborators' data sources and information destinations, and (4) the exportation of specialized, tailored subsystems and/or satellite workstations which may incorporate custom-designed, very-large-scale integrated (VLSI) circuits in order to achieve practical realizations of especially demanding computations.

Individual Projects

A. Ischemic Heart Disease and ECG Analysis

Some of the projects reported in this section continue longstanding work in high-speed ECG analysis. In other projects, modeling and signal-processing endeavors in the field of cardiology have supported collaborations which address other aspects of ischemic heart disease, such as myocardial metabolism and blood flow, the electrophysiologic characterization of abnormal myocardial depolarization, various antidysrhythmic drug studies, infarct-size modification, and the study of ventricular diastolic mechanics.

A real-time computer-based arrhythmia monitoring system, called Argus, in operation in the Barnes Hospital Coronary Care Unit from 1969-1975, was replaced in 1975 by "Argus/Sentinel," a commercially available version developed through collaboration with the Mennen-Greatbatch Company. The experience garnered with Argus led directly to the development of a system, called Argus/H, for the high-speed (60 times real time) processing of long-term ECG recordings. Argus/H has since processed several thousand recordings for a study of ventricular arrhythmias in survivors of myocardial infarction and several hundred recordings for a host of other studies. Extensive evaluations have verified the integrity of the analysis algorithms, proven the value of the quantified results as compared to conventional manual-scanning techniques, and confirmed the consistency of results on reprocessing. The importance of such issues stimulated the development of a stochastic model for the performance evaluation of event detectors.

By the mid-1970's, it was apparent that Argus/H could not support rigorous algorithm development, could not efficiently process the now more-popular dual-channel recordings, and could not meet the demand for the system from the growing volume of recordings resulting from interests in therapeutic trials of antiarrhythmic agents and interventions designed to protect the ischemic myocardium. A newer system, called Argus/2H, emerged in 1977 and was duplicated in 1978. The two Argus/2H systems have processed long-term ECGs for national multicenter clinical studies of interventions to limit infarct size and of post-infarction risk stratification. The systems also provide the power and flexibility necessary for work on algorithm revision and on new signal-processing strategies and they have further served the analysis and documentation needs of other work to generate an annotated digital ECG database for the evaluation of automated arrhythmia detectors. Newer signal-processing strategies employing frequency-domain analysis of the ECG are now bearing fruit and have led to a continuing industrial collaboration to implement the algorithms in a CMOS processor for real-time dysrhythmia analysis in the ambulatory setting.

A-1. Argus Algorithm Development

Personnel: C. N. Mead, BCL
K. W. Clark, BCL
L. J. Thomas, Jr., BCL

Support: RR 01380
Biosensor Corporation
Washington University

During the past year, emphasis has been placed on finalizing the complete set of Argus algorithms developed at BCL over the past 12 years (PR-9 to PR-20). The algorithms include enhanced QRS detection/delineation, and a combination of time-domain (TD) and frequency-domain (FD) correlation and feature-extraction pattern recognition techniques. Stabilization of the algorithms represents the termination of BCL's extensive involvement in ECG processing. Specifically, the goal of developing a set of automated processing strategies which perform with at least the degree of accuracy as the original Argus/H algorithms (PR-11, A-16) after human editing has been achieved. Realization of this objective has underscored BCL's belief that the revised Argus algorithms (referred to as Argus/R) have attained a level of maturity that warrants their export to the commercial sector. In particular, BCL has been working with the Biosensor Corporation of Brooklyn Center MN to transfer the complete set of Argus/R algorithms to a CMOS microprocessor environment (see Industrial Collaboration). Details of the Biosensor system and preliminary evaluation results of Argus/R on both the AHA and MIT annotated ECG databases (Tables 1 and 2) have been reported.[1]

Since September of 1984, code modules for couplet/run detection, channel-independent signal-quality assurance testing, and atrial fibrillation detection have either been developed or enhanced. Additionally, the original 128-point FFT routine was rewritten to process 64-point data sets, thereby allowing for the routine processing of either the traditional 512-msec data window (64 pts. @ 8 msec intervals (every other sample)) or a shorter 256-msec window (64 pts. @ 4 msec intervals)). The use of the 64-point transform window with a variable-length data set solved one of the final remaining difficulties with Argus/R, i.e. the application of the algorithm to ECGs with high heart rates (> 135/min) in which event-to-event proximity caused significant transform window boundary discontinuities. Because the current FD algorithms require no information above 30 Hz, the use of a 512-msec window sampled at 8-msec intervals does not degrade the algorithm's performance compared to the original 128 pt. version. A final evaluation is in progress.

Argus/R is coded in assembly language and runs on DEC PDP 11-34's. Because the code has not been optimized for processing speed nor has any attempt been made to use existing hardware FFT chips, analysis is quite slow, in the range of 2-10 × real time. Although the amount of post-processing human interaction time is negligible for Argus/R when compared to Argus/H, application of Argus/R to routine high-speed Holter tape analysis would still require substantial hardware and software revision. At present, BCL has no plans to undertake such revisions. Except for the final evaluation now in progress, BCL plans no further work in high-speed ECG processing.

1. C. N. Mead, K. W. Clark, J. C. Platt, and L. J. Thomas, Jr., "Argus Algorithm Development: A Decade of Progress - Results of Final System Evaluation and Implementation in a CMOS Environment," Proceedings of the IEEE Conference on Computers in Cardiology, IEEE Catalog No. 84CH2078-4, Park City, UT, pp. 197-200, September 18-21, 1984.

EVALUATION RESULTS: AHA Database

Tape Class		Argus/H Unedited	Argus/H Edited	Argus/R (Unedited)
1	sensitivity	n.a.	n.a.	n.a.
	specificity	.974	1.000	.995
2	sensitivity	.962	.980	.987
	specificity	.992	1.000	.999
3	sensitivity	.779	.927	.963
	specificity	.996	1.000	.999
4	sensitivity	.648	.984	.979
	specificity	.997	1.000	.997
6	sensitivity	.743	.968	.973
	specificity	.999	1.000	.999
7	sensitivity	.806	.964	.982
	specificity	.996	1.000	.999
All	sensitivity	.799	.964	.976
	specificity	.991	1.000	.999

59 Tapes: 10 per class, #2002 excluded
Notes: 5-minute learning period.
All annotated fusion beats excluded.
"n.a." = not applicable.

Argus/R Couplet-and-Run Detection Sensitivity

	Per-Tape Average	(Gross Average)
932 Couplets	.974	(.986)
379 Runs	.928	(.967)

Table 1. AHA tape classes are: 1 = No PVCs, 2 = Unifocal PVCs, 3 = Multifocal PVCs, 4 = Bigeminy, 6 = Ventricular Couplets, 7 = Ventricular Couplets and Runs. Classes 5 (R-on-T) and 8 (Ventricular Fibrillation) are not yet available. All per-class and overall averages are calculated on a per-tape basis except for couplet and run detection, where both per-tape and gross averages are given. Tape #2002 was excluded because it is a paced-rhythm recording.

EVALUATION RESULTS: MIT Database

Tape Class		Argus/H Unedited	Argus/H Edited	Argus/R (Unedited
1	sensitivity	n.a.	n.a.	n.a.
	specificity	1.000	1.000	1.000
	PPV	n.a.	n.a.	n.a.
2	sensitivity	.713	.780	.836 (.929*)
	specificity	.979	1.000	.999
	PPV	.387	1.000	.950
3	sensitivity	.748	.900	.914
	specificity	.988	.996	.993
	PPV	.881	.997	.960
All	sensitivity	.736	.859	.887 (.919*)
	specificity	.990	.998	.997
	PPV	.711	.985	.957

43 Tapes: class 1 = 14, class 2 = 10, class 3 = 19
Notes: Tapes #102, #104, #107, #217, #207 excluded.
10-minute learning period.
All annotated fusion beats excluded.
"n.a." = not applicable.
PPV = positive predictive value.

Argus/R Couplet-and-Run Detection Sensitivity

	Per-Tape Average	(Gross Average)
312 Couplets	.915	(.907)
45 Runs	.861	(.844)

Table 2. MIT database was divided into classes based on PVC content for the last 20 minutes of the annotated records as: class 1 = No PVCs, class 2 = 1-25 PVCs, and class 3 = >25 PVCs. Evaluation began after a 5-minute TD ARGUS learning period followed by a 5-minute FD CYCLE learning period. Tapes #102, #104, #107, and #217 were excluded because of paced rhythms; Tape #207 was excluded because the event of interest was ventricular flutter, which is sensed only as a pause in QRS events.

* Tape #123 contained only 3 PVCs, all interpolated. These were labeled by Argus/R as "Unclassified" because unless a similar morphology has occurred as a "classic" isolated PVC, six occurrences of an interpolated PVC are necessary before it is "learned" as a definite PVC. The supplemental numbers are recomputed averages with tape #123 excluded.

A-2. Holter Tape Processing

Personnel: K. W. Clark, BCL
C. N. Mead, BCL
A. W. Stangl, BCL

Support: RR 01380
Biosensor Corporation
Mead-Johnson

During the past year, BCL processed fewer than 100 Holter ECG recordings; all of these came from a multicenter drug study sponsored by Mead-Johnson (see VI, Industrial Collaboration). The contract with Mead-Johnson expires in October, 1985.

For the Multicenter Investigation of the Limitation of Infarct Size (MILIS) (A-8), we retrospectively analyzed a subset (50 of 298) of Holter recordings collected during the operational phases of MILIS (1978-1983) in order to detect ST-segment changes. The recordings were from patients who, at six months after infarction, underwent an exercise tolerance test (ETT). The objective of this pilot study was to explore correlations between the ETT and the Holter recordings with regard to ST-segment changes. As very few of the Holter recordings showed significant ST-level changes, the study was discontinued.

Biosensor Corporation continues to market a portable device for analyzing ECG signals in real time (see VI, Industrial Collaboration). The device incorporates the frequency-domain-based Argus algorithms (A-1). As Biosensor has made various refinements to their implementation, they have analyzed many different waveforms and sent to us their results to be plotted and reviewed. In this manner, we have been able to assess the accuracy of their implementation.

A-3. Assessment of Vascular Integrity of the Myocardium Following Ischemic Injury

Personnel: R. G. Tilton, Ph.D., Pathology
R. A. Gardner, Ph.D., Mechanical Engineering
K. B. Larson, BCL
S. P. Sutera, Ph.D., Mechanical Engineering
J. R. Williamson, M.D., Pathology
J. D. Zions, Pathology

Support: RR 01380
AM 07296
HL 12839
HL 17646
The Kilo Diabetes and Vascular Research Foundation

We have continued our previously reported studies (PR 15, A-10; PR 16, A-10; PR 17, A-7; PR 18, A-7; PR 19, A-7; PR 20, A-3) of the role of endothelium in the pathogenesis of the vascular hemodynamic and permeability changes associated with ischemia and reperfusion. In these studies, we employed external-detection techniques to quantify radiolabeled albumin transport across the coronary vasculature under physiological conditions, and during reperfusion after ischemia in isolated, buffer-perfused rabbit hearts. The resulting residue-detection data, analyzed on the basis of a two-compartment model of tracer transport, were used to estimate parameters indicative of microvascular integrity such as permeability and ultrafiltration conductance of the endothelium.

In our previous isolated-heart experiments, flow rate was held constant. If perfusion pressure were held constant, presumably the flow rate would decline and left-ventricle contractile function would not recover during reperfusion. In experiments conducted during the past year, we have tested this hypothesis and have examined the impact of these vascular changes on myocardial contractile performance during reperfusion following ischemia. Alternate hearts were perfused under conditions of constant pressure or constant flow using a modified Krebs-Henseleit buffer. When hearts were perfused under conditions of constant flow, myocardial contractile function was preserved but vascular resistance and vascular leakage of albumin were increased significantly during reflow after ischemia. During reperfusion under conditions of constant pressure, vascular leakage and interstitial myocardial edema were somewhat reduced, but flow rate also was reduced, causing deterioration of myocardial contractile function. These experiments have demonstrated the potential importance of compromised vascular integrity, induced by ischemic injury, in the pathogenesis of ischemic heart disease caused by transient vasospasm or vascular narrowing. In experiments currently in progress, we are repeating the above studies using a perfusate containing 40% sheep erythrocytes to more closely reproduce the in vivo hemodynamic conditions.

In additional experiments, we are assessing the effects of galactose feeding (to induce polyol formation) and experimentally induced diabetes (alloxan) on the susceptibility of the coronary vasculature to ischemic injury.

A-4. Modification of Infarct Size

Personnel: A. S. Jaffe, M.D., Medicine
H. D. Ambos, Medicine
P. R. Eisenberg, M.D., Medicine
L. Fields, M.D., Medicine
E. M. Geltman, M.D., Medicine
R. Genton, M.D., Medicine
R. Kopitsky, M.D., Medicine
P. A. Ludbrook, M.D., Medicine
B. E. Sobel, M.D., Medicine
J. J. Spadaro, M.D., Medicine
A. J. Tiefenbrunn, M.D., Medicine
S. Wickline, M.D., Medicine
R. Wolf, M.D. Medicine

Support: RR 01380
HL 17646

Recent evidence confirming the importance of thrombosis to the pathogenesis of acute myocardial infarction has led to an extensive evaluation of the utility of markers of thrombosis and the effects of therapy designed to induce reperfusion. Studies performed in the cardiac care and cardiac catheterization laboratory have been oriented toward the diagnosis of acute thrombosis or the effects of thrombolytic agents. In the past we have utilized positron tomography to document improvement in regional myocardial metabolism induced by successful reperfusion with streptokinase.[1] Because of the promise of tissue-type plasminogen activator, a more clot specific agent, which does not induce circulating products of lysis that impair coagulation we began to utilize this agent in patients. The initial results with the melanoma derived protein (mtPA) were reported in a previous BCL progress report (PR 20, A-4). Subsequently, additional studies were performed to ascertain the potential utility of this agent. Forty-five patients with acute transmural infarction and angiographically confirmed complete coronary occlusion were prospectively randomized to treatment with intracoronary recombinant human tissue-type plasminogen activator (rtPA) or placebo. Five additional patients were treated with high dose rtPA for 2 hours. Twenty-five of 33 patients (75%) receiving .5 to .75 mg per kg of rtPA over 30 to 120 minutes developed angiographically documented reperfusion within 90 minutes of the initiation of therapy. Only 1 of 14 patients given placebo had spontaneous recanalizaiton within 45 minutes. The remaining 13 patients who received placebo were crossed over to an intracoronary rtPA group and 9 exhibited subsequent recanalization in 45 minutes. Levels of circulating fibrinogen decreased after treatment by an average of only 8% from baseline and none of the patients manifested a depletion of fibrinogen below 1 mg/dL. None of the patients unresponsive to rtPA (n=6) responded to intracoronary streptokinase. In addition, the response to intravenous rtPA appeared comparable to the effects of the agent infused directly into the coronary artery in terms of the percentage of patients achieving lysis. However, the time to recanalization was somewhat longer (23 ± 8 compared to 46 ± 18 minutes) when the agent was given intravenously. Thus, both intravenous and intracoronary rtPA induced coronary thrombolysis without eliciting significant fibrinogenolysis in patients with evolving myocardial infarction.[2]

Based on the data of patients treated locally (n=12) the effects of rtPA on coagulation and the kinetics of administration were defined. Serial blood samples were obtained prior to, during and after the infusion of rtPA and analyzed for tPA antigen (immunoassayable rtPA protein), functional fibrinolytic activity attributable to tPA, fibrinogen, plasminogen, alpha 2 antiplasmin, fibrin degradation products, thrombin time, activated partial thromboplasmin time and protamine corrected thrombin time. Prior to therapy all values were normal and the plasma tPA antigen levels averaged 16.5 ± 5 ng/ml. Peak plasma levels were generally proportional to the dose of rtPA, averaging 3,330 ± 1,201 ng/ml. Ninety percent of peak activity was reached in 30 minutes with a plateau reached within 40 minutes. Functional peak tPA activity increased monotonically in a comparable fashion. Curves for disappearance of tPA antigen and functional activity from plasma were monoexponential for at least two half lives and were concordant. The observed half-lives were similar, averaging 8.3 and 9.1 minutes respectively. Changes in fibrinogen were transient and modest (a reduction of 17 ± 6% from baseline). Plasma alpha 2 antiplasma levels had declined moderately (51 ± 6% and 32 ± 7%) from pretreatment phase at the end of the infusion of rtPA. Prothrombin time, protamine-corrected thrombin time and assay of fibrinogen degradation products corroborated the lack of a lytic state. Thus, desirable levels of rtPA can be achieved consistently with short term infusions and without the induction of a systemic lytic state which might induce bleeding.[3]

Based on these initial data a large national trial (Thrombolysis and Myocardial Infarction, TIMI) was initiated comparing rtPA in a dose of .8 mg/kg infused over a 3 hour period (40 mg first hour followed by 20 mg over the subsequent 2 hours) to intravenous streptokinase in a dose of 1,500,000 units. The study was initiated in 13 clinical centers. Eligible patients were taken to the cardiac catheterization laboratory and given intravenous heparin after placement of an arterial sheath. Left ventriculography was performed and coronary angiography thereafter. The infarct related artery was studied last. Two-hundred micrograms of nitroglycerin were injected into the coronary artery prior to the infusion of thrombolytic therapy. Repeat injections were made at 10, 20, 30, 45, 60, 75, and 90 minutes after the start of intravenous therapy. The primary endpoint of the study was the number of patients with total occlusion (grade 0) which progressed to partial or complete reperfusion (grades 2 or 3) by 90 minutes. Thereafter all care was standardized. Three hundred sixteen patients were studied, 26 of whom were not treated because they failed to meet angiographic criteria for treatment. Seventy-six of the 290 remaining patients did not have total occlusion and therefore though treated were not analyzed as part of the primary end point. Of the 214 patients with total occlusion (grade 0) 99 were assigned to tissue-type plasminogen activator and 115 to streptokinase. Baseline clinical and arteriographic findings were similar between the two treated groups as was the time from the onset of chest pain to the start of drug infusion (287 minutes for rtPA and 286 for streptokinase). Of the patients with total occlusion at baseline, 60% of those assigned to rtPA had achieved grade 2 or 3 reperfusion by 90 minutes. This is in contrast to only 35% of those assigned to streptokinase ($P<.001$). When patients with grade 0 and grade 1 occlusion are considered together the relative percentages to reach grade 2 or 3 were 66% compared to 36% ($P<.0001$). There were no clear cut differences in the instances of fatal or central nervous system hemorrhage in either group. Hematoma at the cath site was common occurring in 43% of patients receiving rtPA and 47% of those receiving streptokinase. Gastrointestinal bleeding was noted

in 6% and 10% of the rtPA and streptokinase groups respectively. This was largely due to the large doses of heparin utilized during subsequent management since fibrinogen depletion was quite rare in patients receiving rtPA.[4]

These data confirm the increased efficacy of rtPA in the treatment of patients with acute myocardial infarction. Not only was rtPA less apt to deplete fibrinogen but it was also more efficacious, probably due to its specific binding. For this reason intravenous rtPA has been chosen to be utilized for the continuing phases of the large national TIMI trial.

As a way of assessing the potential utility of thrombolytic and anticoagulant therapy in patients with acute ischemic heart disease, we have for years pursued the study of markers of thrombosis such as platelet factor 4 and beta thromboglobulin (platelet degranulation proteins) in an attempt to find a marker for thrombotic events.[5] Recently we have evaluated the utility of fibrinopeptide A (FPA), 16 amino acid peptide cleaved by the action of thrombin with fibrinogen as a marker. The sensitivity of this marker for thrombosis is well established in patients with acute thrombosis but its use to assess coronary thrombosis in vivo has not been tested explicitly. Since fibrinogen turnover is rapid during the early phase of thrombosis, we reasoned that during acute thrombotic episodes, FPA might be elevated. A quality control system similar to that described above was utilized to obtain samples in 83 patients with acute myocardial infarction. Patients sampled early had marked elevations in FPA. Thirty of 39 patients (77%) with transmural myocardial infarction admitted within 10 hours of the onset of symptoms had markedly elevated levels (>8 ng/ml). In contrast, among patients in whom samples were obtained later than 10 hours after the onset of symptoms, only 2 of the 14 patients had elevations greater than 8 ng/ml. One of these patients had a mural thrombus present at the time of admission and the other had severe pericarditis. Among 10 patients who underwent angiography within 7 hours of the onset of symptoms, all had total thrombotic occlusion. In each, FPA was elevated (mean = 64.4 $\pm$ 26.6 ng/ml) and in 9 of the 10 levels were greater than 8 ng/ml. All of the 13 patients in whom samples were obtained very early (<3 hours of the 13 hours after the onset of symptoms) had values of more than 8 ng/ml. FPA elevations did not correlate with infarct size as measured with creatine kinase. FPA declined in patients with transmural infarction over the initial 24 hours. In response to heparin, FPA fell markedly, compatible with inhibition of ongoing intravascular thrombin activation. The abrupt response to heparin suggests strongly that the likely source of the initial thrombin activation was coronary thrombosis. Three patients had recurrent injury during follow-up. In each, transmural injury was accompanied by reelevation of FPA. Studies are being initiated to assess whether this marker of thrombosis is of utility in defining the risk for recurrent injury.[6]

1. B. E. Sobel, E. M. Geltman, A. S. Tiefenbrunn, A. S. Jaffe, J. J. Spadaro, M. M. Ter-Pogossian, D. Collen, and P. A. Ludbrook, "Improved Regional Myocardial Metabolism After Coronary Thrombolysis with Tissue-Type Plasminogen Activator (t-PA) or Streptokinase," Circulation, vol. 69, pp. 983-989, 1984.

2. D. Collen, E. J. Topol, A. S. Tiefenbrunn, H. K. Gold, M. L. Weisfeldt, B. E. Sobel, R. C. Leinbach, J. A. Brinker, P. A. Ludbrook,

I. Yasuda, B. H. Bulkley, A. K. Robison, A. J. Hutter, Jr., W. R. Bell, J. J. Spadaro, Jr., B. A. Khaw, and E. B. Grossbard, "Coronary Thrombolysis with Recombinant Human Tissue-Type Plasminogen Activator: A Prospective Randomized, Placebo-Controlled Trial," Circulation, vol. 70, pp. 1012-1017, 1984.

3. A. J. Tiefenbrunn, A. K. Robison, P. B. Kurnik, P. A. Ludbrook, and B. E. Sobel, "Clinical Pharmacology in Patients with Evolving Myocardial Infarction of Tissue-Type Plasminogen Activator Produced by Recombinant DNA Technology," Circulation, vol. 71, pp. 110-116, 1985.

4. The TIMI Study Group, "The Thrombolysis in Myocardial Infarction (TIMI) Trial, Phase I Findings," Special Report, New England Journal of Medicine, vol. 312, pp. 932-936, 1985.

5. A. S. Jaffe, R. G. Lee, J. R. Perez, E. M. Geltman, G. D. Wilner, and B. E. Sobel, "Lack of Elevation of Platelet Factor IV in Plasma from Patients with Myocardial Infarction," Journal of the American College of Cardiology, vol. 4, pp. 653-659, 1984.

6. P. R. Eisenberg, L. A. Sherman, K. Schechtman, J. Perez, B. E. Sobel, and A. S. Jaffe, "Fibrinopeptide A: A Marker of Acute Coronary Thrombosis," Circulation, vol. 71, pp. 912-918, 1985.

A-5. Electrophysiological and Biochemical Factors Underlying the Genesis of Dysrhythmias Due to Myocardial Ischemia and Infarction

Personnel: P. B. Corr, Ph.D., Medicine and Pharmacology
S. M. Moore, BCL
J. B. Kramer, M.D., Medicine and Surgery
S. M. Pogwizd, M.D., Medicine
B. E. Sobel, M.D., Medicine
K. A. Yamada, Ph.D., Medicine

Support: RR 01380
HL 28995
HL 17646
AHA 81-108

The overall concept of the research is that potential arrhythmogenic metabolites accumulate in ischemic tissue and exert deleterious effects on membranes and that their effects may be exacerbated by the concomitant influences of the adrenergic nervous system. Over the past several years studies have been completed demonstrating a major electrophysiological role of α-adrenergic stimulation during myocardial ischemia as well as reperfusion. In addition, it has been demonstrated using radioligand binding procedures that there is a reversible increase in α_1-adrenergic binding sites in ischemic and reperfused myocardium. More recently, we have demonstrated that α-adrenergic blockade specifically attenuates the increase in intracellular calcium associated with reperfusion in reversibly injured tissue.[1] Studies performed in our laboratory have also indicated

that lysophosphatides, including lysophosphatidylcholine (LPC) and ethanolamine (LPE) accumulate in ischemic myocardium in situ and have been implicated as potential mediators of arrhythmogenesis in the ischemic heart.[2]

Previous findings indicate that exogenous LPC (20-100 μM) induces electrophysiologic alteration in vitro. To assess whether the compartment in which LPC resides is a critical determinant of its electrophysiologic effects, intracellular micropressure injection of LPC was performed with simultaneous recording of the transmembrane action potential in superfused canine Purkinje fibers. Microelectrode injector properties were calibrated by measuring the diameter of the droplet prior to and after cell impalement at a series of pressures yielding a proportional relese of LPC (r=.99), and the concentration delivered calculated based on measured total cell volume. Intracellular delivery was verified by the generation of slow response action potentials after injection of cyclic AMP in tissue depolarized with 10 mM KCl. Intracellular LPC, in concentrations as high as 500 μM (n=18) did not induce discernible electrophysiologic alterations (RMP = -81 ± 1 to -80 ±1 mV; amplitude = 122 ± 2 to 118 ± 3 mV and APD_{95} = 285 ± 10 to 293 ± 11 ms). Very high concentrations of LPC, 2.5 mM (n=18), induced a slight but rapidly reversible depolarization (RMP = -81 ± 1 to -73 ± 2 mV) and decrease in amplitude (122 ± 2 to 110 ± 4 mV) attributable to changes in volume. Thus, electrophysiolgic effects induced by LPC are markedly dependent on the locus of accumulation. Since electrophysiologic derangements can be induced by LPC in the extracellular compartment at relatively low concentrations compared to that required in the intracellular compartment, concentrations of phospholipids in cardiac lymph during ischemia were assessed in 7 dogs. In each animal, a cannula was inserted into the supracardiac lymph vessel identified with Evan's Blue dye injected into the left ventricular apex. Less than 4% of ^{14}C-PC (phosphatidyl choline) or ^{14}C-LPC incubated in cardiac lymph for 30 min at 4°C or 90 min at 37°C was catabolized (n=5). Lymph was collected on ice at 15 min intervals throughout 2 hr of ischemia induced by LAD coronary ligation, extracted in $CHCl_3$:CH_3OH (2:1) and phospholipids separated by HPLC. Prior to ischemia, PC constituted the major phospholipid (79 ± 2%). Substantial quantities of sphingomyelin (11 ± 2%) and LPC (6 ± 1%) were present. With ischemia, LPC concentration increased 135% from 84 ± 5 to 197 ± 34 μM (n=7, P<.01) judging from the measured concentration and dilution determined with constant infusion of dye into the LV apex. In contrast, PC concentration and efflux did not change. Thus, LPC increases in interstitial fluid concomitant with ischemia to levels sufficient to induce electrophysiologic derangements. Studies are currently underway to delineate the effects of selective inhibitation of PLA_2 in vivo during ischemia with simultaneous three-dimensional cardiac mapping from 240 sites[3] to assess whether the electrophysiologic effects of ischemia are blunted.

A recent series of studies was completed to determine whether endogenous long-chain acyl carnitines alter electrophysiologic function during hypoxia. Sarcolemmal long-chain acyl carnitines and transmembrane action potentials were measured in neonatal rat myocytes rendered hypoxic with or without blockade of synthesis of long-chain acyl carnitines with phenylalkyloxirane carboxylic acid (POCA, 10 μM), an inhibitor of carnitine acyltransferase. Local concentrations in the sarcolemma of endogenous long-chain acyl carnitines were determined by quantitative electron microscopic autoradiography. Hypoxia increased long-chain acyl carnitines

by more than 5-fold (radioactivity increasing from 25 ± 9 in controls to 139 ± 77 (SD) dpm/μg protein) but not with POCA (radioactivity = 11 ± 4 dpm/μg protein). The long-chain acyl carnitines in sarcolemma increases 70-fold with hypoxia from 2 to 140 × 10^5 molecules/μm^3, but not with POCA. Increased long-chain acyl carnitines in hypoxic cells was associated with decreased resting potential (RP) to -25 mV and abolition of depolarizations in contrast to the case in hypoxic but POCA-treated cells (RP = -64 ± 14 vs 76 ± 10 mV in controls; action potential amplitude = 77 ± 17 vs 97 ± 9 mV). These results strongly implicate endogenous long-chain acyl carnitines as a mediator of electrophysiologic impairment secondary to hypoxia. The effect of POCA and oxfenacine, another inhibitor of carnitine acyltransferase are currently being evaluated in vivo during ischemia in an attempt to reverse or modify the electrophysiologic alterations and associated arrhythmias.

To delineate the electrophysiologic mechanisms underlying arrhythmias induced by ischemia, a computerized, three-dimensional mapping system[3] with simultaneous 8-level transmural recording from 232 bipolar sites was used to characterize ventricular tachycardia (VT) after LAD coronary artery ligation in feline hearts in vivo. Within 5 min of ischemia, sinus rhythm was characterized by delayed subendocardial to epicardial total activation time (70 ± 5 vs 25 ± 1 ms prior to ischemia) and the appearance of reverse activation from the epicardium to the midmyocardium were present during sinus rhythm. Spontaneous VT always arose in the subendocardium (n=5) adjacent to the site of the delayed epicardial to midmyocardial conduction of the previous beat. Maintenance of VT was due to further delayed endocardial to epicardial conduction (102 ± 9 ms) with areas of block in the ischemic zone as well as further subsequent delayed epicardial to myocardial conduction. Thus, VT during ischemia is due to intramural reentry. Currently, studies are being performed to assess, for the first time, the electrophysiologic mechanisms responsible for the deleterious effects of catecholamines during ischemia.

We have previously demonstrated that sustained monomorphic ventricular tachycardia (SMVT) during chronic canine myocardial infarction is secondary to intramural reentry and is critically dependent upon epicardial conduction delay and block.[4] The present study assessed the mechanisms responsible for nonsustained polymorphic VT (NSVT) in dogs 3 to 5 days following transient LAD coronary artery occlusion (n=5) with a computerized mapping system which analyzed activity simultaneously from 232 epicardial and intramural sites.[3] In contrast to SMVT, reentry during NSVT elicited by programmed stimulation was confined to the midmyocardium and subendocardium, with only passive epicardial activation. NSVT was maintained when reentrant wavefronts reached nonrefractory endocardium to initiate successive beats. Polymorphism was attributable to different endocardial exit sites between each beat. Endocardial activation time during the last paced beat preceding VT was similar in SMVT and NSVT (92 ± 13 vs 89 ± 10 ms). In contrast, epicardial activation time was prolonged in dogs with SMVT compared with NSVT (170 ± 16 vs 91 ± 12 ms, $P < .01$). This indicates that NSVT can result from reentry confined to the midmyocardium and subendocardium and depends less on transmural electrical dysfunction. These results also identify a mechanism accounting for the frequently lethal VT seen after nontransmural infarction in man.

1. A. D. Sharma, J. E. Saffitz, B. I. Lee, B. E. Sobel, and P. B. Corr, "Alpha-Adrenergic Mediated Accumulation of Calcium in Reperfused

Myocardium," Journal of Clinical Investigation, vol. 72, pp. 802-818, 1983.

2. P. B. Corr, R. W. Gross, and B. E. Sobel, "Amphipathic Metabolites and Membrane Dysfunction in Ischemic Myocardium," invited review for Circulation Research, vol. 55, pp. 135-154, 1984.

3. F. X. Witkowski and P. B. Corr, "An Automated Simultaneous Transmural Cardiac Mapping System," American Journal of Physiology, vol. 247, pp. H661-H668, 1984.

4. J. B. Kramer, J. E. Saffitz, F. X. Witkowski, and P. B. Corr, "Intramural Reentry as a Mechanism of Ventricular Tachycardia During Evolving Canine Myocardial Infarction," Circulation Research, vol. 56, pp. 736-754, 1985.

A-6. Research Projects Utilizing the Isolated-Probe Data-Acquisition System

Personnel: K. A. A. Fox, M.B., Ch.B., Medicine
H. D. Ambos, Medicine
D. E. Beecher, BCL
S. R. Bergmann, M.D., Ph.D., Medicine
T. L. Rosamond, M.D., Medicine
B. E. Sobel, M.D., Medicine

Support: RR 01380
HL 13851
HL 17646

The research in this project is designed to define the kinetics of positron-emitting radiotracers that are potentially useful for the noninvasive characterization of myocardial perfusion and metabolism. Studies in this project are conducted in isolated rabbit hearts perfused with washed sheep erythrocytes suspended in a modified Krebs-Henseleit buffer, and in open-chest dogs with controlled, extracorporeal circulation. Both of these animal preparations have been used extensively in our laboratories, and presage the implementation of approaches of proven value in studies using positron-emission tomography. The development of accurate, quantitative, noninvasive measurements of myocardium metabolism and perfusion are dependent on the characterization of the factors that can influence tracer kinetics. Since fatty acid is the major fuel of the myocardium, we have continued our studies on the characterization of 1-^{11}C-palmitate.

Assessment of myocardium metabolism with radiolabeled palmitate and positron-emission tomography has generally assumed that the clearance of radiolabel from the myocardium is attributable solely to the efflux of the products of oxidative metabolism. However, interpretations would differ if this assumption differed with altered metabolic states, such as ischemia or reperfusion. Accordingly, we studied 21 open-chest anesthetized dogs with

the coronary circulation perfused with a extracorporeal bypass pump, and monitored the extraction and clearance of 1-^{11}C-palmitate (administered as a bolus into the coronary artery) under baseline conditions. After radioactive decay, a second intracoronary bolus was administered during ischemia (n=6), hypoxia (perfusion at normal flow rates but with venous blood, (n=9), or with maintained baseline conditions (n=6). Myocardial time-activity curves were measured with a beta-probe with radioactive data fed into the isolated-probe data acquisition system. The results of the time-activity curves were correlated with products of oxidative metabolism measured directly from analysis of the arterial and regional coronary venous blood. Under control conditions, 95.2 ± 3.8% (mean ± SD) of initially extracted ^{11}C-palmitate was metabolized to $^{11}CO_2$, while 6.2 ± 2.6% back diffused in an unaltered form. In contrast, with ischemia (perfusion 26% of baseline flow), only 16.9 ± 9.8% of administered tracer evolved as $^{11}CO_2$, and 18.8 ± 11.7% back diffused (P<.001). Overall, from 1-40 min. after intracoronary injection of tracer, back diffusion of palmitate contributed to 40.6% of the total radioactivity in the effluent with ischemia, 48.7% with hypoxia, but only 8.9% under control conditions. Despite the increased back-diffusion of non-metabolized palmitate seen during ischemia and hypoxia, the overall residue of ^{11}C-activity in the myocardium was increased, consistent with the diminished clearance observed in the myocardial time-activity curves and the increase in tissue lipid content. These results suggest that estimates of oxidative metabolism based upon external detection of the clearance of radiolabeled fatty acid must take into account the efflux of initially extracted but non-metabolized fatty acid.

Our division is currently involved in studies designed to evaluate the efficacy of coronary reperfusion in the restoration of myocardial metabolism and function after coronary thrombolysis. To determine whether myocardial intermediary metabolism recovers promptly with reperfusion after brief (20 min) ischemia, the LADs in 22 open-chest anesthetized dogs were perfused extracorporally, and 1-^{11}C-palmitate was given intravascularly under baseline or repeat control conditions (n=6) 66 ± 11% of initially extracted ^{11}C-palmitate was oxidized to $^{11}CO_2$. In contrast, with ischemia, (22% of baseline flow, n=6) only 26 ± 14% was oxidized. Recovery of $^{11}CO_2$ was incomplete (42 ± 19%) after 30 min. of reperfusion (n=7, P<.05). Back diffusion of non-metabolized ^{11}C-palmitate increased from 10.5 to 17.2% and clearance of residual ^{11}C-palmitate detected externally with the beta-probe system was prolonged ($t_{1/2}$ increasing from 4.2 to 12.5 min, P<.05), and recovered only incompletely. Recovery of all parameters was complete in positive control experiments (3 min ischemia followed by 30 min reperfusion). Thus impairment of myocardial intermediary metabolism persists after transitory ischemia followed by reperfusion, a phenomenon necessitating consideration for interpretation of clinical metabolic images. As reported (D-1), we have looked sequentially at the recovery of perfusion and metabolism in an intact-dog preparation of ischemia and reperfusion.

Since 1-^{11}C-palmitate is subject to initial extraction but then can back-diffuse from either intracellular or interstitial compartments during ischemia, hypoxia, or reperfusion, we studied the use of a fatty-acid analog, 1-^{11}C beta methyl heptadecanoic acid (BMHA). BMHA was given as a bolus injection proximal to an occluded circumflex marginal branch in 5 open-chest, anesthetized dogs. Extraction fraction, determined by collection of myocardial time-activity curves with the beta-probe and the

isolated probe data acquisition system averaged 25 ± 5 (mean ± SD) % in normal, and 45 ± 15% in ischemic zones. In normal zones, 5% of extracted BMHA was oxidized to $^{11}CO_2$ in twenty minutes, and 3% egressed unaltered via the coronary venous effluent. In contrast, less than 1% was oxidized while 45% egressed unaltered from ischemic zones. Ischemia increased the proportion of total activity in trigylerides (from 55 ± 11 to 73 ± 8%) and decreased the proportion in phospholipid. Thus, although BMHA has been suggested as a fatty-acid analog that would not be subject to limitations of 1-^{11}C-palmitate, its kinetics do not simulate those of circulating fatty acids. However, since BMHA accumulates predominately in tricyleride without undergoing substantial beta oxidation, this tracer may be useful to study neutral lipid pools in normal and ischemic myocardium.

The studies performed in the laboratory in the past year with 1-^{11}C-palmitate and BMHA have permitted a better understanding of the factors that influence the uptake of these tracers. In the coming year, we will continue our characterization of the kinetics of these tracers, with a special emphasis on the recovery of metabolism during reperfusion. Since during ischemia and reperfusion, the myocardium may switch from fatty acid metabolism to utilization of carbohydrates for energy production, we plan to begin characterizing the use of ^{11}C glucose, as well as ^{11}C-deoxy-glucose, in an isolated heart model preparation of ischemia and reperfusion. Clarification of the kinetics of these tracers under controlled laboratory conditions will enhance understanding of the tomographic data that is acquired in our studies of experimental animals (D-1) as well as positron-emission tomographic studies in humans (D-2).

1. K. A. A. Fox, D. R. Abendschein, H. D. Ambos, B. E. Sobel, and S. R. Bergmann, "Efflux of Metabolized and Non-Metabolized Fatty Acid from Canine Myocardium: Implications for Quantifying Myocardial Metabolism Tomographically," Circulation Research, vol. 57, pp. 232-243, 1985.

2. D. R. Abendschein, K. A. A. Fox, R. M. Knabb, H. D. Ambos, D. R. Elmaleh, and S. R. Bergmann, "The Metabolic Fate of ^{11}C-Beta Methyl Heptadecanoic Acid (BMHA) in Myocardium Subjected to Ischemia," Circulation, vol. 70 supplement II, p. II-148, 1984, (abstract).

3. K. A. A. Fox, D. R. Abendschein, B. E. Sobel, and S. R. Bergmann, "Persistent Impairment of Myocardial Metabolism and Clearance of Labeled Fatty Acid after Brief Ischemia: Implications for Positron Emission Tomography (PET)," Journal of the American College of Cardiology, vol. 5, p. 451, 1985, (abstract).

A-7. Analysis of Plasma CK Isoforms

Personnel: D. R. Abendschein, Ph.D., Medicine
S. R. Devries, M.D., Medicine
A. M. Grace, Medicine
A. S. Jaffe, M.D., Medicine
J. Markham, BCL
B. E. Sobel, M.D., Medicine
A. W. Strauss, M.D., Medicine

Support: RR 01380
HL 17646

Early and reliable detection of acute myocardial infarction and characterization of its time course are important for timely initiation of therapy and evaluation of the effects of therapy. Conventional analysis of enzyme time-activity curves in blood is neither rapid nor a reliable method to assess the chronology of infarction. However, analysis of profiles of isoforms of creatine kinase (CK) MM isoenzyme in plasma may permit prompt detection of infarction and differentiation of events punctuating the time course of infarction.

In the past year, we have shown in dogs subjected to coronary artery occlusion that the predominant MM CK isoform in myocardium, MM_A, is converted quickly and sequentially to MM_B and MM_C isoforms in plasma.[1] Conversion combined with disappearance of each isoform from the circulation results in a consistent, time-dependent change in the proportions of isoforms in plasma with rapid return to the baseline proportions. Changes in isoform proportions are independent of infarct size and are not affected by marked variations in the contours of total CK and isoform time-activity curves in plasma. Moreover, because of continuous elimination of MM_A from plasma, the proportions of isoforms in plasma are altered markedly by egress of modest amounts of MM_A from myocardium. Thus, changes in isoform proportions indicative of recent tissue damage occur very early after the onset of ischemia and are more sensitive to early myocardial damage than total CK activity in plasma.

Recent studies (in review) have also shown that the fraction of total CK activity in plasma represented by MM_A (MM_A%) changes very early after the onset of myocardial reperfusion in conscious dogs. The rate of change of MM_A% in plasma after reperfusion is remarkably consistent and strikingly different (at least 5-fold) from the rate in the absence of reperfusion regardless of the duration of preceding ischemia, magnitude of absolute plasma CK activity, or infarct size. Thus, analysis of changes in MM_A% in plasma may provide an early and reliable index of myocardial reperfusion.

In order to apply isoform analysis clinically for early detection of reperfusion and other disparate biological events in the chronology of infarction, it is necessary to rigorously define the kinetics of conversion and elimination of isoforms in plasma in vivo. Accordingly, we have initiated development of a physiologically based, mathematical model of MM CK isoform kinetics during myocardial infarction in dogs which will provide a basis for recognition of kinetic parameters characterizing different cardiac events.

Previous observations from our laboratory[2] indicating that greater than 95% of total MM CK in myocardium is MM_A and that MM_A is converted sequentially and irreversibly to MM_B and MM_C in plasma have led to the formulation of a three-compartment, vascular model of isoform kinetics. For preliminary testing, we have assumed that the kinetics of isoform conversion are first-order. In the past year, estimates of the conversion and disappearance rates of each isoform using the vascular model have been obtained in vivo after intravenous injection of purified MM_A into conscious dogs and in vitro after incubation of purified MM_A in canine plasma. Close agreement of the in vivo and in vitro rate constants estimated from plasma time-activity curves by non-linear least squares approximation suggested the suitability of the vascular model to define isoform kinetics during myocardial infarction. However, subsequent experiments in which the kinetic rate constants estimated in vivo were used to simulate isoform time-activity curves in plasma after myocardial infarction proved unsuccessful. The vascular model predicted that the amount of each isoform in plasma would be about equal over time when, in fact, the time-activity curves in plasma showed a progressive increase in the amount of MM_B relative to MM_A and MM_C relative to MM_B. Judging from these preliminary results, it appears that a simple vascular model will not adequately define isoform kinetics during myocardial infarction in dogs.

A possible explanation for the disparity between simulated isoform time-activity curves derived from the rate constants after intravenous injection of MM_A, and actual isoform activity curves in plasma after myocardial infarction is that the input into plasma during infarction may consist of all three isoforms reflecting conversion of MM_A in more than one biological pool. Because we have shown that MM_A is the primary isoform in both normal and necrotic myocardium, it is reasonable to consider that additional pool(s) may be located extracellularly.

Preliminary experiments have been conducted to examine the isoform converting capability of extracellular fluid. Isoforms leaving the heart via cardiac lymph were assessed and compared to isoforms in plasma at 6 hours and 14 hours after coronary artery occlusion in dogs. At 6 hours, most of the CK activity in lymph was in the form of MM_A. A small amount of MM_B but no MM_C was detected in lymph compared with high quantities of MM_B and MM_C in plasma. However, at 14 hours, corresponding to the time of peak total CK activity in plasma, more than half of the isoform activity in cardiac lymph was in the form of MM_B and MM_C. Thus, it appears that conversion of isoforms occurs in cardiac lymph after infarction, but at a slower rate than in plasma. Although the volume flow of lymph leaving the heart is small, the amount of MM_B and MM_C egress from the heart may be sufficient to account for the disparity observed in earlier modeling experiments. Accordingly, the model to define isoform kinetics in vivo during myocardial infarction may need to include a cardiac lymph pool.

Additional experiments are planned to determine the time course of isoform activities in cardiac lymph and plasma simultaneously after myocardial infarction in dogs. For this purpose, we are developing a procedure for obtaining serial cardiac lymph samples from conscious dogs. The results of these studies should identify the input function for isoforms entering plasma during infarction and facilitate the delineation of the appropriate model to define the kinetics of isoforms in plasma after acute myocardial infarction. This model will then be employed to identify kinetic parameters that might differentiate acute infarction from

myocardial reperfusion, recurrent infarction in previously ischemic zones, and extention of infarction in previously non-ischemic zones in conscious dogs and ultimately in human subjects.

1. H. Hashimoto, D. R. Abendschein, A. W. Strauss, and B. E. Sobel, "Early Detection of Myocardial Infarction in Conscious Dogs by Analysis of Plasma MM Creatine Kinase Isoforms," Circulation, vol. 71, pp. 363-369, 1985.

2. H. Hashimoto, A. M. Grace, J. J. Billadello, R. W. Gross, A. W. Strauss, and B. E. Sobel, "Non-Denaturing Quantification of Subforms of Canine MM Cratine Kinase Isoenzymes (Isoforms) and Their Interconversion," Journal of Laboratory Clinical Medicine, vol. 103, pp. 470-484, 1984.

A-8. Multicenter Investigation of the Limitation of Infarct Size

Personnel: A. S. Jaffe, M.D., Medicine
H. D. Ambos, Medicine
D. R. Biello, M.D., Radiology
K. W. Clark, BCL
E. D. Galie, R.N., Medicine
E. M. Geltman, M.D., Medicine
D. S. Payne, Medicine
J. E. Perez, M.D., Medicine
B. A. Siegel, M.D., Radiology
B. E. Sobel, M.D., Medicine
P. H. Stone, M.D., Peter Bent Brigham Hospital
L. J. Thomas, Jr., BCL
R. A. Wettach, R.N., Medicine
A. L. Ysaguirre, Medicine

Support: RR 01380
HV 72941

The MILIS protocol was initiated on August 1, 1978. In previous progress reports the goals and aims of the study as well as the end-point data for propranolol have been delineated. The hyaluronidase arm of the study was terminated on December 31, 1983. By that time 9,444 patients had been screened for eligibility and a total of 985 patients had been randomized. Washington University contributed 244 patients (25% of the overall recruitment). The primary end-point was infarct size measured by serial determinations of MB creatine kinase. It has previously been shown that there were close relationships between MB CK infarct size and the size of infarction as determined by morphometric measurements in patients who died early ($r=.79$, $n=19$).[1] Ancillary end-points included mortality, electrocardiographic findings, pyrophosphate scintigraphy, radionuclide ventriculography and exercise treadmill tests. Of the 851 patients who received blinded therapy, 166 who received hyaluronidase and 172 who received placebo were in group A (those patients eligible medically to

receive propranolol). In group B (patients not eligible to receive propranolol) 254 patients received hyaluronidase and 259 received placebo. The baseline characteristics between these groups were quite comparable although patients treated with hyaluronidase had slightly higher blood pressures. The mean time from the onset of chest pain to the administration of blinded therapy was 9.3 ± 0.2 hours for hyaluronidase and 9.4 ± 0.2 hours for placebo. Four patients were treated within 3 hours of the onset of pain, 26 within 4 hours and 161 within 6 hours. The numbers of patients in the entire group (0 to 18 hours) were such that a 20% reduction in infarct size index at the $P<.05$ level (2 sided) could be accomplished at a power of .82. However the power given similar assumptions to assure that early treatment had not been beneficial in the subgroup randomized between 0 and 8 hours was only .56. Hyaluronidase was well tolerated; urticaria developed in 9 patients (2.1%) compared to 2 patients in the placebo group (.5%, $P=0.04$). The incidence of acute myocardial infarction was not altered by hyaluronidase therapy (86% for hyaluronidase compared to 88% for placebo-treated patients). There were no differences in the infarct size index or MB, peak MB CK between groups (Table 1).[2] Similarly there was no significant mortality during a 48 month followup for the entire cohort of patients (Figure 1). There were minor differences in other parameters of cardiac performance including radionuclide ventriculograms, ECGs, stress tests performance and pyrophosphate images.

These negative results were in sharp conrast to results of other studies with hyaluronidase and likely were in large part due to the relatively late administration of therapy in this study. It was clear that hyaluronidase given to patients with acute infarction within the confines of this study failed to show significant benefit.

Although no benefit was found overall, an interesting observation was made retrospectively in a subgroup of patients. Since at the time of the initiation of the trial, little was known concerning reperfusion or the fact that rapid peaking of MB CK might be a marker of acute reperfusion, the possibility that patients who mainfested reperfusion would have a different response to hyaluronidase was not considered. Subsequently, as data in this area were developed, the need to evaluate this patient group was recognized. Accordingly, a retrospective analysis was done to assess whether patients who fell in the first quartile of time from onset of symptoms to peak CK behaved differently than those in the other 3 quartiles. Patients with early peaking of MB CK treated with hyaluronidase had a markedly reduced mortality over time compared to control patients who peaked similarly early. This effect was not seen on any of the other quartiles of patients. Additional effects delineated retrospectively included improvement in mortality and ejection fraction in patients with ST depression, especially for those in group B treated 8 to 18 hours after the onset of infarction. The mechanisms for both of these effects are unclear. It is conceivable that early reperfusion allows hyaluronidase to reach the infarcted area and to prevent further extension or to reduce the initial size of infarction. The effects in patient with nontransmural infarction may be seen similarly mediated if a partially open artery is present. The possibility that this finding is due to statistical artifact must be strongly considered.

A large number of on going data bank studies continue from the MILIS data bank with active participation from our contingent at Washington University.[3-8]

For example, Peter Stone, M.D., proposed a preliminary investigation of ischemia in MILIS patients who had survived 6 months post-MI and who had received at 6 months both an exercise tolerance test (ETT) and a 24-hour Holter ECG recording. Of 298 patients who had both tests performed, 94 patients had exertional ST-segment depression (>1 mv) on the ETT. Since the original analyses of the Holter recordings did not include estimates of ST-segment deviations, a sample of 50 of the 94 Holters were retrospectively analyzed for significant ST-segment changes. Because the Holter recordings were not calibrated to measure ST-segment deviations in the traditional sense of absolute millivolts, ST-segment deviation was expressed as a percentage of QRS height, for which 25% was arbitrarily chosen as significant. As only 2 of the 50 recordings showed significant ST-segment changes, the investigation was discontinued.

1. D. B. Hackel, K. A. Reimer, R. E. Ideker, E. M. Mikat, T. D. Hartwell, C. B. Parker, E. B. Braunwald, H. K. Gold, A. S. Jaffe, D. S. Raabe, R. E. Rude, B. E. Sobel, P. H. Stone, M. Buja, J. E. Muller, R. Roberts, and the MILIS Study Group, "Comparison of Enzymatic and Anatomic Estimates of Myocardial Infarct Size in Man," Circulation, vol. 70 pp. 824-835, 1984.

2. A. S. Jaffe, for the MILIS Study Investigators, "The Adminstration of Hyaluronidase to Patients with Acute Myocardial Infarction: Results of the MILIS Study," Journal of the American College of Cardiology, vol. 5, p. 447, 1985.

3. J. Mukharji, R. E. Rude, K. W. Poole, L. J. Thomas, H. W. Strauss, A. S. Jaffe, J. E. Muller, R. Roberts, D. S. Raabe, C. H. Croft, E. Passamani, E. Braunwald, J. T. Willerson, and the MILIS Study Group, "Late Sudden Death Following Acute Myocardial Infarction: Multivariate Analysis of Risk Factors," American Journal of Cardiology, vol. 54, pp. 31-36, 1984.

4. D. E. Jansen, J. R. Corbett, S. E. Lewis, C. L. Wolfe, G. Galiani, N. Filipchuk, G. Redish, R. W. Parkey, M. Buja, A. S. Jaffe, B. E. Sobel, and J. T. Willerson, "Measurement of Myocardial Infarct Size: A Comparison of Single Photon Emission Computed Tomography with Pyrophosphate and Serial CK-MB Measurements," Circulation, vol. 72, pp. 327-333, 1985.

5. J. E. Muller, Z. G. Turi, P. H. Stone, R. E. Rude, D. S. Raabe, A. S. Jaffe, H. K. Gold, N. Gustafson, K. W. Poole, E. Passamani, T. W. Smith, E. Braunwald, and the MILIS Group: Digoxin Therapy and Mortality Following Myocardial Infarction: Experience in the MILIS Study," submitted for publication.

6. Z. G. Turi, J. D. Rutherford, R. Roberts, J. E. Muller, A. S. Jaffe, R. E. Rude, C. Parker, D. S. Raabe, P. H. Stone, T. D. Hartwell, S. E. Lewis, R. W. Parkey, H. K. Gold, T. L. Robertson, B. E. Sobel, J. T. Willerson, E. Braunwald, and the Multicenter Investigation for the Limitation of Infarct Size (MILIS), "Electrocardiographic, Enzymatic and Scintigraphic Criteria of Acute Myocardial Infarction as

Determined from Study of 726 Patients," American Journal of Cardiology, vol. 55, pp. 1463-1468, 1985.

7. J. E. Muller, P. H. Stone, Z. G. Turi, J. D. Rutherford, C. Czeisler, C. Parker, K. W. Poole, T. D. Hartwell, E. Scheiner, H. K. Gold, A. S. Jaffe, D. S. Raabe, R. E. Rude, E. Passamani, R. Roberts, T. Robertson, B. E. Sobel, J. T. Willerson, E. Braunwald, and the MILIS Study Group, "Circadian Variation in the Frequency of Onset of Acute Myocardial Infarction," submitted for publicaiton.

8. H. C. Croft, R. E. Rude, N. Gustafson, P. H. Stone, K. W. Poole, R. Roberts, H. W. Strauss, D. S. Raabe, L. J. Thomas, A. S. Jaffe, J. Muller, P. Hoagland, B. E. Sobel, E. R. Passamani, E. Braunwald, J. T. Willerson, and the MILIS Study Group, "Abrupt Beta-Blockade Withdrawal in Patients with Acute Myocardial Infarction. Effects on Infarct Size, Left Vetricular Function, and Hospital Course," submitted for publication.

Table III
PLASMA MB-CK ANALYSIS FOR ALL PATIENTS

	Hyaluronidase	Placebo	Significance of the Difference (P value)
MB-INFARCT SIZE INDEX			
Total Population			
Number of Patients	364	374	
Mean (MBCK-g-eq/m^2)	14.6	15.2	0.62
SE	0.8	0.8	
Range	0.0-123.5	0.0-103.0	
Early Randomization (0.8 hrs)			
Number of Patients	174	171	
Mean	16.3	16.5	0.89
SE	1.1	1.1	
Range	0.0--123.5	0.0-70.4	
Late Randomization (8-18 hrs)			
Number of Patients	190	203	
Mean	13.1	14.1	0.54
SE	1.1	1.0	
Range	0.0-84.0	0.0-103.0	
PEAK PLASMA MBCK			
Total Population			
Number of Patients	415	429	
Mean	131.0	128.1	0.71
SE	5.9	5.2	
Range	0-848	0-612	
Early Randomization (0-8 hrs)			
Number of Patients	192	191	
Mean	154.9	148.4	0.60
SE	9.0	8.4	
Range	0-848	3-612	
Late Randomization (8-18 hrs)			
Number of Patients	223	238	
Mean	110.5	111.7	0.90
SE	7.5	6.2	
Range	0.754	0.454	

A-9. Model Development for Cardiac Diastolic Mechanics

Personnel: M. L. Ridner, M.D., Medicine
M. R. Courtois, M.A., Medicine
P. A. Ludbrook, M.D., Medicine
J. Markham, BCL

Support: RR 01380
HL 17646
HL 25430
Barnes Hospital
Washington University

During the past year, our studies of cardiac diastolic mechanics (PR 20, A-9), i.e., the passive mechanical properties of the left ventricular (LV) muscle and chamber, have continued with emphasis on evaluation of the effects of early reperfusion on the stiffness of the left ventricle (LV) in dogs where the stiffness index is computed from stress-radius relationships.

Values for stress are computed from several variables measured in the cardiac catheterization lab including intra- and extra-cavitary pressures, and the radii of the cavity are calculated from the area and the longest chord of the ventricle as measured from single-plane angiographic silhouettes. Stress is then derived as a function of strain, and strain is expressed as a function of radius to yield a stress-radius relationship (a power function of radius) for estimating elastic stiffness of the LV muscle.

Until recently, we had attempted to fit stress-radius curves over the entire diastolic range; however the rapidly changing curvature of the early portion of the curve precludes a fit with any smooth function. We are presently following the example of other researchers[1] and fitting only the mid- and late-diastolic phases starting with the end of the rapid filling phase. It has been suggested that the stress-radius curves reflect viscous effects in the rapidly filling or early diastolic phase.[2] Curve fits obtained after omitting the early diastolic phase show a closer fit of the power function to the data.

Future efforts will be directed toward determining the portion of the stress-radius curve to be fit and the best function for characterizing the stiffness of the LV.

1. A. Fester and P. Samet, "Passive Elasticity of the Human Left Ventricle: The "Parallel Elastic Element"," Circulation, vol. 50,p. 609, 1974.

2. L. Kirk, J. T. Peterson, A. Johnson, J. DiDonna, and M. LeWinter, "Diastolic Left Ventricular Pressure-Volume and Stress-Strain Relations in Patients with Valvular Aortic Stenosis and Left Ventricular Hypertrophy," Circulation, vol. 58, no. 1, pp. 77-89, July 1978.

A-10. SCOR Patient Information Database

Personnel: K. B. Schechtman, BCL
H. D. Ambos, Medicine
E. M. Geltman, M.D., Medicine
A. S. Jaffe, M.D., Medicine
J. Markham, BCL
B. E. Sobel, M.D., Medicine

Support: RR 01380
HL 17646

The Specialized Center for Research (SCOR) database currently contains information on more than 2000 patients who suffered acute myocardial infarction. The data describe each patient's cardiovascular history, in-hospital course, and long term progress via follow-up examination. The data are stored as a SAS database on the University's IBM System/370 computer. Data are entered using interactive SAS under the Conversational Monitoring System (CMS) operating system. A total of 24 data-entry screens have been designed for this purpose. All data analysis and management facilities of SAS are available for interactive application.

Studies which have utilized the SCOR database include a consideration of whether coronary thrombosis in vivo is reflected by elevations in levels of fibrinopeptide A (FPA) in plasma; an analysis of the factors which are responsible for the initial success or failure of coronary thrombolysis; and a prospective evaluation of platelet factor IV plasma levels in patients with myocardial infarction suggesting that these levels do not provide a definitive criterion for coronary thrombosis.

A-11. Software Support for Cardiological Image Processing

Personnel: D. E. Beecher, BCL
E. M. Geltman, M.D., Medicine
T. O. Videen, BCL

Support: RR 01380
HL 17646

A software system for cardiological image processing has recently been completed and is now in routine use in the Coronary Care Unit. The highly modular system was written in FORTRAN on a Perkin-Elmer 3230 processor and structured for maintainability as well as portability.

This software system was developed for analyzing PET images of the heart. Regions of interest may be created in a variety of ways including defining high and low thresholds of activity or by drawing or subdividing regions free-hand with a trackball. Regions may be defined on zoomed images and may be moved to new locations with the trackball. Statistical analysis may be carried out on individual PET images when the regions are

defined. However, analysis is speeded significantly by allowing multiple regions to be stored and later analyzed on a series of PET images automatically.

Heart imaging has some unique problems posed by the large blood pool and by the fluidity of the heart and movement of the chest. The automatic analysis allows the user to enter coordinates specifying relative shifts between the images on which regions were created, the images of the blood pool, and the images of metabolic activity.

B. Quantitative Imaging: Ultrasonic Tissue Characterization

Although ultrasound has proven to be a useful source of diagnostic information, results of examinations based on current ultrasonic methods are primarily qualitative and pictorial. In a collaborative effort with Cardiology and the Department of Physics work has continued on methods of tissue characterization via ultrasound. Our overall goal is to use ultrasound for the non-invasive identification of tissue pathologies within two-dimensional images of tissue properties. Specific objectives of this effort are 1) to investigate the magnitude and character of anisotropy in tissue, 2) to systematize the representation of the ultrasonic field and to reduce the data needed to describe that field by determining the moments of the spatial distribution of energy over the receiver aperture, 3) to seek improvement in measurement capability of imaging systems via interactive, adaptive beamforming for both linear and variable-aperture transducer arrays, 4) to test the hypothesis that quantitative images based on intrinsic tissue properties can be produced with reflected ultrasound, and 5) to construct a digital multiprocessor system to perform post-echo ultrasonic estimation of attenuation, phase velocity and backscatter in two dimensions.

Quantitative images based on ultrasonic tissue properties have been made at the BCL for several years using transmitted ultrasound with a multiple-frequency tomographic reconstruction system. In the past year we added a multiuser, color-graphics workstation for generating and manipulation images to our processing environment (B-10), which supports acquisition, storage, and processing of reflected ultrasound from arrays, as well as transmitted ultrasound using single-element transducers.

Our investigation of the anisotropy of tissue was extended in four studies conducted over the past year. We constructed a tissue phantom from graphite fibers imbedded in gelatin which reproduces the fiber organization of muscle (B-1). The attenuation (B-2) and backscatter (B-3) of this phantom were studied as functions of ultrasonic frequency and angle of incidence of the ultrasonic beam. Predictions of the change of properties relative to the axis of the fibers agrees well with experimental measurements, and the nature of these changes mimick those observed in dog myocardium and skeletal muscle (B-4). An isotropic, dispersive tissue model based on a single pole (relaxation frequency) was used to predict attenuation of material both linearly and quadratically dependent on frequency (B-7).

Transducers and initial processing of received ultrasound were also the subject of four studies. The frequency and angular responses of elements in a typical linear array were characterized (B-8). A two-dimensional array was simulated by scanning a point-like receiver to measure the spatial moments (B-5) of azimuthally symmetric beams (B-6). The point-like array significantly reduced phase-cancellation errors and the moments allowed beam description in terms of its energy; centroid; and beam width, incidence angle, and divergence angle. We are also processing received ultrasonic fields by adaptively forming beams, i.e., forming beams in ways that depend on the insonified medium (B-9).

B-1. Construction of Anisotropic Tissue-Mimicking Phantoms

Personnel: J. G. Mottley, BCL
J. G. Miller, BCL

Support: RR 01362
HL 17646
HL 28998

Background

Early investigations, ranging as far back as that of Hueter in 1948,[1] have indicated that the ultrasonic attenuation and speed of sound are different when ultrasound propagates parallel to the fibers of the muscle than when it travels perpendicular to those fibers.[2-7] Due to an error in labeling a figure in the Hueter article, the direction of maximum ultrasonic attenuation relative to the fiber direction was in doubt for some time. Further, the articles referenced above indicate only the values of attenuation measured parallel to and perpendicular to the fibers, with no indication of the detailed angular dependence of the parameter.

Research from this laboratory has endeavored to determine the angular dependence and magnitude of these anisotropic effects, in order to permit more rational application of quantitative imaging techniques (PR 18, B-3, B-4).[8] Such anisotropy in the attenuating properties of soft tissues could have a profound impact on the interpretation of ultrasonic images and on measurements which require the use of data acquired from multiple angles of view. In addition, the presence of anisotropic media violates the initial assumptions of back projection reconstructive tomography. Studies and simulations from this laboratory have shown that anisotropy of the attenuation introduces false and misleading values into reconstructed images.[9,10]

Isotropic tissue-mimicking phantoms have frequently been prepared in this laboratory from suspensions of graphite powder in gelatin using procedures described by Madsen and co-workers. These "phantoms" provide relatively accurate mimicking of the attenuation of soft tissues such as liver, but do not exhibit the dependence of attenuation on the angle of insonification that is exhibited by tissues which are oriented into fibers, such as muscular tissue. We thus undertook a project to construct anisotropic phantoms from materials similar to those which proved successful in the prior experiments. We used fibers of graphite which were suspended in gelatin with the axes of the fibers approximately aligned with the procedure described below.

Construction of Anisotropic Phantoms

Short fibers (approximately 400 μm long and 8 μm in diameter) of graphite were obtained by washing them from lumps of fibers as supplied (Alpha Chemical) and were concentrated by settling and decanting. This water and fiber mixture was then mixed with gelatin powder (Fisher Scientific). The mixture was placed in a pre-heated beaker and a warmed cylindrical insert was submerged in the gelatin. The insert was spun while the beaker remained fixed, creating a velocity gradient between the beaker walls and the insert, and also between the bottom of the beaker and a lip

on the insert, with the resulting forces tending to align the fibers circumferentially. The entire apparatus was allowed to cool gradually while the insert was spun.

When the viscosity of the mixture became large, the beaker, mixture, and insert were refrigerated in order to solidify the gelatin rapidly. Subsequently, the ring of gelatin was removed from the beaker and fixed in formaldehyde. After fixation, phantoms were kept immersed in water.

1. T. Hueter, "Messung der Ultraschallabsorption in tierischen Geweben und ihre Abhangigkeit von der Frequenz," Naturwissenschaften, vol. 35, pp. 285-286, 1948.

2. K. T. Dussik, D. J. Fritch, M. Kyriazidou, and R. S. Sear, "Measurements of Articular Tissues with Ultrasound," American Journal of Physiology Medicine, vol. 37, pp. 160-165, 1958.

3. D. E. Goldman and J. R. Richards, "Measurement of High-Frequency Sound Velocity in Mammalian Soft Tissues," Journal of the Acoustical Society of America, vol. 26, pp. 981-983, 1954.

4. W. Buschmann, M. Voss, and S. Kemmerling, "Acoustic Properties of Normal Human Orbit Tissues," Ophthalmology Research, vol. 1, pp. 354-364, 1970.

5. R. C. Chivers and R. J. Parry, "Ultrasonic Velocity and Attenuation in Mammalian Tissues," Journal of the Acoustical Society of America, vol. 63, no. 3, pp. 940-953, 1978.

6. S. A. Goss, R. L. Johnston, and F. Dunn, "Compilation of Empirical Ultrasonic Properties of Mammalian Tissues. II," Journal of the Acoustical Society of America, vol. 68, pp. 93-108, 1980.

7. D. K. Nassiri, D. Nicholas, and C. R. Hill, "Attenuation of Ultrasound in Skeletal Muscle," Ultrasonics, pp. 230-232, September 1979.

8. J. G. Mottley and J. G. Miller, "Anisotropy of Ultrasonic Attenuation in Canine Heart and Liver," Ultrasonic Imaging, vol. 4, p. 180, 1982 (abstract).

9. G. H. Brandenberger, J. R. Klepper, J. G. Miller, and D. L. Snyder, "Effects of Anisotropy in the Ultrasonic Attenuation of Tissue on Computed Tomography," Ultrasonic Imaging, vol. 3, pp. 113-143, 1981.

10. G. H. Brandenberger, J. R. Klepper, D. L. Snyder, and J. G. Miller, "Consequences of Anisotropy on Computed Ultrasonic Tomography," Proceedings of the Sixth International Symposium on Ultrasonic Imaging and Tissue Characterization, Ultrasonic Imaging, vol. 3, p. 197, 1981 (abstract).

B-2. The Attenuation of the Anisotropic Tissue Phantom as a Function of Angle

Personnel: J. G. Mottley, BCL
J. G. Miller, BCL

Support: RR 01362
HL 17646
HL 28998

When particles are suspended in viscous fluids or viscoelastic media, the propagation of ultrasound is affected in several ways, including an increase in the absorption coefficient over that of the medium and the existence of scattering. Further, if the particles are not totally symmetric (i.e., spherical), but are partially symmetric (e.g., cylinders or spheroids), and are suspended with their symmetry axes aligned, then the attenuation and backscatter can be expected to be anisotropic with respect to the direction of insonification (PR 18, B-4).

The systematic theoretical investigations of Avtar S. Ahuja have approached several aspects of this problem. In a series of articles from 1972 to 1979, Ahuja examined the phenomena of the attenuation and scattering due to spherical and spheroidal inhomogeneities distributed in a viscous fluid. The papers show a progression from calculations involving spherical inhomogeneities to those which consider the inhomogeneities to be spheroidal. We summarize the results of the calculations in the early papers of the absorption coefficient due to "viscous relative motion" (described in detail below) of spherical particles, and then examine Ahuja's extensions of this theory to include spheroidal particles.

The Absorption Due to Symmetric Particles Suspended in a Fluid

In 1972, Ahuja published a paper[1] in which he formulated the wave equation for sound propagation in suspensions, and from this derived the velocity of sound. This theory was extended in 1973 and 1974 to include viscous and thermal attenuation coefficients.[2,3] We will present the results from these papers, with slightly modified notation, and then consider the limit of Ahuja's results for the case of rigid particles.

We consider the case in which a fluid of density ρ and shear viscosity η has particles suspended in it. The particles have properties denoted by a subscript p (e.g., the density is ρ_p). In this section, the radius will be designated by the symbol, a, with $a \ll \lambda$. The number density of the particles, n, is assumed to be such that there are many particles in a cube one wavelength on a side.

The results of Ahuja's calculations show that the dominant absorption mechanism in suspensions is that a viscous relative motion, in which viscous, or transverse, waves are generated in the fluid by the relative motion of the particles and the suspending fluid due to the insonifying field. These transverse waves are damped rapidly, leading to energy loss from the incident ultrasonic beam. The amplitude of the relative motion and the difference in phase of that motion, and thus the magnitude of energy loss, increase as the difference in density between the fluid and the particles becomes larger.

Ahuja's expression for the absorption coefficient due to viscous relative motion is

$$\alpha_{vis} = \frac{1}{2}\left(\frac{w}{c}\right)\phi\,\frac{\left[\frac{\rho_p}{\rho} - 1\right]^2 3}{\left(\frac{\rho_p}{\rho} + \tau\right)^2 + s^2}, \tag{2.1}$$

where $\phi = 4/3\pi a^3 n$ is the fractional volume concentration of particles, τ and s are factors which account for the shape and internal viscosity of the particles,

$$\tau = 1/2 + \frac{\delta_t}{4a}\,\frac{(2\eta + 3\eta_\rho)^2}{\left(\eta + \eta_\rho + \frac{a\eta}{3\delta_t}\right)^2 + \left(\frac{a\eta}{3\delta_t}\right)^2}, \tag{2.2}$$

$$s = \frac{3}{4}(2\eta + 3\eta_\rho)\left(\frac{\delta_t}{a}\right)^2\,\frac{\left(1 + \frac{a}{\delta_t}\right)\left[(\eta + \eta_\rho) + \frac{a\eta}{3\delta_t}\right] + \frac{1}{3}\eta\left(\frac{a}{\delta_t}\right)^2}{\left(\eta + \eta_\rho + \frac{a\eta}{3\delta_t}\right)^2 + \left(\frac{a\,\eta}{3\,\delta_t}\right)^2}. \tag{2.3}$$

Here the leading term of $\frac{1}{2}$ in τ is the inertia coefficient of a sphere, and δ_t is the viscous wave skin depth derived in classical viscosity theory,

$$\delta_t = \left(\frac{2\eta}{\rho w}\right)^{1/2}.$$

In the limit of a rigid particle, $\frac{\eta}{\eta_p} \to 0$, the expressions for τ and s become,

$$\tau = \frac{1}{2} + \frac{9}{4}\,\frac{\delta_t}{a}, \tag{2.4}$$

and,

$$s = \frac{9}{4}\left(\frac{\delta_t}{a}\right)\left[1 + \left(\frac{\delta_t}{a}\right)\right], \tag{2.5}$$

and the expression for the absorption coefficient reduces to that obtained by other investigators through different formulations, such as Epstein and Carhart,[4] Urick,[5] and Urick and Ament.[6]

Using the reduced forms of r and s, we calculated the absorption due to viscous relative motion for a substance which is used to manufacture isotropic tissue-mimicking phantoms,[7] using the published descriptions of the materials. The results of these calculations are shown in Figure 1. Fitting the summed absorption coefficient as a function of frequency over the range 1 to 10 MHz, we obtain a slope of 0.5 dB/(cm/MHz), a value that is to be compared to the published measured attenuation coefficient of 0.7 dB/(cm/MHz). Since additional signal loss mechanisms, especially those due to viscous absorption in the gelatin and to scattering of longitudinal waves to longitudinal waves, have not been included in the calculation, the consistency between theory and experiment seems reasonable.

Absorption Due to Non-Symmetric Particles Suspended in a Fluid

Ahuja introduced the possibility of non-symmetric inhomogeneities into his model for viscous relative motion by distorting the particles from spheres of radius a into prolate or oblate spheroids and calculating the absorption coefficient when the particle was insonified either along or perpendicular to the major axis of symmetry of the spheroid. The dimensions of the particles will be denoted by a, the semiminor axis of a prolate or the semimajor axis of an oblate spheroid, and b, the semimajor axis of a prolate or the semiminor axis of an oblate spheroid. Since the case of interest here is that of long thin scatterers, we will limit further discussion to that of prolate spheroids, and refer the reader to Ahuja's papers for information concerning oblate spheroids.

The results of the calculations of the absorption coefficient due to suspended spheroids are similar to those obtained for spheres, with appropriate modifications to the definitions of r and s,

$$r = L + \frac{9}{4}\frac{\delta_t}{b} K^2 \tag{2.6}$$

and,

$$s = \frac{9}{4}\frac{\delta_t}{b} K^2 \left(1 + \frac{1}{K}\frac{\delta_t}{a}\right). \tag{2.7}$$

In these expressions, L is the inertia coefficient of the spheroid, for a particular orientation of the symmetry axis relative to the insonifying field, and K is a shape factor. The calculation of these two factors will be discussed below, both for the general case and in the limit of a long thin prolate spheroid, i.e., $\frac{a}{b} \to 0$. We note that for b = a and appropriate L and K for a sphere, these two expressions are the same as those presented above for the isotropic case.

Drawing on the results of others,[8] Ahuja writes the inertia coefficient for a prolate spheroid of eccentricity

$$e = \left(1 - \frac{a^2}{b^2}\right)^{1/2},$$

as

$$L = \frac{\zeta}{2 - \zeta} , \tag{2.8}$$

where ζ is calculated differently for motions parallel to and perpendicular to the axis of symmetry. For motions parallel to the axis, this factor is

$$\zeta_{\parallel} = \frac{2(1 - e^2)}{e^3} \left\{ \frac{1}{2} \ln\left[\frac{(1 + e)}{(1 - e)}\right] - e \right\}.$$

In the limit of a long thin object,

$$\zeta_{\parallel} \rightarrow 2\left(\frac{a}{b}\right)^2 \left[\ln\left(\frac{2b}{a}\right) - 1\right],$$

which for all practical purposes leads to $L_{\parallel} \rightarrow 0$.

For fluid motion perpendicular to the axis, the factor is

$$\zeta_{\perp} = \frac{1}{e^2}\left[1 - \frac{(1-e^2)}{2e} \ln\left(\frac{1+e}{1-e}\right)\right],$$

which reduces, in the limit of a long thin spheroid, to

$$\zeta_{\perp} \rightarrow 1 - \left(\frac{a}{b}\right)^2 \ln\left(\frac{2b}{a}\right).$$

In this limit we obtain $L_{\perp} \rightarrow 1$.

Ahuja calculates the shape factors K, again making use of the results of others.[9] With the abbreviation $h = \frac{b}{a}$, the shape factor for motion parallel to the axis is

$$K_{\parallel} = \frac{8}{3} \left\{ - \frac{2h}{h^2 - 1} + \frac{2h^2 - 1}{\left(h^2 - 1\right)^{3/2}} \ln \left[\frac{h + \left[h^2 - 1\right]^{1/2}}{h - \left(h^2 - 1\right)^{1/2}}\right] \right\}^{-1} . \tag{2.10}$$

For a long thin needle, this reduces to

$$K_{\parallel} \approx \frac{2h}{3(\ln 2h - 0.5)}$$

For fluid motion perpendicular to the symmetry axis,

$$K_{\perp} = \frac{8}{3}\left\{\frac{h}{h^2 - 1} + \frac{2h^2 - 3}{\left[h^2 - 1\right]^{3/2}} \ln\left[h + (h^2 - 1)^{1/2}\right]\right\}^{-1}. \qquad (2.11)$$

In the limit h>>1, this becomes,

$$K_{\perp} \approx \frac{4h}{3(\ln 2h + 0.5)}.$$

In Figure 2 we illustrate the values of τ and s for a range of the parameter b/a, with the radius taken as 4 μm, which is equal to that of the fibers used in the construction of the anisotropic phantom which was described in Section 1, and the skin depth δ_T selected to correspond to 5-MHz sound in gelatin. We see that for this value of the radius and skin depth the parameters are approximately equal for propagation parallel to the fibers and that τ is approximately 1.5 times s for propagation parallel to the fibers.

Similarly, we calculated the absorption coefficients for propagation parallel to and perpendicular to the axis of a prolate spheroid as functions of the ratio b/a and of frequency. The absorption coefficients at 5 MHz for spheroids with radius, density, and concentration approximating the fibers used to construct the anisotropic phantom are shown in Figure 3, where the length of the spheroid is the independent parameter. The vertical line shows the value of the average b/a for the fibers used in the anisotropic phantom.

In Figure 4 we illustrate the absorption due to viscous relative motion of spheroids having the average length of the fibers used in the anisotropic tissue phantom as a function of frequency. We note that the absorption is maximum when the sound travels parallel to the long axis of the spheroids, or fibers, and is a minimum when the sound travels perpendicular to the fibers.

We note that the absorption for both directions of insonification is approximately linear with frequency, having a slope of 0.62 dB/(cm•MHz) for insonification parallel to the fibers, and a slope of 0.52 dB/(cm•MHz) for ultrasound travelling perpendicular to the fiber axes.

Measurement and Analysis Techniques in the Determination of the Anisotropy of Attenuation

The experiments described in this section were conducted on cylindrical specimens. We measured both the attenuation and the backscatter along scan lines of samples cut from anisotropic phantoms made of graphite fibers in gelatin. The attenuation will be described in this section, and backscatter results described in the next section.

Attenuation and backscatter were measured at several frequencies (16 frequencies from 1.5 to 9 MHz), at many points in a scan line (from 31 to 51 points at 1 mm spacing, depending on the specimen size). Scan lines were obtained at 65 angles through 360 degrees. The edges of the sample were detected in the scan line by finding the points on each side where the value exceeded 10% of the peak value. The midpoint of these two points was

taken to be the center of the object at that angle. The slope and intercept of the attenuation as a function of frequency were calculated at the center point.

Results

Figure 5 illustrates the results of these measurements. In this figure, zero degrees corresponds to propagation parallel to the dominant fiber direction. We note that the slope of attenuation is greatest along the fibers and minimum perpendicular to the fibers, as predicted by the theory and in accord with results on heart tissue previously reported from this laboratory. The ratio of maximum slope to minimum slope is approximately 2, in accord with the prediction of the theory.

1. A. S. Ahuja, "Formulation of Wave Equation for Calculating Velocity of Sound in Suspensions," Journal of the Acoustical Society of America, vol. 51, pp. 916-919, 1972.

2. A. S. Ahuja, "Wave Equation and Propagation Parameters for Sound Propagation in Suspensions," Journal of the Acoustical Society of America, vol. 44, pp. 4863-4868, 1973.

3. A. S. Ahuja, "Acoustical Properties of Blood: A Look at the Basic Assumptions," Medical Physiology, vol. 1, pp. 311-316, 1974.

4. P. S. Epstein and R. R. Carhart, "The Absorption of Sound in Suspensions and Emulsions. I. Water Fog in Air," Journal of the Acoustical Society of America, vol. 25, pp. 553-565, 1953.

5. R. J. Urick, "The Absorption of Sound in Suspensions of Irregular Particles," Journal of the Acoustical Society of America, vol. 20, pp. 283-289, 1948.

6. R. J. Urick and W. S. Ament, "The Propagation of Sound in Composite Media," Journal of the Acoustical Society of America, vol. 21, pp. 115-119, 1949.

7. E. L. Madsen, J. A. Zagzebski, R. A. Banjavic, and R. E. Jutila, "Tissue Mimicking Materials for Ultrasound Phantoms," Medical Physiology, vol. 5, pp. 391-394, 1978.

8. H. Lamb, Hydrodynamics, Dover, New York, 1945.

9. J. Happel and H. Brenner, Low Reynolds Number Hydrodynamics, Prentice-Hall, Englewood Cliffs, NJ, 1965.

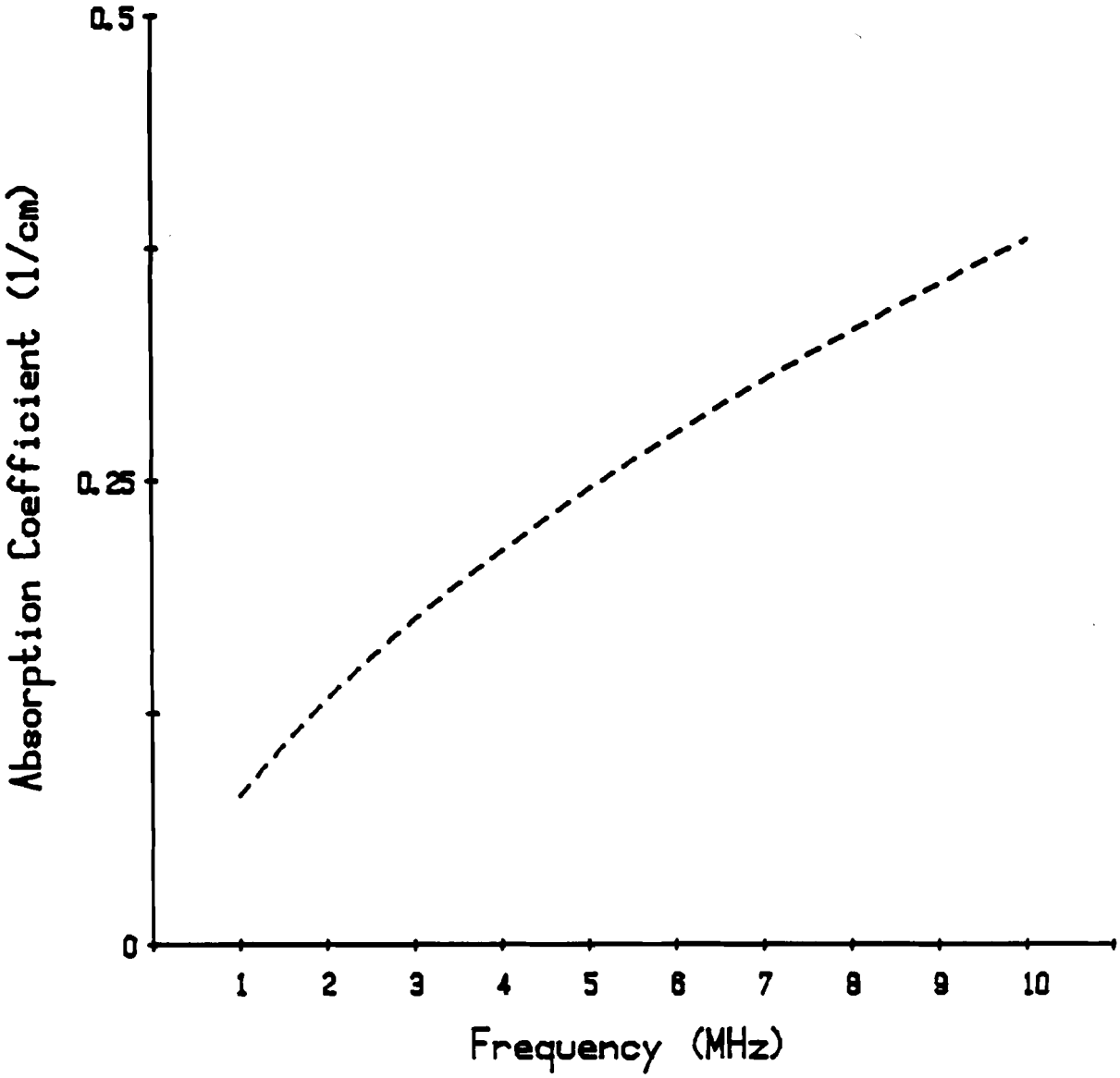

Figure 1. The theoretical viscous relative motion absorption coefficient as a function of frequency for tissue mimicking material made from graphite powder suspended in gelatin. Parameters of the material were obtained from published sources.

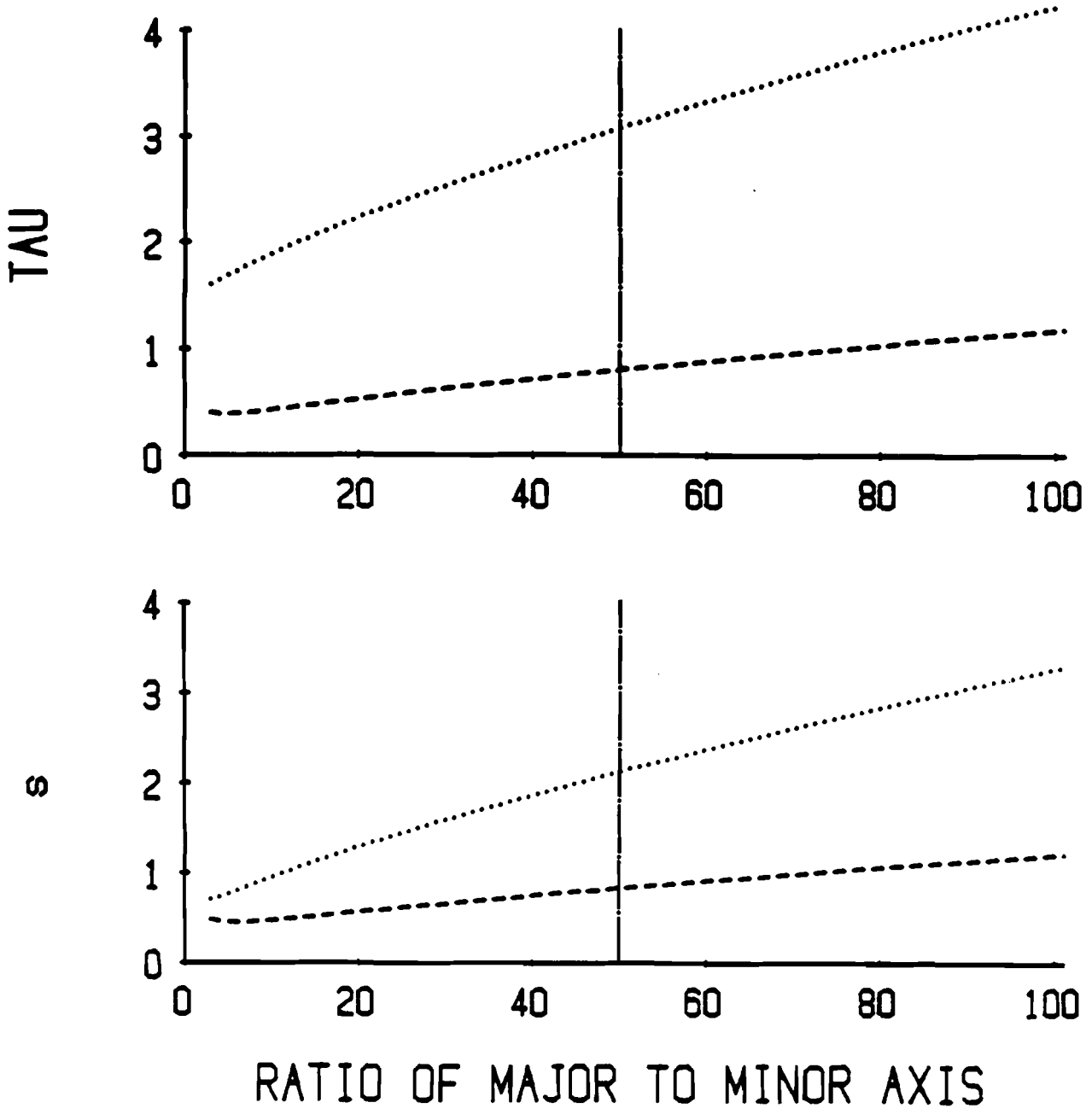

Figure 2. The factors τ and s as a function of major- to minor-axis ratio b/a for 5-MHz ultrasound in gelatin. The minor axis a was selected to be 4 μm, the same as the graphite fibers used to construct the anisotropic phantom described in Section 1. The vertical lines show the value of b/a for the average fiber length used.

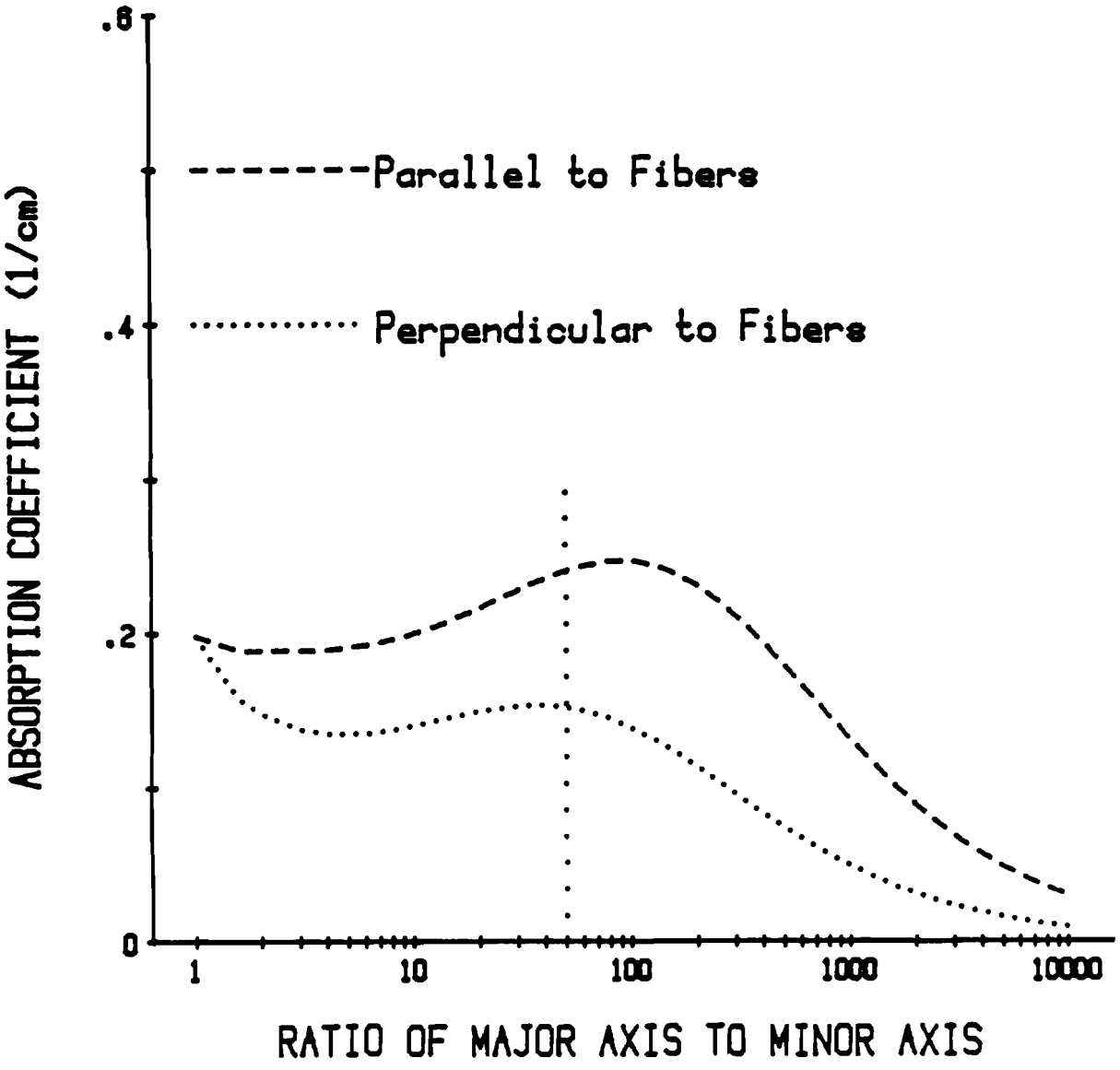

Figure 3. The theoretical absorption coefficient of 5-MHz ultrasound due to viscous motion of prolate spheroids suspended in gelatin for motion parallel and perpendicular to the axis of the spheroids. Parameters of spheroids are taken to be those of graphite fibers used to construct anisotropic tissue phantoms.

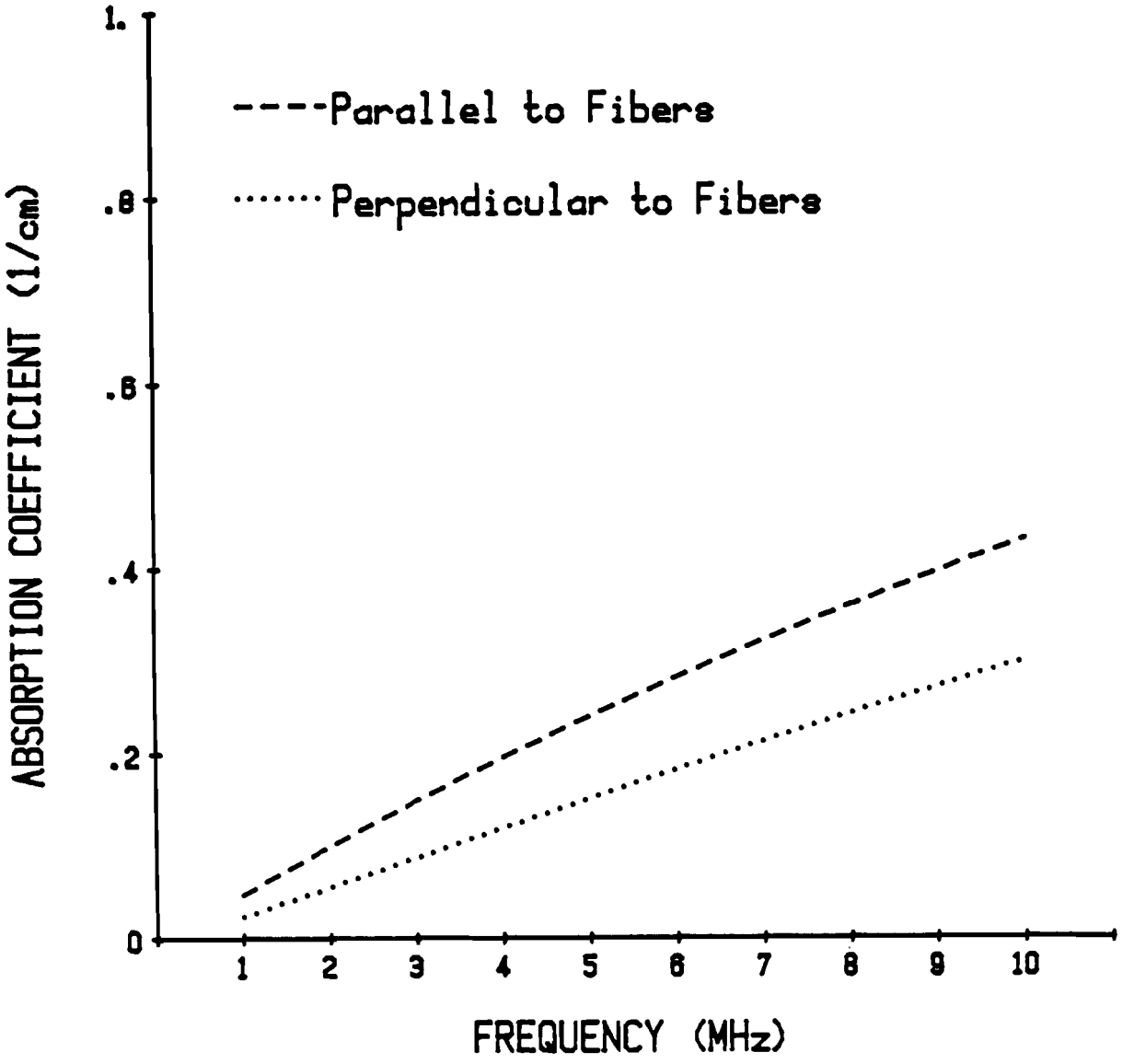

Figure 4. The absorption coefficient due to relative motion of prolate spheroids suspended in gelatin as a function of frequency, with motion either parallel to or perpendicular to the axis of the spheroids. Values were calculated using parameters appropriate to graphite fibers.

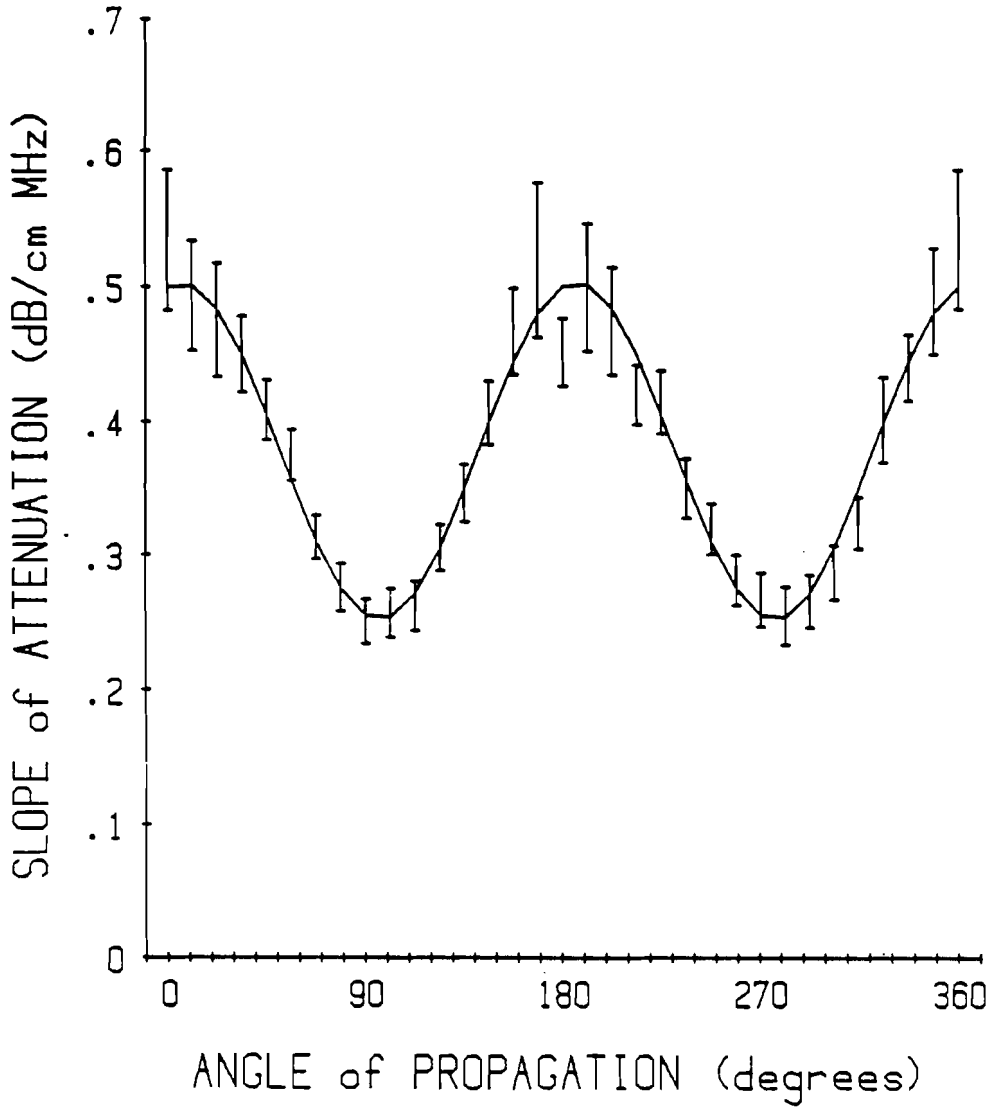

Figure 5. The slope of attenuation as a function of angle as measured in the anisotropic phantoms described elsewhere in this report.

B-3. The Backscatter Properties of the Anisotropic Tissue Phantom

Personnel: J. G. Mottley, BCL
J. G. Miller, BCL
R. M. Glueck, M.D., Medicine
J. E. Perez, M.D., Medicine
B. E. Sobel, M.D., Medicine

Support: RR 01362
HL 17646
HL 28998

The dependence of the scattering from muscle tissues on angle was first reported anecdotally by Wild and Reid in 1953[1] but the subject has not received much attention in the literature since then. As in the case of attenuation anisotropy, dependence of the scattering properties on the angle of insonification can profoundly affect the interpretation of information contained in quantitative images. In this section we will present a method for predicting the angular dependence of the scattering from cylinders, a representation of the fibers used to construct the anisotropic phantom and of muscle fibers, and then present the results of experiments designed to measure the extent of anisotropy in the backscatter from those phantoms (PR 18, B-5).

The Theory of Scattering Due to Non-symmetric Inhomogeneities

We examine the scattering properties of collections of inhomogeneities that are non-symmetric, e.g., cylindrical or spheroidal particles, which are relatively well aligned, i.e., the axes of the cylinders or spheroids are oriented in approximately the same direction. This configuration does not appear to have received much attention in the ultrasonic tissue characterization literature. The technique called the "Time Domain Born Approximation" of Rose and Richardson[2] described below can be applied to the problem in a straightforward manner.

Scattering From Arbitrarily-Shaped Inhomogeneities Using the Born Approximation

In the calculation of scattering due to inhomogeneities, one can make the approximation that the properties of the particle do not differ greatly from those of the surrounding medium and then substitute the form of the incident pressure into the differential equations which govern the total pressure. This is referred to as the Born approximation, and has been applied to the estimation of the time-domain scattering response of single particles by Rose and Richardson.[2] In this technique, the authors calculated the time domain impulse response of a particle of arbitrary shape. In the limit of an observation point at a large distance from the object and for plane-wave insonification, the impulse response is related to the cross-section of the object in a plane perpendicular to the bisector of the scattering angle, as the plane is swept through the object in the direction of the incident wave. In symbols, the displacement response at a long distance, $U_s(r,t')$ is given by

$$U_s(r,t') \to \frac{\hat{o}}{r}\, g(\hat{i},\hat{o}) \frac{1}{c^2} \frac{d^2}{dt^2} \iiint d^3r \gamma(r) \delta(t' - \frac{r}{c} - \frac{\hat{i} - \hat{o}}{c} \cdot r), \qquad (3.1)$$

where, $\hat{i}$ denotes the unit vector in the incident direction, and $\hat{o}$ is the unit vector in the scattered direction. The characteristic function $\gamma(r)$ is 1 inside the object and 0 outside and therefore delineates the object. The function g depends on the scattering angle,

$$g(\hat{i}\cdot\hat{o}) = \frac{1}{4\pi} \left[\frac{\delta p}{p}\, \hat{i}\cdot\hat{o} - \frac{\delta\lambda + 2\delta G(\hat{i}\cdot\hat{o})^2}{\lambda + 2G} \right], \qquad (3.2)$$

and t' is the time at which the signal is measured.

Setting $t = t' - \frac{r}{c}$, we can write the impulse response as

$$R(t,\hat{i},\hat{o}) = \hat{o}\, \frac{r U_s(r,t)}{u_o}$$

$$R(t,\hat{i},\hat{o}) = g(\hat{i},\hat{o})\hat{o}\, \frac{1}{c^2} \frac{d^2}{dt^2} \iiint d^3r \gamma(r) \delta\left[t - \frac{(\hat{i} - \hat{o})\cdot r}{c} \right]. \qquad (3.3)$$

Here we have normalized by the incident pulse amplitude u_0 and for the distance r. The quantity R therefore does not depend on the incident pulse amplitude nor on the distance at which the measurement is performed. R corresponds to the time domain signal which would be received by a transducer in the direction of o due to an incident impulse displacement from the direction i.

We recast these formulas to be more explicit functions of the scattering angle θ by writing the projection of the incident and outgoing directions as

$$\hat{i}\cdot\hat{o} = -\cos\theta.$$

The angular function $g(\theta)$ becomes

$$g(\theta) = -\frac{1}{4\pi} \left[\frac{\delta\rho}{\rho} \cos\theta - \frac{\delta\lambda + 2\delta G\cos^2\theta}{\lambda + 2G} \right], \qquad (3.4)$$

from which we obtain,

$$R(t,\theta) = -\hat{o}\, \frac{1}{4\pi} \left[\frac{\delta\rho}{\rho} \cos\theta + \frac{\delta\lambda + 2\delta G\cos^2\theta}{\lambda + 2G} \right] \frac{1}{c^2} \frac{d^2 A(t,\theta)}{dt^2}, \qquad (3.5)$$

where we have introduced

$$A(t,\theta) = \iiint d^3r\gamma(r)\delta\left(t - \frac{(\hat{i} - \hat{o})\cdot r}{c}\right).$$

This integral has an intuitive meaning. The signals selected by the impulse function

$$(\hat{i} - \hat{o})\cdot r = ct$$

defines a plane in which the time of flight between the transmission and reception of the pulse is a constant. In the plane-wave limit, and for the Born approximation in which the velocity of the wave inside the object is the same as outside, this defines a plane at angle $\frac{\theta}{2}$ with the incident direction. The remaining two integrations over the characteristic function calculate the cross-sectional area of the object in this plane. This area is a function of time as the selected plane sweeps through the object in the direction of the incident sound. The second time derivative of this area leads to scattering which responds to changes in the cross-section, and most strongly to those shapes in which there are discontinuities in the cross-section which are impulsive in the second derivative.

The time-domain impulse response function $R(t,\theta)$ is the Fourier transform in the k-domain of the angular function in the frequency domain $f(\omega,\theta)$. Since only the time derivative of the cross-section contains any time dependence, the transform operates only on this term, and we may write,

$$f(\omega,\theta) = g(\theta)\,\frac{1}{c}\,\text{F.T.}\left[\frac{d^2}{dt^2}\,A(t,\theta)\right], \tag{3.6}$$

where F.T.[Q(t)] denotes the Fourier transform of a time domain function Q. From the well-known properties of the Fourier transform of derivatives, we obtain

$$f(\omega,\theta) = g(\theta)\,\frac{1}{c}\,(-\omega^2)\,\text{F.T.}\left[A(t,\theta)\right]. \tag{3.7}$$

As an example, consider the sphere shown in Figure 1. To calculate the backscattering from this sphere (i.e., $\theta = 180°$), let us write the area A of the sphere when cut by the plane at an angle of 90° with respect to the incident direction as a function of time, where the time origin is defined to be when the point of intersection of the plane and the incident direction passes through the center of the sphere,

$$A = \begin{cases} \pi\{a^2 - c^2t^2\} & |ct| \le a \\ 0 & |ct| > a \end{cases} \tag{3.8}$$

Substituting this into Eq. 3.27, performing the Fourier transform, taking the magnitude squared, and performing the limit ka→0, we obtain the differential backscattering cross-section for ka<<1,

$$|f(\omega,180°)|^2 = \left[\frac{\delta\lambda+2\delta G}{\lambda+2G} + \frac{1}{4\pi}\frac{\delta\rho}{\rho}\right]^2 \frac{16\pi}{9} a^2(ka)^4. \qquad (3.9)$$

For a fluid suspending medium, G=0. Substituting the relationship for the Lame' constant in terms of the bulk and shear moduli,

$$\lambda = B - \frac{2}{3}G,$$

and that the compressibility is the reciprocal of the bulk modulus, we derive

$$\frac{\delta\lambda+2\delta G}{\lambda+2G} = -\frac{\delta\kappa}{\kappa_p} + \frac{4}{3}\kappa G p.$$

In the Born approximation $\kappa_p \chi\kappa$, and $G_p \chi G$. For a fluid medium this becomes

$$\frac{\delta\lambda+2\delta G}{\lambda+2G} \quad -\frac{\delta\kappa}{\kappa}$$

and we can write

$$|f(\omega,180°)|^2 \quad \left[\frac{\delta\kappa}{\kappa} - \frac{\delta\rho}{\rho}\right]^2 \frac{16\pi}{9} a^2(ka)^4.$$

For an object which is not totally symmetric, this expression must be written to include a dependence on the orientation of the object with respect to the "plane of measurement," the plane containing the incident and outgoing unit vectors. For example, we could define "object angles" ϕ and ψ, such that ϕ is the angle between an axis of symmetry of the object and the plane of measurement and ψ is the angle in the measurement plane between the incident unit vector and the projection of the object's axis into that plane. In the case of backscattering, the scattering angle is taken to be fixed at $\theta = 180°$, and the plane of measurement reduces to a line. The angle ψ is then indeterminate, and the only necessary angle is the angle ϕ.

We consider the backscattering from a cylindrical object. The previous equation can now be written in the form

$$f(\omega,180°,\phi) = g(180°)\frac{1}{c^2}(-4\pi^2\omega^2)\text{F.T.}\left[A(t,\theta)\right] \qquad (3.10)$$

where $A(t,\phi)$ is the cross-sectional area of the cylinder as a function of time for a particular orientation of the incident sound and the axis of the cylinder. We will perform these calculations for backscatter from a cylinder of radius a and half-length b at an arbitrary angle ϕ between the axis of the cylinder and the direction to the transducer (see Figure 2).

Calculation of Cross-Sectional Area of a Cylinder in a Plane at Arbitrary Angle and Distance

Referring to Figure 1, at angle ϕ and range r, we note that there will be some range at which the plane first touches the cylinder. This will be denoted r_{max}, where

$$r_{max} = b\cos\phi + a\sin\phi. \tag{3.11}$$

The range at which the plane goes through the point at z = b, y = a is called r_1,

$$r_1 = b\cos\phi - a\sin\phi. \tag{3.12}$$

The plane will then pass through the origin, and subsequently pass through z = -b, y = a when $r = -r_1$, and then exit the cylinder when $r = -r_{max}$. We subdivide the situation into four possible cases and examine each separately, writing the area of intersection.

The first possibility is the $\phi = 0°$. Then the sound is incident along the cylinder axis and the intersection is a circle of radius a, and the area A_C is simply

$$A_C(r,\phi) = \pi a^2 \qquad |r| \le b. \tag{3.13}$$

The second (simple) case is that the angle ϕ is 90°, in which event the cross-section is a rectangle whose area is

$$A_C(r,\phi) = 4\left[a^2 - r^2\right]^{1/2} b \qquad |r| \le a. \tag{3.14}$$

The third case is that in which, due to the angle ϕ, $r_1 \ge 0$. In this case, as the plane sweeps through the cylinder the area of intersection will first be a truncated ellipse for $r_1 \le r < r_{max}$, then the area changes to an ellipse for $|r| \le r_1|$, and then the shape reverts to a truncated ellipse between $-r_{max} < r \le -r_1$. Making the substitution

$$\frac{b\cos\phi - r}{a\sin\phi} = Q(r), \tag{3.15}$$

the area is then

$$A_C(r,\phi)=\frac{a^2}{\cos\phi}\begin{cases}\left[Q(r)\left[1-Q(r)^2\right]^{1/2}+\sin^{-1}Q(r)+\frac{\pi}{2}\right] & r_1\le r\le r_{max}\\ \pi & |r|<|r_1|\\ \left[Q(-r)\left[1-Q(-r)^2\right]^{1/2}+\sin^{-1}Q(-r)+\frac{\pi}{2}\right] & -r_{max}\le r\le -r_1\end{cases} \quad (3.16)$$

The fourth case is that in which, due to the choice of angle ϕ the quantity $r_1 < 0$. For this case, the area of intersection is an ellipse truncated at one end for $|r_1|\le|r|\le|r_{max}|$. For the range in the interval $|r|\le|r_1|$, the area is an ellipse which is truncated at both ends. The area is given by,

$$A_C(r,\phi)=\frac{a^2}{\cos\phi}\begin{cases}Q(r)\left[1-Q(r)^2\right]^{1/2}+\sin^{-1}Q(r)+\frac{\pi}{2} & -r_1\le r\le r_{max}\\ Q(r)\left[1-Q(r)^2\right]^{1/2}+\sin^{-1}Q(r)\\ \quad +Q(-r)\left[1-Q(-r)^2\right]^{1/2}+\sin^{-1}Q(-r) & r_1<r<-r_1\\ Q(-r)+\left[1-Q(-r)+\right]^{1/2}+\sin^{-1}Q(-r)+\frac{\pi}{2} & -r_{max}\le r\le r_1\end{cases} \quad (3.17)$$

These functions of time for selected angles ϕ are plotted in Figure 3. For this Figure the ratio of length to diameter was chosen to be 50, the same as for the fibers used in constructing the anisotropic phantoms. The area is normalized to the maximum possible area (4ab) for the purposes of plotting.

Calculation of Backscatter Properties of a Cylinder at Arbitrary Angle as a Function of Frequency

The Fourier transform of the cross-sectional area as a function of time may be performed easily in the first two cases (ϕ=0° and 180°). The other cases are far more complex, but have been accomplished numerically. In the case of sound incident parallel to the axis of the cylinder, the backscatter differential cross-section becomes

$$|f(\omega,180°,0°)|^2 = 256\pi^6\,\frac{(ka)^4}{\omega^2}\sin^2\left[\frac{b\omega}{c}\right]\left[g(180°)\right]^2, \quad (3.18)$$

where,

$$g(180°) = \frac{1}{4\pi}\,\frac{\delta\rho}{\rho} - \frac{\delta\lambda+2\delta G}{\lambda+2G}\,.$$

From this expression, the scattering end-on to a cylinder is determined from the cross-section (the $(ka)^4$ factor) and is modulated by the distance between the ends (the $\sin^2(b\omega/c)$ factor).

For the case of $\phi = 90°$, the backscatter differential cross-section is given by

$$|f(\omega,180°,90°)|^2 = 256\pi^6 \frac{(ka)^2(kb)^2}{\omega^2} J_1^2\left[\frac{a\omega}{c}\right]\left[g(180°)\right]^2. \qquad (3.19)$$

Here we see that the backscattering strength is proportional to the length squared, and the modulation pattern is determined by the radius.

We performed the Fourier transforms of the cross-section vs. time plots of Figure 3 numerically, and then selected the frequency components which correspond to frequencies in our range of interest, assuming that one time-domain sample corresponded to one μm in distance, for a velocity of sound of 1500 m/sec, and taking the dimensions of the cylinder to be $a=4\mu m$ and $b=200\mu m$. The results of these calculations are illustrated in Figure 4, where the power spectral component at several frequencies is plotted as a function of the angle ϕ. Here 0° corresponds to the sound incident along the axis of the cylinder and 90° denotes sound incident perpendicular to the cylinder axis, and the frequencies are 2 MHz ($ka=3.4\times10^{-2}$), 5 MHz (8.5×10^{-2}), and 10 MHz (17×10^{-2}). The values at each frequency are normalized to the maximum at that frequency and are expressed logarithmically.

The Prediction of Backscattering Properties of a Suspension of Cylinders

A rich structure is present in these calculated backscattering properties of s single particle. If in a collection of particles the symmetry axes were perfectly aligned, the backscatter properties would scale as N, the number of scatterers in the interrogated volume. Actual suspensions of fibers have a distribution of lengths and not a single orientation, but rather a distribution of fiber orientations which are more or less tightly grouped about a single direction. (The anisotropic phantoms studied here had an average fiber length of 400μm and a distribution in angle with a standard deviation of approximately 20°.) We calculated the angular distribution of backscatter for cylinders of 5 different lengths (160, 180, 200, 220, and 240 μm) and performed a weighted average at each angle over the lengths. To accomodate the frequency-dependent volume insonified, we multiplied by the area of a typical beam. Gaussians were constructed with standard deviations of 10, 20, 30, 40, and 50° and convolved with the backscatter as a function of angle, to yield predictions of the angular dependence of the backscatter properties of the anisotropic phantoms.

The results of this process for the angular distribution with a standard deviation of 20° are shown in Figure 5. The values at each frequency were then normalized to the maximum value and plotted on a logarithmic scale.

We then calculated the equivalent of the integrated backscatter as a function of angle of insonification by averaging the relative backscatter

over frequency for each angular distribution. The results of this are illustrated in Figure 6. We see that the amplitude of change of the integrated backscatter with angle ranges from approximately 12 dB to 6 dB, and that the structure seen in Figure 3 has been blurred due to both the angular distribution of the scatterers and the averaging over frequency.

Experiments to Measure the Anisotropy of the Backscatter from Tissue Phantoms

The experiments described in this section were designed to detect the presence of and to determine the angular dependence of anisotropy in the backscatter properties of tissue-mimicking phantoms. We measured both the attenuation and the backscatter of samples cut from anisotropic phantoms made of graphite fibers in gelatin. The results of the attenuation measurements are reported in Section 2 of this report.

Experimental Design

Both the attenuation and the backscatter were measured along scan lines of samples cut from anisotropic phantoms made of graphite fibers in gelatin. Only the backscatter at the center of the sample will be reported.

Attenuation and backscatter were measured at several frequencies (16 frequencies from 1.5 to 9 MHz) at many points in a scan line (from 31 to 51 points at 1 mm spacing, depending on the specimen size). Scan lines were obtained at 65 angles through 360 degrees. The edges of the sample were detected in the scan line by finding the points on each side where the value exceeded 10% of the peak value. The midpoint of these two points was taken to be the center of the object at that angle. The slope and intercept of the attenuation as a function of frequency were calculated at the center point.

The apparent backscatter as a function of frequency, or apparent backscatter transfer function, was computed at the center and at the points on the scan line on each side of center, and these transfer functions were averaged. The average apparent backscatter transfer functions were compensated for the attenuation of the intervening tissue and the tissue within the gate. Then the integrated backscatter was calculated at each angle.

Results

The results of measurements of backscatter from the anisotropic tissue phantom are shown in Figure 7, along with a fit to a cosine form. We note that the amplitude of variation with the angle of insonification is approximately 7 dB, very similar to the predicted angular variation of Figure 5.

1. J. J. Wild and J. M. Reid, "The Effects of Biological Tissues on 15-mc Pulsed Ultrasound," Journal of the Acoustical Society of America, vol. 25, pp. 270-280, 1953.

2. J. H. Rose and J. M. Richardson, "Time Domain Born Approximation," Journal of Nondestructive Evaluation, vol. 3, pp. 45-53, 1982.

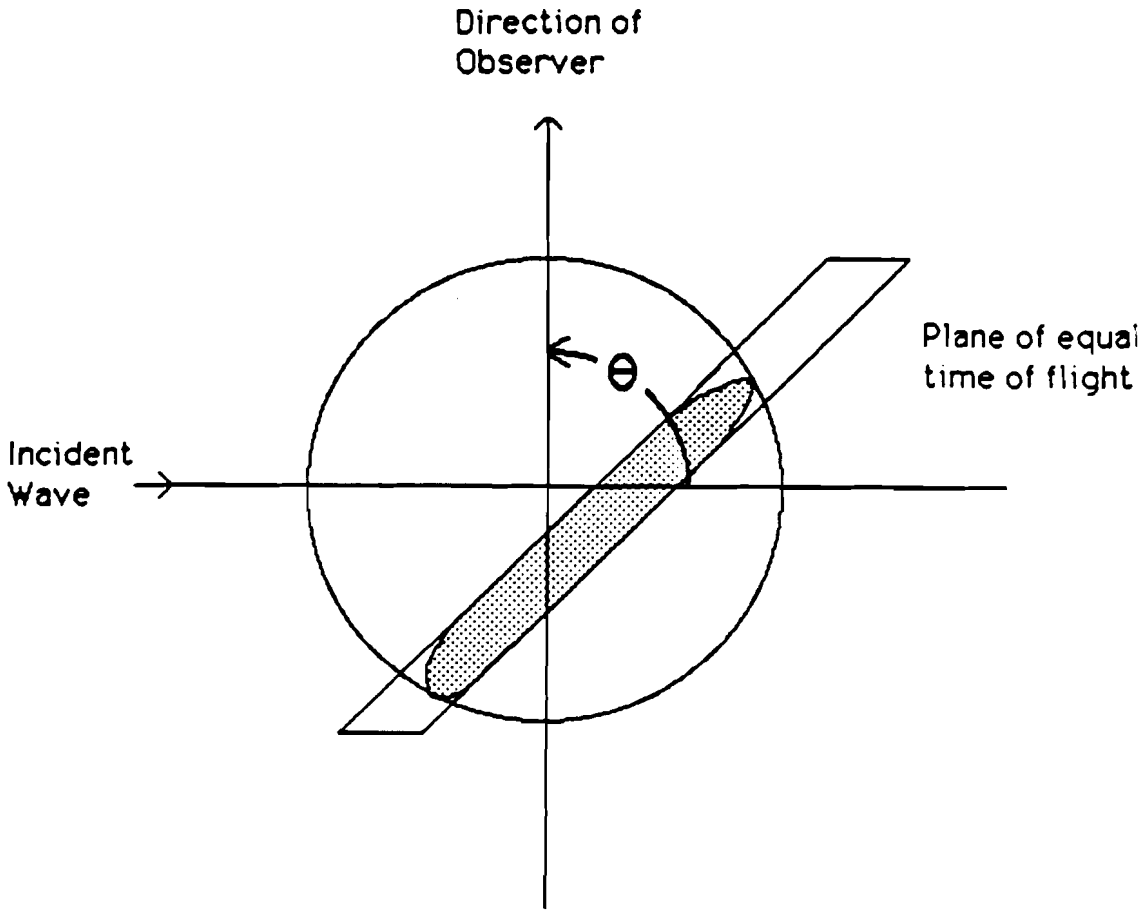

Figure 1. A sphere of radius a and the plane of constant-time-of-flight which defines the contributions to the scattering at time t.

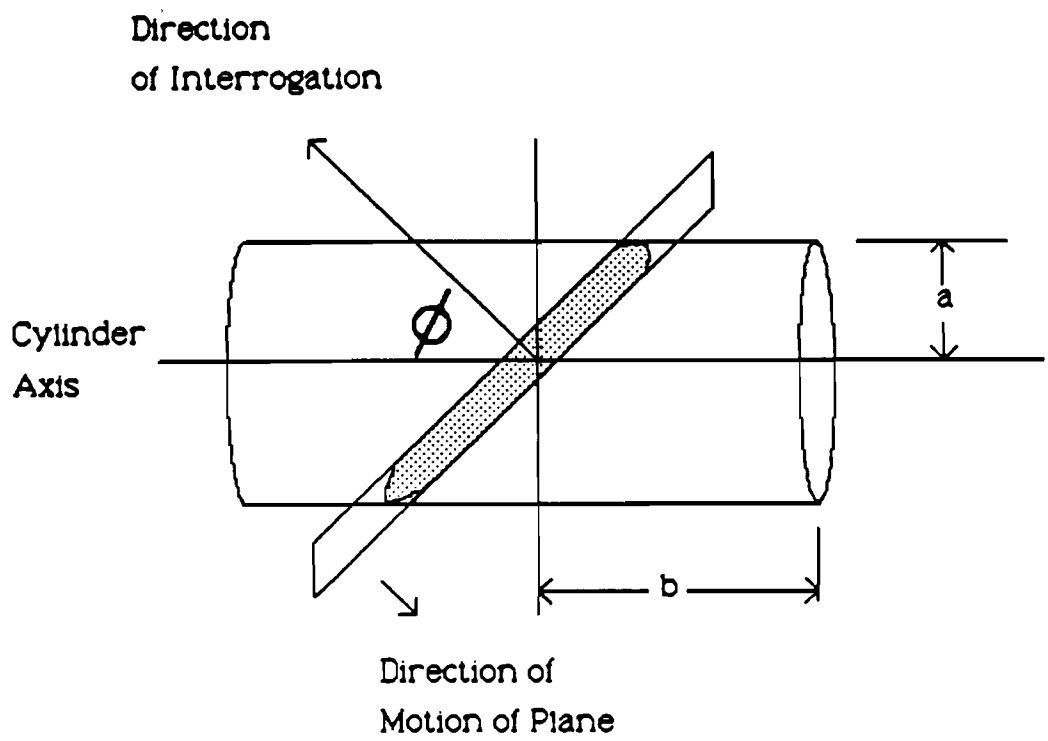

Figure 2. Schematic illustration of the geometry used for the calculation of backscattering from a cylinder of radius a and half-length b using the time-domain Born approximation.

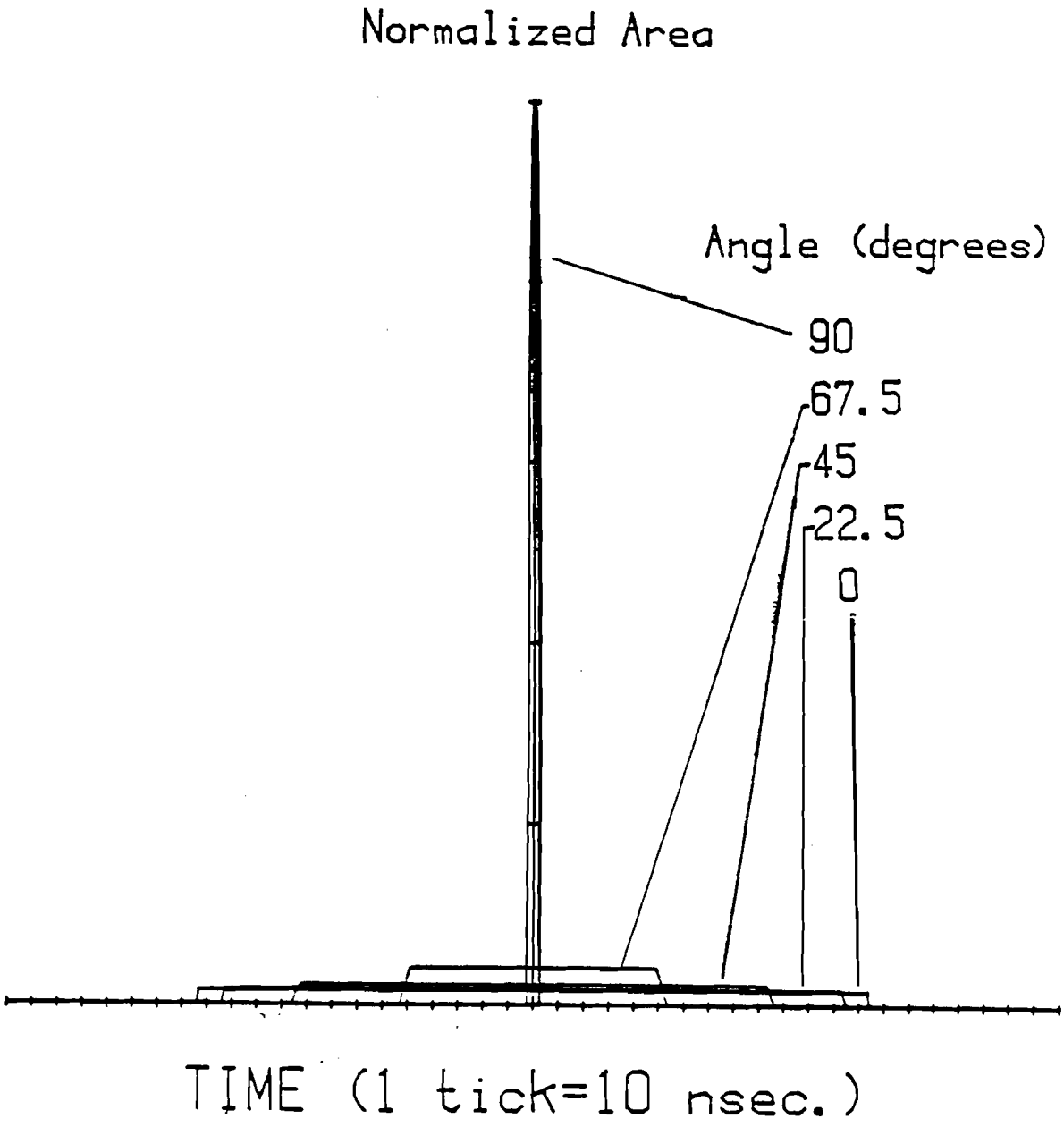

Figure 3. The area of intersection of a plane at angle ϕ with a cylinder having a length to radius ratio of 50. The area is plotted as a function of time for angles ϕ=0, 22.5, 45, 67.5, and 90 degrees.

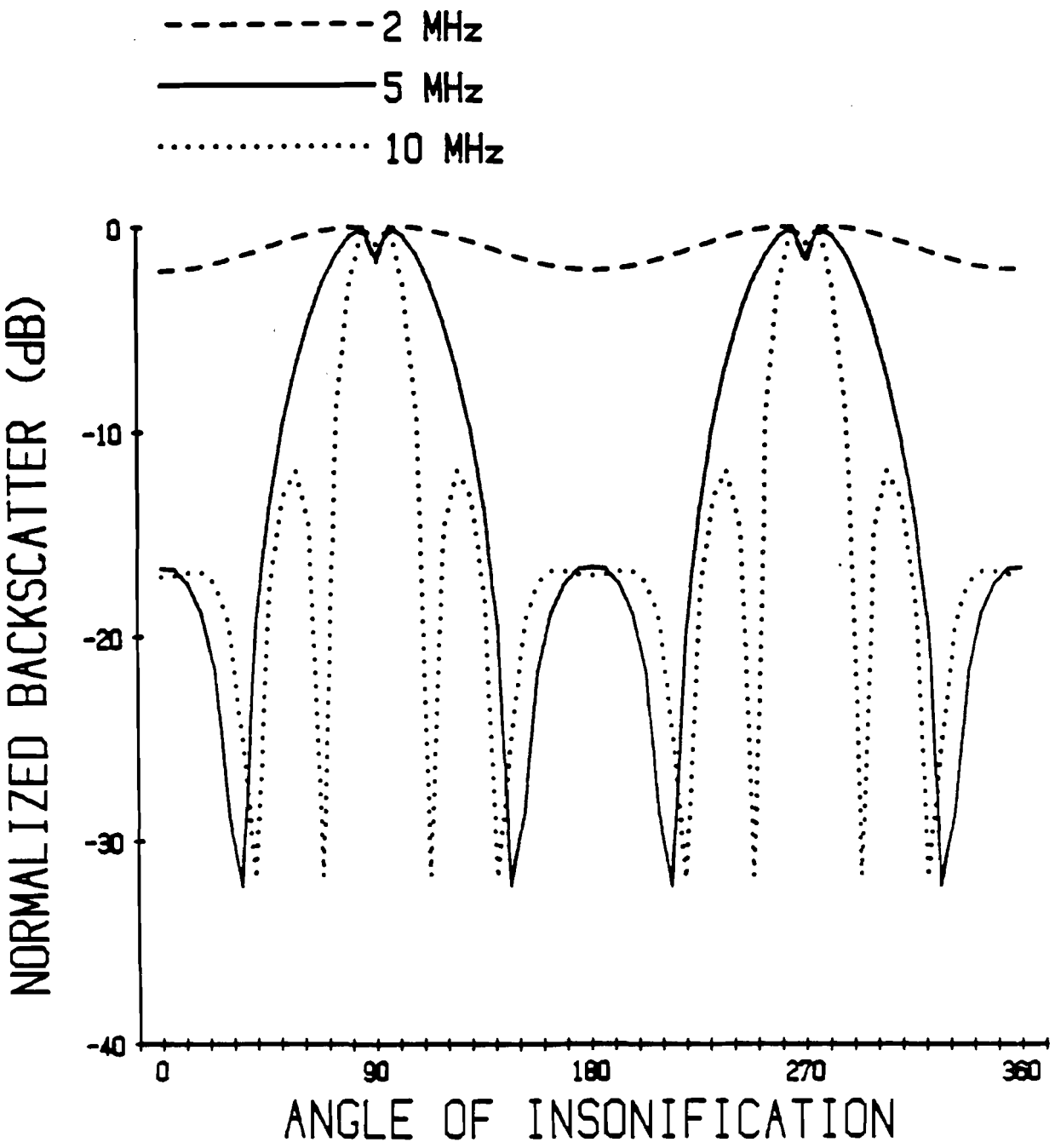

Figure 4. The normalized backscatter from a cylinder as a function of angle relative to the cylinder axis at three frequencies. Cylinder dimensions were a=4 μm, b=200 μm, and the frequencies were approximately 2, 5, and 10 MHz.

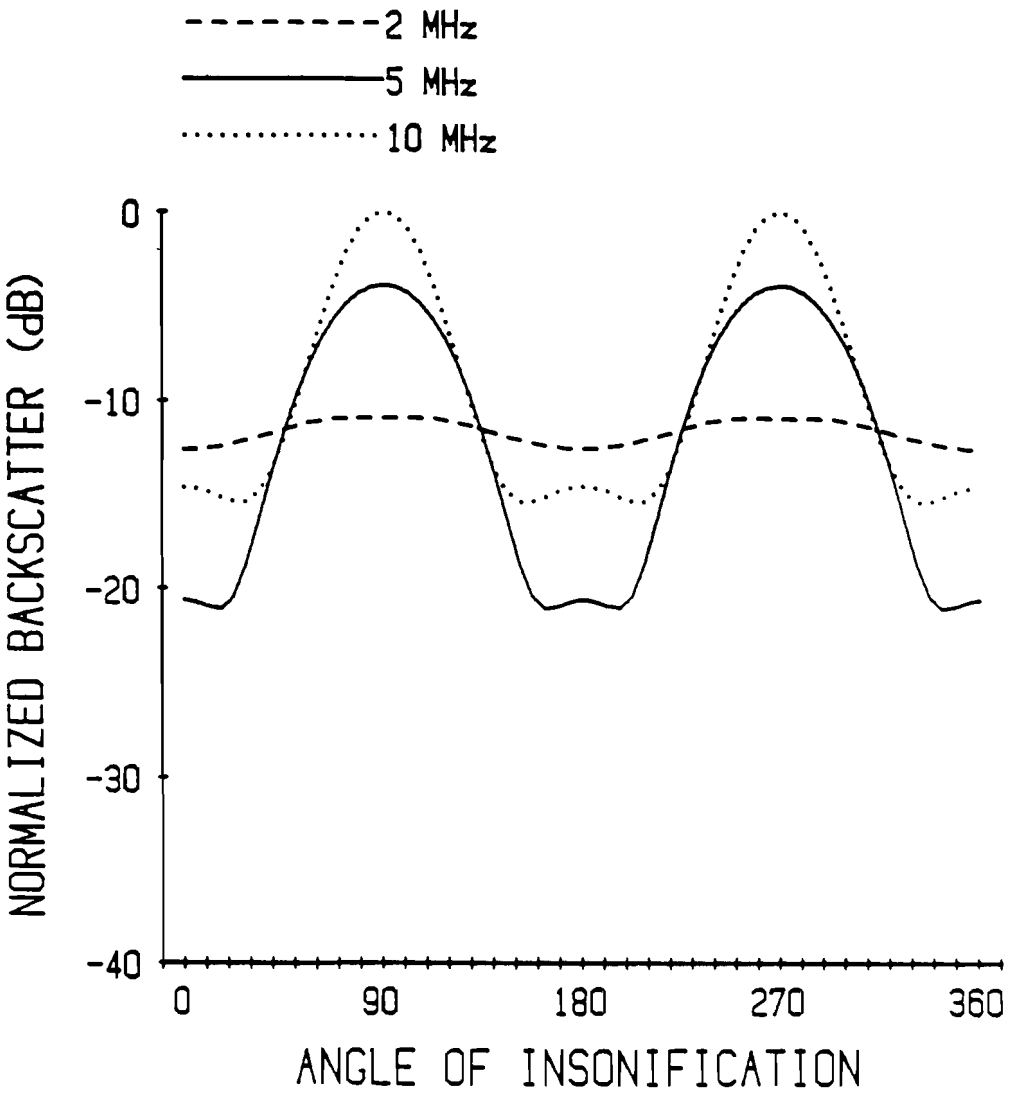

Figure 5. The backscatter from a suspension of cylinders as a function of angle relative to the dominant fiber orientation at frequencies of 2, 5, and 10 MHz. Suspension properties are described in text.

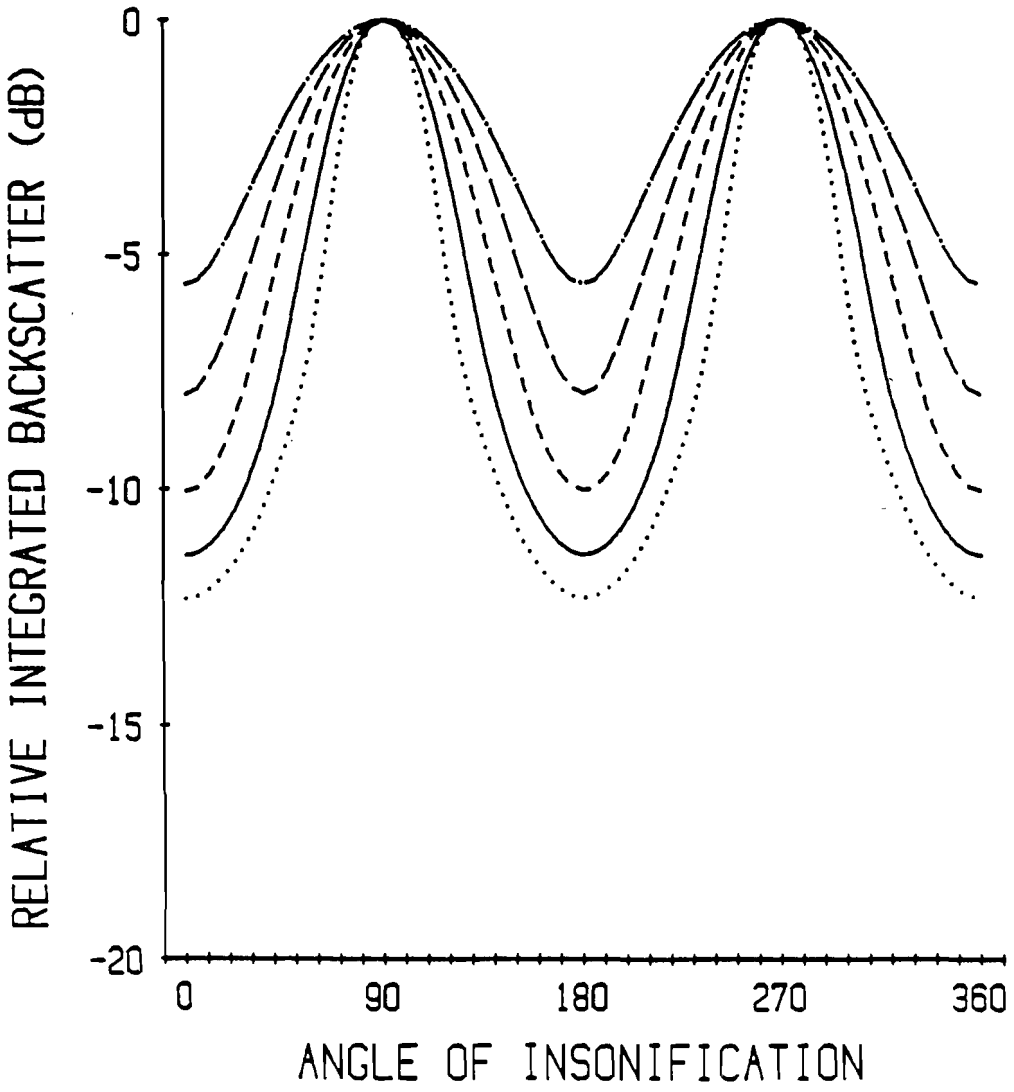

Figure 6. The theoretical relative integrated backscatter of a graphite-fiber-in-gelatin tissue phantom as a function of angle for values of the width of the distribution of fibers in angle of 10°, 20°, 30°, 40°, and 50°.

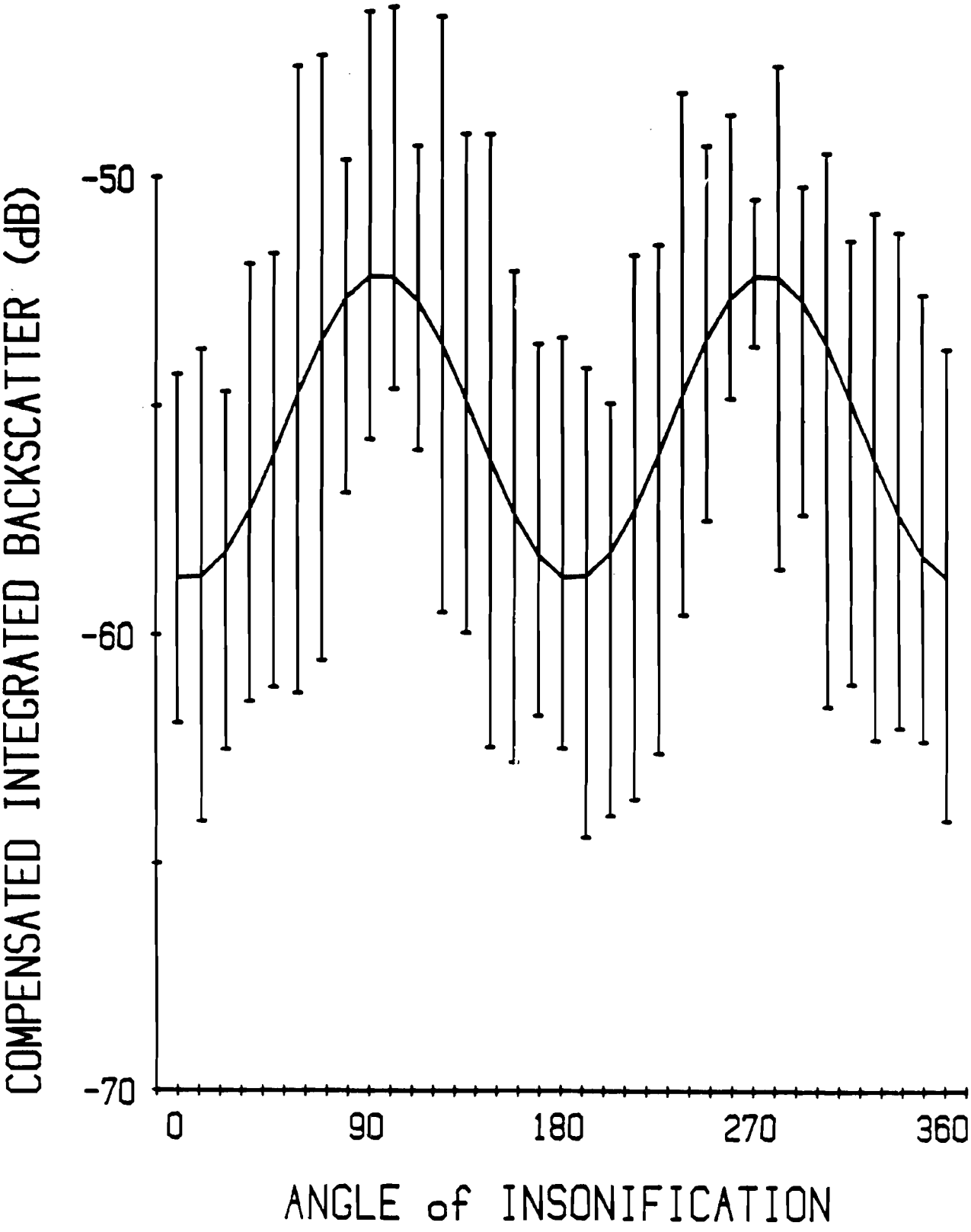

Figure 7. The measured integrated backscatter as a function of angle of insonification from a graphite-fiber-in-gelatin phantom.

B-4. Anisotropy of the Backscatter of Canine Skeletal Muscle and Heart Tissue

Personnel: J. G. Mottley, BCL
R. M. Glueck, M.D., Medicine
J. G. Miller, BCL
J. E. Perez, M.D., Medicine
B. E. Sobel, M.D., Medicine

Support: RR 01362
HL 17646
HL 28998

The experiments described in this section were designed to detect the presence of and to determine the angular dependence of anisotropy in the backscatter properties of tissues. Both the attenuation and the backscatter were measured along scan lines of samples cut from canine myocardium and from canine skeletal muscle, using the techniques described in B-3. The compensated integrated backscatter is reported here.

Results

The results of backscatter measurements on canine myocardium are shown in Figure 1. Here we see an angular variation of approximately 8 dB in the integrated backscatter.

The results of backscatter measurements on canine skeletal muscle are shown in Figure 2. For the oriented fibers of skeletal muscle, the angular variation of the integrated backscatter is approximately 2.5 dB.

Discussion

The backscatter properties of canine myocardium and skeletal muscle vary with the angle of interrogation, measured relative to the local dominant fiber orientation. In addition, suspensions of small fibers have been constructed which exhibit similar angular variations, and the angular variations of these suspensions can be accurately predicted.

These variations of scattering properties can have profound effects on efforts to measure the ultrasonic parameters of tissue in vivo and on the interpretation of ultrasonic images of soft tissue structures. For example, efforts to measure the attenuation coefficient of soft tissues using backscattered signals depend on the scattering process remaining constant with depth. If the region under examination crosses from an area with one fiber orientation into an area with a different fiber orientation, incorrect values of the attenuation will be inferred.

Conversely, the existence of such anisotropy of the backscatter from oriented tissues may provide an index to the degree of organization of the tissue, and could find applicability in diagnosis or serial monitoring of degenerative diseases which destroy the fibrillar structure of the tissue.

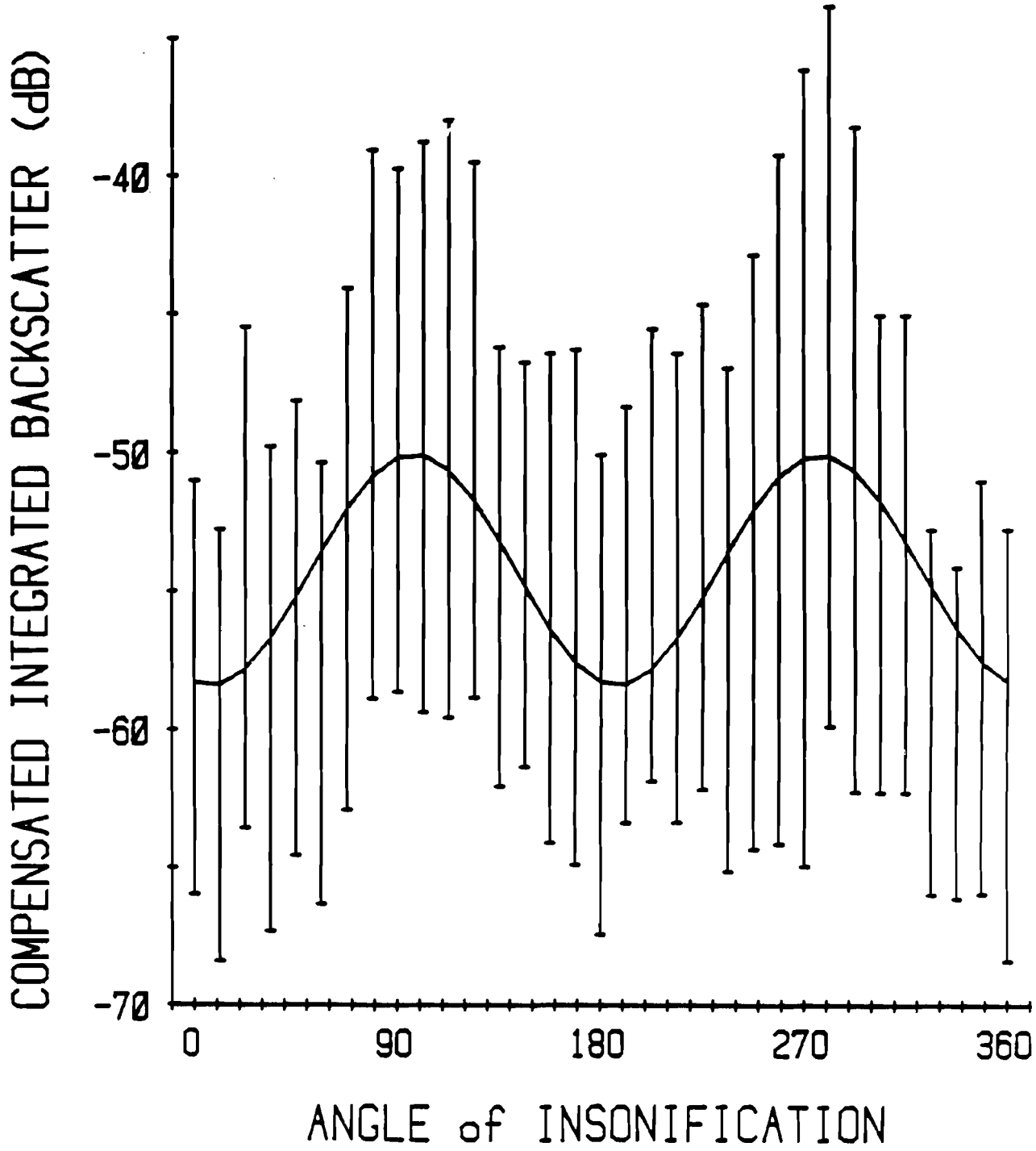

Figure 1. The measured integrated backscatter as a function of angle of insonification from canine myocardium.

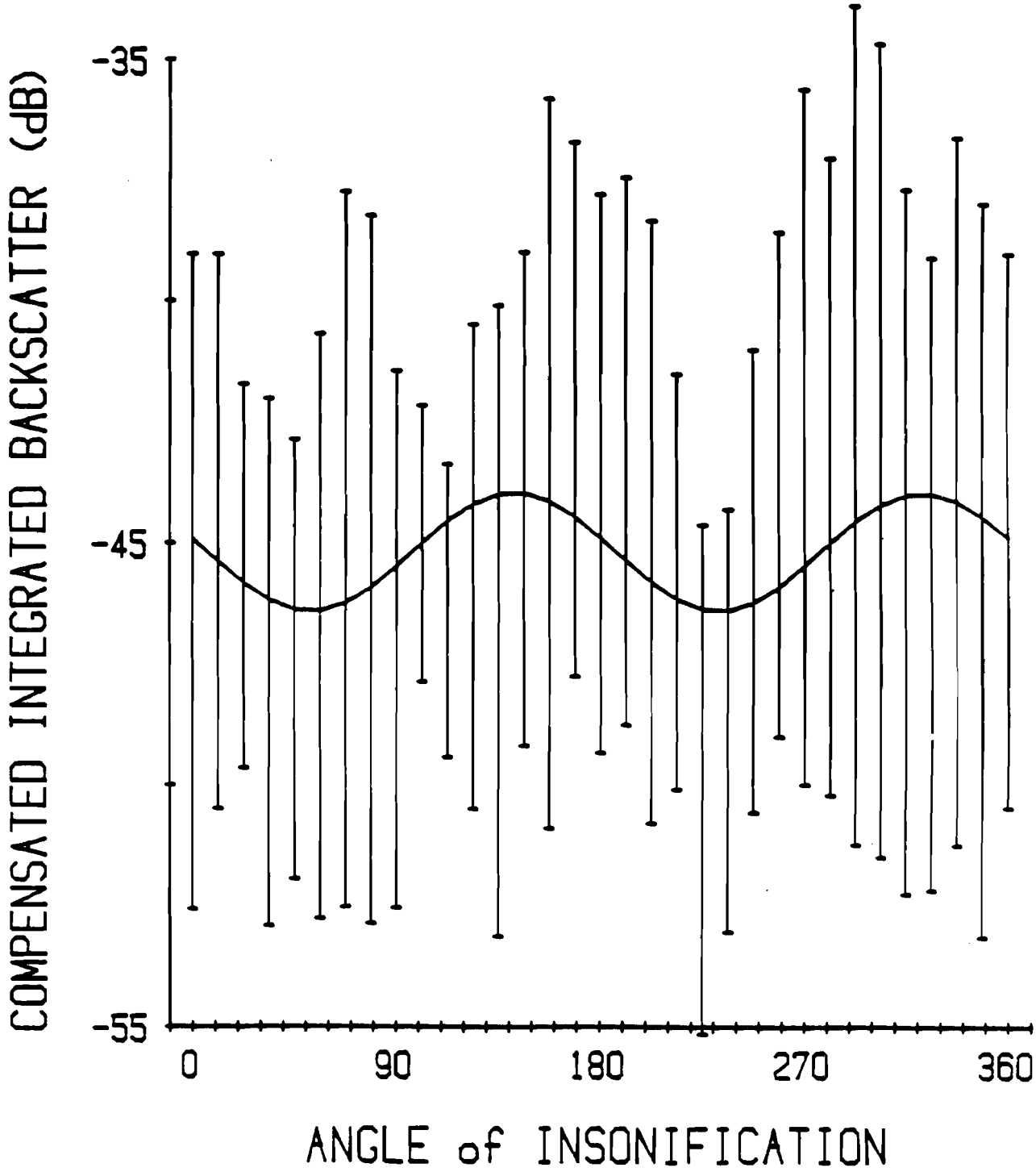

Figure 2. The measured integrated backscatter as a function of angle of insonification from canine skeletal muscle.

B-5. Formalism for Two-Dimensional Spatial Moments

Personnel: P. H. Johnson, BCL
J. G. Miller, BCL

Support: RR 01362
HL 17646
HL 28998

We have been considering applications of the two-dimensional spatial moments of measured distributions of energy in ultrasonic beams (PR 20, B-4). In this section we summarize the formalism we have adopted for the several types of moments used.

The general two-dimensional spatial moments of a function $f(\vec{r})$ is defined as

$$m_{pq} = \int_A x^p \, y^q \, f(\vec{r}) dx \, dy \tag{5.1}$$

where A is the area of the receiving aperture. We say that the general 2-dimensional moment m_{pq} is of order $n = p + q$.

One special class of two-dimensional moments is the radial moments. The nth order radial moment M_n is defined as the integral of the function $f(\vec{r})$ over the aperture A weighted by the nth power of the radius vector $\vec{r}$

$$M_n = \int_A \vec{r}^n \, f(\vec{r}) dx \, dy. \tag{5.2}$$

The notation $\vec{r}^n$ expands as

$$\vec{r}^n = \begin{cases} 1 & , n=0 \\ \vec{r} & , n=1 \\ \vec{r}\cdot\vec{r} & , n=2 \\ (\vec{r}\cdot\vec{r})\vec{r} & , n=3 \\ (\vec{r}\cdot\vec{r})^2 & , n=4 \\ \ldots & . \ldots \end{cases} \tag{5.3}$$

Examination of the weighting factor $\vec{r}^n$ reveals that the even-order radial moments are scalars and the odd-order radial moments are vectors.

An appealing property of the lower-order radial moments is that they yield to physical interpretation. The scalar zeroth-order radial moment is the definite integral of $f(\vec{r})$ over the aperture A, the "total energy" or "total mass," the most global characteristic of $f(\vec{r})$. The vector

first-order moment of $f(\vec{r})$ is related to the "centroid" or "center of gravity," a global property specifying the center of concentration of the function $f(\vec{r})$. The scalar second-order radial moment represents the spread of $f(\vec{r})$ about the origin of coordinates, or the "moment of inertia." Third- and fourth-order radial moments are related to the "skewness" and "kurtosis" of the function, respectively. These interpretations provide much of the motivation for the use of radial moments in this work to characterize the distribution of ultrasonic energy.

The radial moments are defined relative to the origin of the particular coordinate system in use. Alternatively, the weighting factor of radial moments may be defined relative to any other point in space. If the point of reference is chosen to lie at the centroid of the function $f(\vec{r})$ defined as

$$\vec{C} = \frac{\vec{M}_1}{M_0} , \tag{5.4}$$

then the moments are referred to as radial central moments of $f(\vec{r})$. These are denoted as U_n and are given by

$$U_n = \int_A \left[\vec{r} - \vec{C}\right]^n f(\vec{r}) dx\ dy. \tag{5.5}$$

In addition, general central moments in a form analogous to Equation (5.1) may be defined as

$$\mu_{pq} = \int_A (x-C_x)^p (y-C_y)^q f(\vec{r}) dx\ dy. \tag{5.6}$$

A summary of the notation for the various types of moments defined above is presented in Table 1.

The different types of moments are interrelated by relatively simple expressions. An important set of relationships is the equality of all the moments of order zero

$$m_{00} = M_0 = U_0 = \mu_{00} = \int_A f(\vec{r}) dx\ dy. \tag{5.7}$$

Based on these equalities we use the several notations interchangeably, but in appropriate context. Another set of equalities exists in the case of one dimension, where the general moments become identical to the corresponding radial moments, i.e.

$$\left.\begin{aligned} m_n &= M_n \\ \mu_n &= U_n \end{aligned}\right\} \quad \text{in one dimension.} \tag{5.8}$$

The relationships between the first order moments are contained in the definition of the centroid

$$\vec{M}_1 = \left[m_{10}, m_{01}\right] = M_0 \vec{C} \tag{5.9}$$

$$\vec{U}_1 = \left[\mu_{10}, \mu_{01}\right] = 0. \tag{5.10}$$

Equation (5.9) defines the position of the centroid of $f(\vec{r})$ relative to an arbitrary origin of coordinates on A. Because the central moments are by definition calculated about the centroid, the first-order central moments are all equal to zero.

The second-order moments are related to each other and to lower-order moments by

$$\begin{aligned} \mu_{11} &= m_{11} - m_{00} C_x C_y \\ \mu_{20} &= m_{20} - m_{00} C_x^2 \\ \mu_{02} &= m_{02} - m_{00} C_y^2 \\ U_2 &= \mu_{20} + \mu_{02} \\ M_2 &= m_{20} + m_{02}. \end{aligned} \tag{5.11}$$

Each of the scalar radial moments and the components of the vector radial moments and each of the general central moments can be expanded in terms of the general moments given by Equation (5.1). The general moments m_{pq} are the most readily computed quantities, so we choose these as the basis set of moments. In many applications, it is frequently most useful to consider the central moments. Thus, in practice we compute the m_{pq} first, then find the centroid and compute U_n and μ_{pq} for orders $n \geq 2$.

Summary of Moments		
Moment Type	Non-Central	Central
General	m_{pq}	μ_{pq}
Radial	M_n	U_n

Table 1. Summary of notation for various types of moments.

B-6. Two-Dimensional Spatial Moments for Azimuthally Symmetric Beams

Personnel: P. H. Johnston, BCL
J. G. Miller, BCL

Support: RR 01362
HL 17646
HL 28998

In this section we describe an approach for characterizing ultrasonic beams using two-dimensional spatial moments (PR 20, B-4). In particular, we present formulas derived for beams exhibiting azimuthal symmetry and linear divergence, such as those produced by circular piezoelectric transducers.

For this analysis, we consider our receiving aperture to be continuous, rather than discretely sampled. Further, we assume that the receiver is sensitive to the intensity of the beam rather than to the pressure. This assumption of phase insensitivity is based on the model of a practical receiving aperture consisting of point-like receiving elements, which can be considered sensitive to the local incident intensity.[1] Under these assumptions, we express the measured energy flux at position $\vec{R}$ on the receiving aperture as

$$E(\omega,\vec{R}) = H(1)\vec{\Phi}(\omega,\vec{R})\cdot\hat{n}, \tag{6.1}$$

where $\vec{\Phi}(\omega,\vec{R})$ is the incident ultrasonic intensity, $\hat{n}$ is the unit normal to the surface of the receiving aperture, and $H(\omega)$ represents the transfer function of the mechanical and electrical loading of the receiver. We compute the nth-order two-dimensional spatial radial moments of the distribution $E(\vec{R})$ over the receiver according to

$$M_n = \int_A \vec{R}^n E(\vec{R})\,dA \tag{6.2}$$

where A is the area of the receiver. The energy flux is weighted in the moment integral by the vector distance $\vec{R}$ from the center of the receiving aperture raised to the nth power.

In the far field of a transmitting transducer or in the focus of a focused transmitter the phase fronts exhibit little curvature, and may be considered planar to a good approximation. Thus, the intensity incident upon a receiving aperture placed in either of these regions may be approximated by the plane waveform

$$\vec{\Phi} = \frac{|p|^2}{\rho c}\,\hat{k} \tag{6.3}$$

where p is the pressure and ρ and c are the density and speed of sound respectively in the medium at the face of the receiver, and k is a unit

vector normal to the wavefronts. The two-dimensional spatial moments are expressed under this condition as

$$M_n = \int_A \vec{R}^n \, E_0(\vec{R}) \cos\theta \, dA \tag{6.4}$$

where $E_0 = |p|^2/pc$ and $\hat{n}\cdot\hat{k} = \cos\theta$ is the cosine of the angle of incidence of the beam.

The lower-order moments of the energy distribution provide information about the beam such as the total energy defined as

$$I_0 = M_0, \tag{6.5}$$

the vector centroid

$$\vec{C} = \frac{\vec{M}_1}{M_0}, \tag{6.6}$$

and the mean squared beam width

$$W^2 = \frac{U_2}{U_0} = \frac{M_2}{M_0} - \frac{|\vec{M}_1|^2}{M_0^2}. \tag{6.7}$$

The total energy I_0 is useful for the determination of signal loss, i.e. attenuation, through a specimen. Deviations of the centroid $\vec{C}$ from zero indicate the effects of gross refraction as shown in Figure 1. In panel (a) we show a lateral shift due to refraction by a specimen in which the faces are parallel to each other. The transmitted beam is refracted within the specimen and the beam exits the tissue slab shifted laterally but parallel to its original path. This is in contrast with the case shown in panel (b) of Figure 1, where the tissue slab has a wedge shape. The refraction suffered by the beam upon exiting the tissue in this case does not bring the beam back parallel to its original direction, and the measured centroid will depend upon the range between the specimen and the receiving aperture. These qualitatively different conditions suggest that it is important to know not only the magnitude and direction of the centroid in the plane of the receiver, but also the angle of incidence θ.

The beam width W, or lateral extent of the energy distribution, may also be modified by propagation through tissue. Because tissue exhibits a nonunity refractive index, a specimen will effectively act as a lens, with concomitant changes in beam shape related to the geometry of the tissue. Further, scattered waves from inhomogeneities in the tissue can combine with the transmitted wave to effectively broaden the received beam.

The effects just outlined serve to present to a receiving aperture a transmitted beam which appears to have emanated from a transmitting transducer positioned at some location which differs from the actual position of the source of the beam. Thus, providing that distortions of the beam are small, the nature of the beam at the receiving aperture may be considered to define a virtual transmitting transducer positioned such that it would produce the measured field in a homogeneous medium in the absence of a specimen.

We now investigate some of the general features of the two-dimensional spatial moments of azimuthally symmetric beams and develop a scheme for the determination from these moments of the total transmitted energy, the direction of incidence of the beam, and the mean squared width of the beam. We mimic the refraction effects of a specimen by varying the position of a simulated virtual transmitting transducer. In order to calculate the two-dimensional spatial moments of a transmitted beam across a receiving aperture, we must express the intensity distribution within the beam in terms of the coordinate system of the receiver. Let us fix a coordinate system (x,y,z) to the transmitting aperture and coordinates (X,Y,Z) to the receiving aperture. Beginning with these apertures coincident, we perform the following sequence of translations and rotations:

(a) translate (x,y,z) by (X_0,Y_0) in the Z=0 plane

(b) rotate result by angle ϕ about the new z axis

(c) rotate result by angle (θ) about the new y axis

(d) translate result by Z_0 along the new z axis

(e) invert sense of z axis so that positions of points on receiver are positive.

Figure 2 graphically depicts these coordinate transformations. The resulting transformations between receiver coordinates (X,Y,Z) and transmitter coordinates (x,y,z) are given by

$$x = \cos\theta\left[(X-X_0)\cos\phi + (Y-Y_0)\sin\phi\right] + Z\sin\theta$$

$$y = \left[-(X-X_0)\sin\phi + (Y-Y_0)\cos\phi\right]$$

$$z = Z_0 - \sin\theta\left[(X-X_0)\cos\phi + (Y - Y_0)\sin\phi\right] - Z\cos\theta \qquad (6.8)$$

and

$$X = X_0 + \cos\phi\left[x\cos\theta + (Z_0-z)\sin\theta\right] - y\sin\phi$$

$$Y = Y_0 + \sin\phi\left[x\cos\theta + (Z_0-z)\sin\theta\right] + y\cos\phi$$

$$Z = (Z_0 - z)\cos\theta - x \sin\theta \tag{6.9}$$

Because the elements of the receiving array lie on the plane Z=0, Equation (6.9) requires that

$$z = Z_0 - x \tan\theta \tag{6.10}$$

and Equation (6.8) and Equation (6.9) reduce to

$$\begin{aligned} x &= \cos\theta\left[(X-X_0)\cos\phi + (Y-Y_0)\sin\theta\right] \\ y &= \left[-(X-X_0)\sin\theta + (Y-Y_0)\cos\phi\right] \\ z &= Z_0 - \sin\theta\left[(X-X_0)\cos\phi + (Y-Y_0)\sin\phi\right] \end{aligned} \tag{6.11}$$

and

$$\begin{aligned} X &= X_0 + x\,\frac{\cos\phi}{\cos\theta} - y\sin\phi \\ Y &= Y_0 + x\,\frac{\sin\phi}{\cos\theta} + y\cos\phi \end{aligned} \tag{6.12}$$

The spatial distribution of a beam produced by a circular-piston radiator has the form

$$\Phi(r) \sim \frac{1}{z^2}\,\frac{4J_1^{\,2}(kar/z)}{(kar/z)^2} \,. \tag{6.13}$$

A beam having a Gaussian intensity profile represents a more analytically tractable distribution than this. Gaussian beam shapes may be approximated experimentally by appropriately apodizing a transmitting transducer with an amplitude weighting factor of approximately Gaussian shape.[2] Here we present calculations of the two-dimensional spatial moments of a beam exhibiting an intensity profile given by

$$\Phi(r) = \Phi_0\,\frac{a^2}{\sigma^2}\exp\left[-\frac{r^2}{\sigma^2}\right] \tag{6.14}$$

where the beam width σ is a function of range z and frequency k

$$\sigma = \frac{\zeta z}{ka} . \tag{6.15}$$

The constant a represents the radius of the transmitting transducer, such that the beam exhibits similar dependences as the Bessel function beam given in Equation (6.13). The parameter ζ may be interpreted as a fitting factor which allows one to match the Gaussian form with the beam width of a beam of Bessel function form. For example, ζ might represent the value for which $4J_1^2(\zeta)/\zeta^2 = 1/2$, that is $\zeta = 1.56$. An alternative interpretation is to consider a/ζ to be an effective radius for the transducer, where the value of ζ is determined by the form of an applied apodization function. For simplicity in what follows we consider a to be the effective radius and drop ζ. The normalization condition imposed on this beam is that the total power passing a plane perpendicular to the z axis is equal to the intensity at the transducer face Φ_0 times the effective area of the transducer πa^2.

In order to calculate the two-dimensional spatial moments of this beam it is convenient to change variables to transmitter coordinates. The Gaussian beam smoothly falls off with r, and thus does not define boundaries to use as limits of integration. This means that the boundaries of the receiving aperture should be used. To facilitate computation, we note that 99% of the energy in this beam falls within a radius $r \approx 3\sigma$. We take the receiving aperture to be much larger than this so that we may safely extend the limits of integration to infinity. Further, we see from Equation (6.10) that points on the receiving aperture lie at distance

$$z = Z_0 - r \cos\psi \tan\theta \tag{6.16}$$

from the transmitter, where we have expressed x in polar coordinates r and ψ. Thus, writing out explicitly the range dependence of Equation (6.14) we obtain

$$\Phi(r) = \Phi_0 \frac{k^2a^4}{(Z_0 - r\cos\psi\tan\theta)^2} \exp\left[-\frac{k^2a^2r^2}{(Z_0 - r\cos\psi\tan\theta)^2}\right]. \tag{6.17}$$

To investigate the behavior of the spatial moments of the Gaussian beam we note that $r \sim \sigma_0 \ll Z_0$ in a typical experimental situation, so we may expand Equation (6.17) in a Taylor series with respect to z about Z_0

$$\Phi(z) \approx \Phi(Z_0) + \frac{\partial\Phi}{\partial z}\bigg|_{Z_0}(z-Z_0) + \frac{1}{2!}\frac{\partial^2\Phi}{\partial z^2}\bigg|_{Z_0}(z-Z_0)^2 + \ldots \tag{6.18}$$

The first two partial derivatives of Φ evaluated at Z_0 are

$$\left.\frac{\partial \Phi}{\partial z}\right|_{Z_0} = -\frac{2\Phi(Z_0)}{ka\sigma_0}\left(\frac{r^2}{\sigma_0^2} - 1\right) \tag{6.19}$$

$$\left.\frac{\partial^2 \Phi}{\partial z^2}\right|_{Z_0} = -\frac{2\Phi(Z_0)}{k^2a^2\sigma_0^2}\left(2\frac{r^4}{\sigma_0^4} - 7\frac{r^2}{\sigma_0^2} + 3\right) \tag{6.20}$$

where the beam width σ_0 is Z_0/ka. We refer to the terms of the expansion Equation (6.18) as being a zeroth, first, and second order and denote this order by superscripts

$$\Phi(z) \approx \Phi^{(0)} + \Phi^{(1)} + \Phi^{(2)} \tag{6.21}$$

where

$$\Phi^{(0)} = \Phi_0 \frac{a^2}{\sigma_0^2} \exp\left(-\frac{r^2}{\sigma_0^2}\right) \tag{6.22}$$

$$\Phi^{(1)} = \frac{2\Phi^{(0)}}{ka\sigma_0}\left(1 - \frac{r^2}{\sigma_0^2}\right) r \cos\psi \tan\theta \tag{6.23}$$

$$\Phi^{(2)} = \frac{\Phi^{(0)}}{k^2a^2\sigma_0^2}\left(2\frac{r^4}{\sigma_0^4} - 7\frac{r^4}{\sigma_0^2} + 3\right) r^2 \cos^2\psi \tan^2\theta. \tag{6.24}$$

The nth spatial moment may be written in a corresponding series of increasing order as

$$M_n = M_n^{(0)} + M_n^{(1)} + M_n^{(2)} \tag{6.25}$$

where

$$M_n^{(k)} = \int_0^{2\pi}\int_0^{\infty} d\psi \int_0^{\infty} r\, dr\, E^{(k)}\left[X(r,\psi), Y(r,\psi)\right]^n \tag{6.26}$$

and

$$E^{(k)} = H(w)\Phi^{(k)}(w). \tag{6.27}$$

To estimate the relative magnitudes of the expansion terms of Equation (6.21) we observe that, assuming that r is of the order of a few times σ_0,

$$\Phi^{(1)} \sim \frac{2\Phi^{(0)}}{k\,a} \text{ and } \Phi^{(2)} \sim \frac{\Phi^{(0)}}{k^2\,a^2} . \tag{6.28}$$

For a typical laboratory transducer of effective radius a = 4 mm radiating 5 MHz ultrasound into a water bath (with speed of sound c = 1.5 mm/μsec) we have ka = $2\pi fa/c$ = 84 and the first and second order terms are thus on the order

$$\Phi^{(1)} \sim 0.02\Phi^{(0)} \text{ and } \Phi^{(2)} \sim 0.0001\Phi^{(0)}. \tag{6.29}$$

Thus, we retain only the first two terms in Equation (6.21) for our calculations of spatial moments for the Gaussian beam. We define the small quantity

$$\varepsilon = \frac{1}{k\,a} \tag{6.30}$$

and note that it corresponds to the angle of divergence of the beam.

Calculation of the two-dimensional spatial moments for this Gaussian beam is straightforward, but tedious. A summary of the results of these calculations is given in Table 1. The total energy within the beam I_0 is equal to the zeroth-order two-dimensional spatial moment M_0. The integral yields E_0 times the effective area of the transmitter, according to the normalization condition. Thus, for any angle of incidence, the receiving aperture measures the total energy in the beam, as required by conservation of energy. The vector centroid $\vec{C}$ is found to be modified by a small shift proportional to the product of the divergence angle of the beam and the beam width. The dependence on polar angle is weak for small angles. The apparent mean squared beam width W^2 increases with polar angle of incidence.

Other combinations of spatial moments provide further information on the orientation of the beam relative to the receiving aperture.[3] One such combination represents the difference between the spread of energy about the X axis and the spread about the Y axis. This quantity is referred to here as the squared width difference, denoted by D. The corresponding quantity defined about axes rotated by 45° is denoted by D_R. These two quantities are found to vary sinusoidally with twice the azimuthal angle of incidence. Finally, we have defined the skewness vector $\vec{S}$ as the third order spatial radial central moment $\vec{U}_3/U_0$.

These quantities tabulated in Table 1 provide a set of characterizable features of a transmitted ultrasonic beam. If the beam exhibits azimuthal symmetry and linear divergence as modeled here, the expressions in the rightmost column offer a means for describing the beam more fully. We may take the ratio of the two squared width differences to obtain an estimate of the azimuthal angle of incidence

$$\tan 2\phi = \frac{D_R}{D} \quad . \tag{6.31}$$

Clearly, this can only determine the azimuthal angle to within an uncertainty of π. The X and Y components of skewness are proportional to $\cos\phi$ and $\sin\phi$ respectively, and are independent of (X_0,Y_0). The sinusoidal behavior of the skewness allows the removal of the ambiguity in the determination of azimuthal angle. The octants defined by the (X,Y) and $(X_R Y_R)$ axes are shown in Figure 3 with the signs of the squared width differences D and D_R and the skewness components S_X and S_Y indicated. The relative signs of D and D_R are the same in opposite octants, producing an ambiguity of π in azimuthal angle. However, the signs of the components of skewness change with the quandrants determined by (X,Y). Thus, if $S_X<0$, the angle ϕ lies in the first or the fourth quandrant, as determined by whether S_Y is negative or positive, respectively. A value of S_X greater than zero implies that ϕ lies in the second or third quandrant, again determined by the sign of S_Y being negative or positive, respectively.

Equation (6.31) also implies that

$$\cos 2\phi = \frac{D}{\left[D^2 + D_R{}^2\right]^{1/2}} \quad . \tag{6.32}$$

We substitute this into the expression for D and use the result to eliminate $\tan^2\theta$ in the expression for W^2 and solve for $\sigma_0{}^2$, yielding

$$\sigma_0{}^2 = W^2 - \left[D^2 + D_R{}^2\right]^{1/2} \quad . \tag{6.33}$$

Finally, we solve for $\tan^2\theta$ to obtain

$$\tan^2\theta = \frac{2\left[D^2 + D_R{}^2\right]^{1/2}}{W^2 - \left[D^2 + D_R{}^2\right]^{1/2}} \quad . \tag{6.34}$$

Thus, for azimuthal symmetry and linear divergence, we may in principle determine the actual width and the angles of incidence of the beam.

As shown by the results in Table 1, divergence of the ultrasonic beam produces a small deviation of the components of the centroid vector $\vec{C}$ from the correct value (X_0,Y_0). Also, the X component of the skewness is proportional to the deviation of C_X from X_0

$$\frac{S_X}{C_X - X_0} = \frac{\sigma_0{}^2}{2}\left(3\tan^2\theta + 4\right), \tag{6.35}$$

the proportionality constant being given in terms of the quantities σ_0 and θ which are fully determined by other moments-based quantities. Thus we may compensate the centroid for this deviation to accurately locate the center of the beam as

$$X_0 = C_X - \frac{2S_X}{\sigma_0^2 \left[3\tan^2\theta + 4\right]} \tag{6.36}$$

and the corresponding result for the Y direction

$$Y_0 = C_Y - \frac{2\,S_Y}{\sigma_0^2\left[3\tan^2\theta + 4\right]} \,. \tag{6.37}$$

The parameter $\varepsilon = 1/ka$ corresponds to the angle of divergence of the beam. The skewness as defined in Table 1 offers a means for estimating ε. One way to express an estimate of ε is

$$\varepsilon = \frac{2\,|\,S\,|\,\cos\theta}{\sigma_0^3\,\tan\theta}\left[\frac{3}{\cos^2\theta} + 1\right]^{-1} . \tag{6.38}$$

Further, the divergence angle is given by

$$\varepsilon = \frac{1}{k\,a} = \frac{c}{2\pi\,f\,a} \tag{6.39}$$

where f is the frequency and c is the speed of sound in the medium. Thus, for example, for a given transmitting transducer with known effective radius a, Equation (6.38) offers a means of extracting some information about the speed of sound of the media lying between the transmitter and receiving array. Alternatively, in a homogeneous medium Equation (6.38) could be used to infer the effective radius of the transmitting transducer.

We have described methods for describing a measured beam using two dimensional spatial moments. Specifically, we derived expressions for the total energy, centroid, mean squared beam width, polar and azimuthal angles of incidence, and divergence angle of the beam. These are summarized in Table 2. These results may be considered to describe the beam from a virtual transmitting transducer located at some position possibly different from that of the actual transmitter. Implicit to this interpretation is the assumption that the transmitted beam retains its form as it is refracted by the media between the actual transmitter and the receiver. We note that when the transmitted beam loses its azimuthal symmetry during passage through a medium, although the expressions in Table 2 no longer hold, the quantities defined in terms of moments in Table 1 are still valid descriptors of the beam.

1. L. J. Busse and J. G. Miller, "Detection of Spatially Nonuniform Ultrasonic Radiation with Phase Sensitive (Piezoelectric) and Phase Insensitive (Acoustoelectric) Receivers," Journal of the Acoustical Society of America, vol. 70, pp. 1377-1386, 1981.

2. R. O. Claus and P. S. Zerwekh, "Ultrasonic Transducer with a Two-Dimensional Gaussian Field Profile," IEEE Transactions on Sonics and Ultrasonics, vol. SU-30, pp. 36-39, 1983.

3. M-K. Hu, "Visual Pattern Recognition by Moment Invariants," IRE Transactions on Information Theory, vol. IT-8, pp. 179-187, 1962.

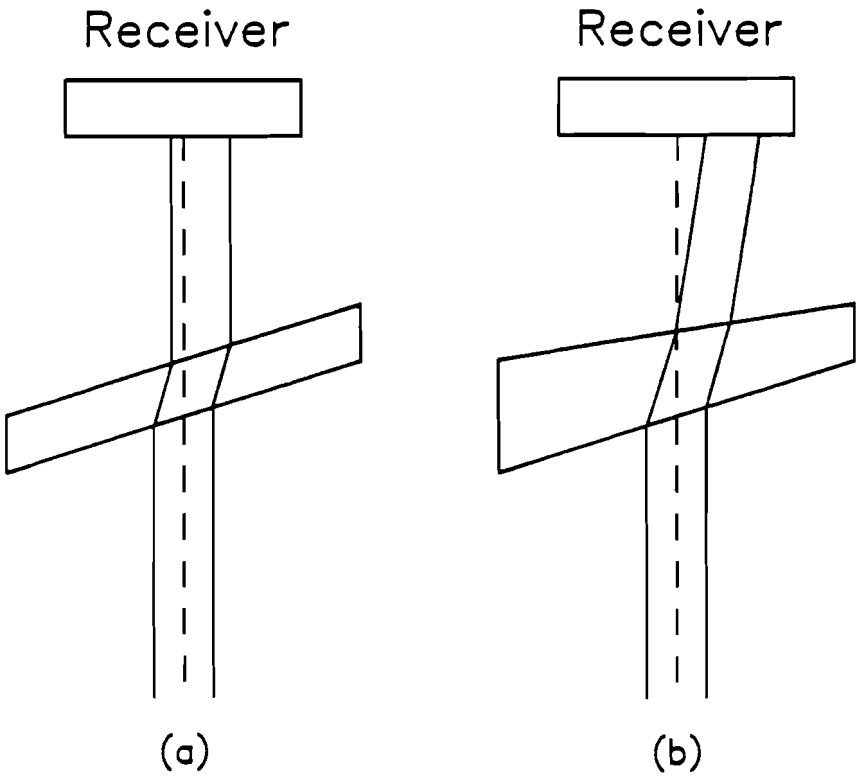

Figure 1. Demonstration of two types of refraction conditions. In panel (a) the specimen has flat and parallel sides so the transmitted beam exits parallel to its incident direction. In the more general case (b) the surfaces of the specimen are nonparallel, and the beam exits at some angle to its original direction.

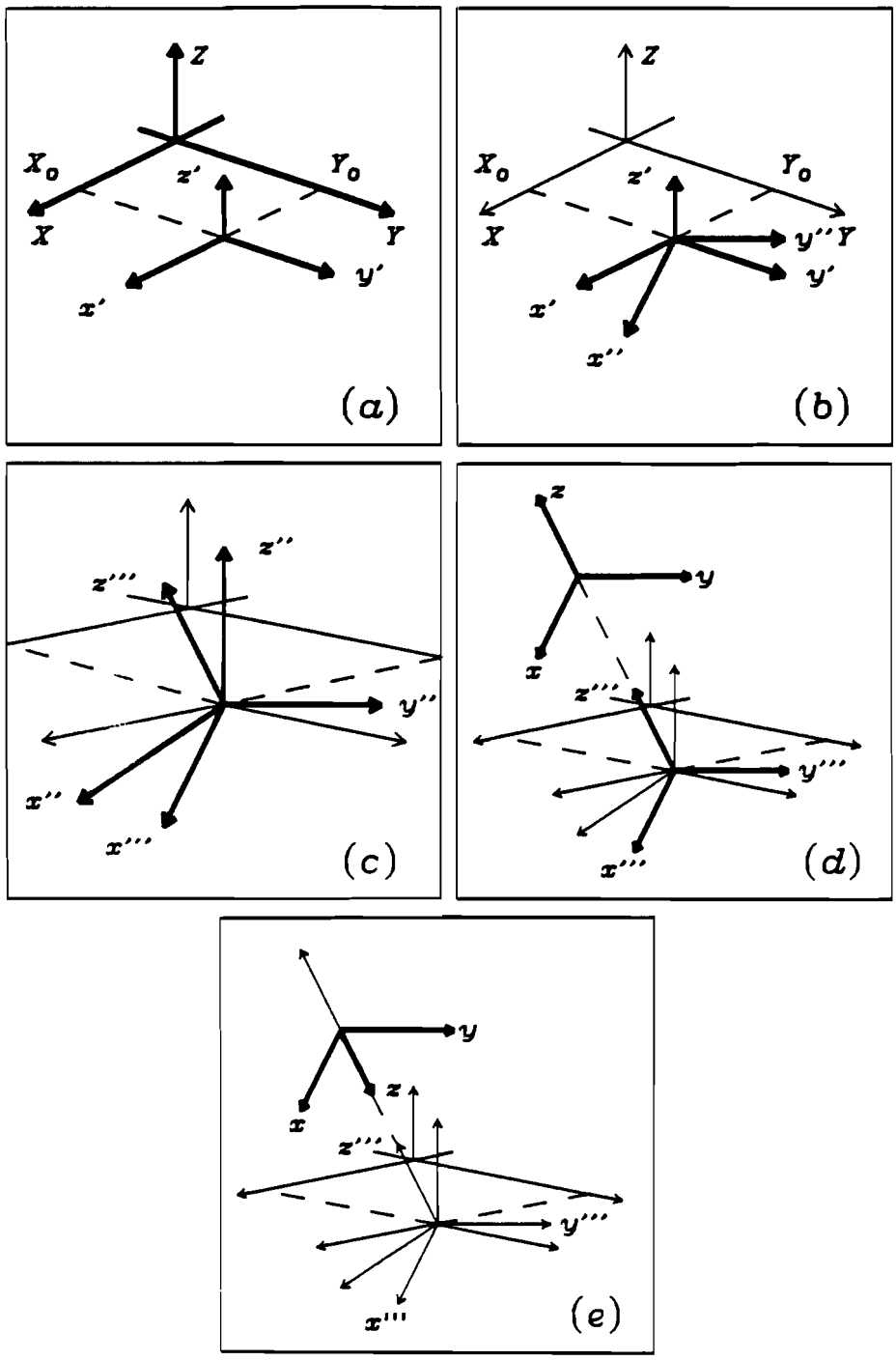

Figure 2. Pictorial representation of coordinate transformations between receiver coordinates (X,Y) and virtual transmitter coordinates (x,y).

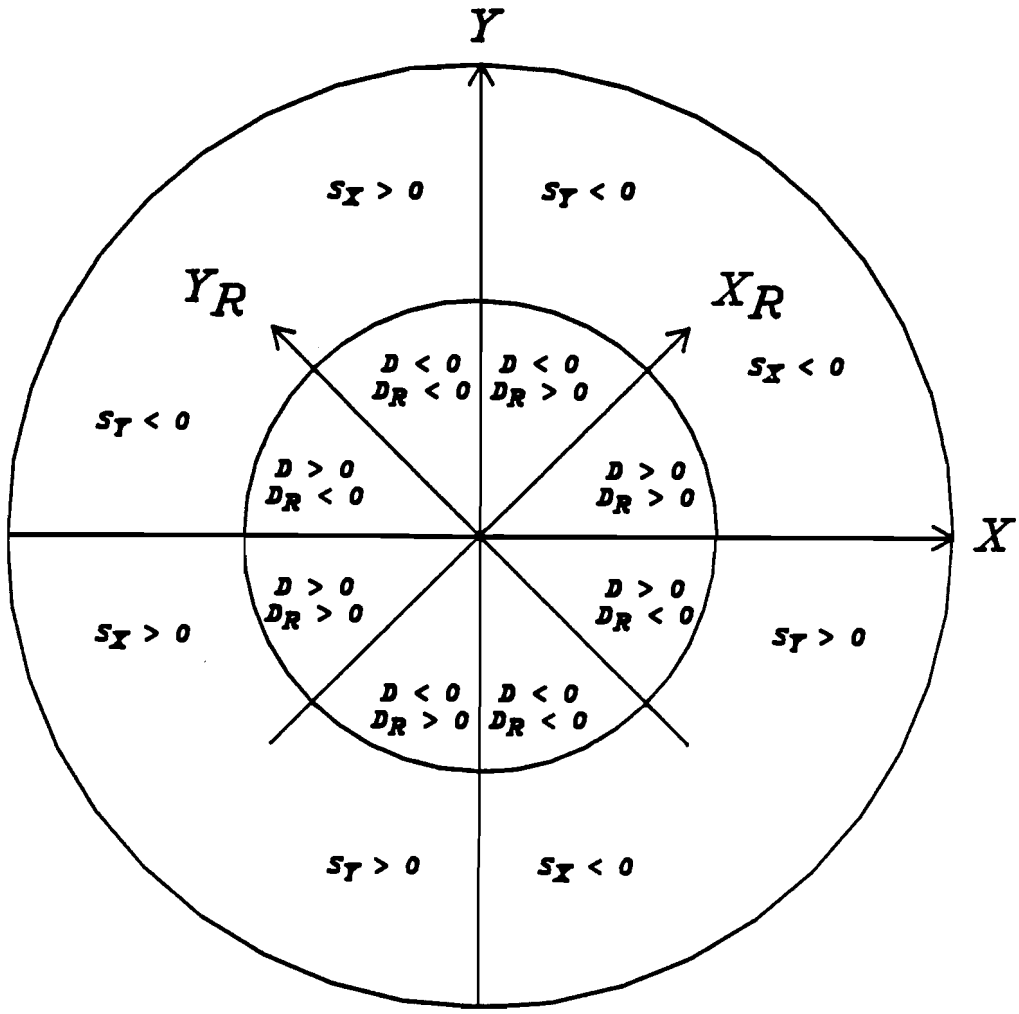

Figure 3. Octants formed by the crossed axes (X,Y) and (X_R,Y_R). Analysis of squared beam width differences leaves an ambiguity in the determination of azimuthal angle which is removed by analysis of the signs of the skewness parameter.

B-7. A Pole-Zero Model for the Transfer Function of Soft Tissue

Personnel: R. M. Arthur, BCL

Support: RR 01362

Although soft tissue is both dispersive and inhomogeneous, conventional B-scan imaging systems focus signals received by phase-sensitive, linear arrays as if tissue were a homogeneous medium with constant phase velocity. Previously we described two nearly equivalent causal models for representing dispersion and inhomogeneity in tissue (PR 16, B-5; PR 19, B-4). One, which is based on the Hilbert transform, assumes attenuation is a linear function of frequency. The other, a pole-zero model, can be synthesized from the magnitude of the frequency response of any experimental data.

A single-pole matched experimental data reported in the literature to within a few percent, which was comparable to a straight line fit. A single-pole model, however, has several advantages beyond its ability to match the magnitude of the frequency response of tissue. The pole location of the single-pole model is a relaxation frequency. This frequency was inversely proportional to the concentration of hemoglobin, directly proportional to the temperature of dog myocardium, and inversely proportional to the collagen content of dog myocardium. In addition phase velocity can be predicted by the single-pole model.

$$V(f) = 1/[\tau_b + \tan^{-1}(f/P)/2\pi f] \ ,$$

where P is the pole location and τ_b is the bulk propagation delay. The prediction was within measurement error for hemoglobin solutions. In contrast to the Kramers-Kronig or Hilbert transform predictions for phase velocity, which depend on the logarithm of frequency, the single-pole prediction of phase velocity is well-behaved at both low and high frequencies and consistent with a linear-phase (constant velocity) model.

$$V(0) = P/(\pi_b P + 1) \simeq 1/\tau_b; \quad V(\infty) = 1/\tau_b \ .$$

The phase velocity of the single-pole model at both low and high frequencies is just the constant velocity of a conventional linear-phase tissue model. Finally the single-pole model has an equivalent circuit representation, which is a low-pass filter coupled with a delay.

This year we determined the attenuation functions for which the single-pole model is a good match. Attenuation of soft tissue is often described by a power function

$$\alpha(f) = \alpha_o \ f^{\gamma}$$

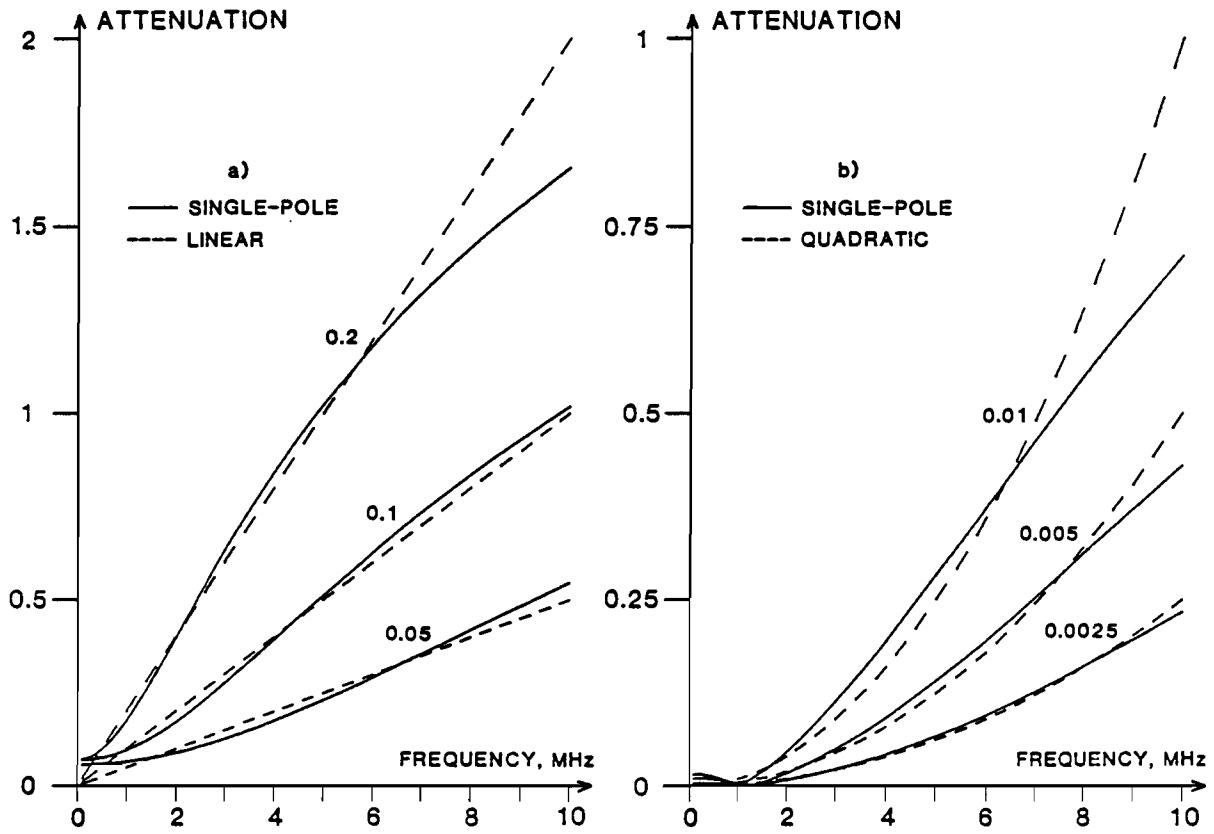

Figure 1. Attenuation predicted by a single-pole tissue model for linear (a) and quadratic (b) dependence of attenuation of frequency. In (a) γ=1 and in (b) γ=2. The number next to each pair of curves is the attenuation coefficient α_o.

where α_o is the attenuation coefficient and f is frequency. α_o and γ are constants that depend on the tissue type. For soft tissue γ is about one; it is about two for liquids. To test the limits of the single-pole model in the 0.1 to 10 MHz range, we matched a single-pole model to attenuation which was linearly and quadratically dependent on frequency.

For the case in which attenuation was assumed to increase linearly with frequency (Figure 1a), the RMS error in the single-pole approximation was a minimum equal to 2.0% of the full-scale attenuation for α_o = 0.12/MHz. The RMS error approached an asymptote of 7.0% of full scale as α_o decreased. It was <7.0% for α_o <0.20/MHz. If, for example, the slope of attenuation β = 0.05/cm/MHz, which is typical of dog myocardium, then the single-pole model could represent a layer up to 4 cm thick with an RMS error of <7% over the 0.1 to 10 MHz range. Where attenuation was assumed to increase quadratically with frequency (Figure 1b), the RMS error in the single-pole approximation increased monotonically from nearly zero for small values of α_o to 7% of the full-scale value for α_o = 0.08/MHz^2. Again the thickness of the layer of tissue which can be described within a given error depends on the type of tissue.

1. R. M. Arthur, and K. V. Gurumurthy, "A Single-Pole Model for the Propagation of Ultrasound in Soft Tissue," Journal of the Acoustical Society of America, vol. 77, pp. 1589-1597, 1985.

B-8. The Transfer Function of Linear Transducer Arrays

Personnel: R. M. Arthur, BCL
S. R. Broadstone, BCL
M. L. Sieger, B.S., Electrical Engineering

Support: RR 01362
Washington University

Transducer behavior must be taken into account in order to make quantitative ultrasonic measurements (PR 20, B-5). Clearly, the content of the beam of a phased array is dependent on the beam profiles of the individual elements in that array. The energy transmitted or received by a transducer element is dependent on signal frequency and on the angle of propagation or incidence.

We mapped the response of individual elements of an array by rotating the array within its image-plane. The axis of rotation passed through the center of the element face. The rotation was performed by a stepper motor under computer control. Another motor fixed the range between the array element under study and a hydrophone or reflector. We measured the pressure field generated by an element of interest with the hydrophone. We also captured signals received by the element when the transmitted signal was scattered by a slotted tube. Broadband pulses were used to excite transducer elements in order to calibrate the element for quantitative pulse-echo imaging. The excitation pulse, the pressure field

recovered by a hyrophone, and the scattered signal received by the element itself were recorded as a function of hydrophone or scatterer range and angle. Signals were sampled at 50 MHz with 8 bits of precision. Spectra were determined by Fourier transform. We used this technique to measure elements of 3.5 and 5 MHz, 32-element linear arrays, composed of piezoelectric material.

Typically beam profiles are determined by measuring the peak pressure received as a function of range and angle. Unfortunately, this approach does not describe the frequency content of the ultrasound delivered to a particular region in the field of view, when the excitation is a pulse. One measure of the usable field of an array for broadband tissue characterization is the energy available within appropriate frequency bands at a given range and angle. By comparing pressures or scattered signals to the excitation pulse we calculated the ability of the element to insonify a given region of its field of view. The energy in various frequency bands was calculated to find the energy present at a given range and viewing angle. Figure 1 shows the energy delivered in the 2 to 5 MHz band at 7 cm from an element of a 3.5-MHz array as a function of off-axis angle. At 30 degrees, for example, the 2-5 MHz energy (a 3 MHz band about the center frequency of the element) was 14 dB below the total energy according to reflection from the slotted tube and 18 dB below as measured by the hydrophone. At 30 degrees the energy delivered by this element is in a 0.5 MHz band centered at 2.0 MHz. Clearly the field of view of this array for broadband tissue characterization is much more limited than it is for conventional imaging. If a signal energy 15 dB below that on axis is sufficient for generating an acceptable image, then the field of view of this array for conventional imaging is about ± 40 degrees. For broadband tissue characterization the field is reduced to about ± 15 degrees.

In addition we have attempted to infer transducer vibration modes by removing diffraction effects from the calibration studies described above. To characterize the transfer function of a given transducer we modeled each element as a collection of facets or subelements. The diffraction patterns of these facets was calculated using the impulse-response method of Lockwood and Willette.[1] Facet motion was inferred from responses measured along scans in azimuth and elevation on a least-squares-error basis. Figure 2 shows the relative magnitudes of three frequencies delivered by a single element of a 3.5 MHz array as a function of off-axis angle in azimuth (a) and elevation (b). Also included is the 16-facet fit of those scans. Whereas there is general agreement between theoretical and measured quantities, the RMS error with 16 facets is not significantly better than the match obtained when the transducer element was assumed to be a uniform rectangular piston. This effect is due to our inability to precisely located the measurement points with respect to the element surface. The least-squares-error method fails if the location of a given field point with respect to other field points is not known to within a few μm, which is the distance over which phase changes by 1 degree in soft tissue at 3.5 MHz. Presently we are exploring maximum likelihood techniques to assess facet motion field point by field point. These results can be averaged and perhaps used iteratively to infer facet motion.

1. J. C. Lockwood, and J. G. Willette, "High-Speed Method for Computing the Exact Solution for the Pressure Variations in the Nearfield of a

Baffled Piston," Journal of the Acoustical Society of America, vol. 53, pp. 735-741, 1973.

2. M. L. Sieger, "Characterization of Phased-Array Medical Ultrasonic Transducers," Master's Thesis, Washington University, 1985.

3. R. M. Arthur, M. L. Sieger, and D. W. Stein, Jr., "Assessing Ultrasonic Arrays for Imaging Tissue Properties," Ultrasonic Imaging, vol. 6, p. 209, 1984 (abstract).

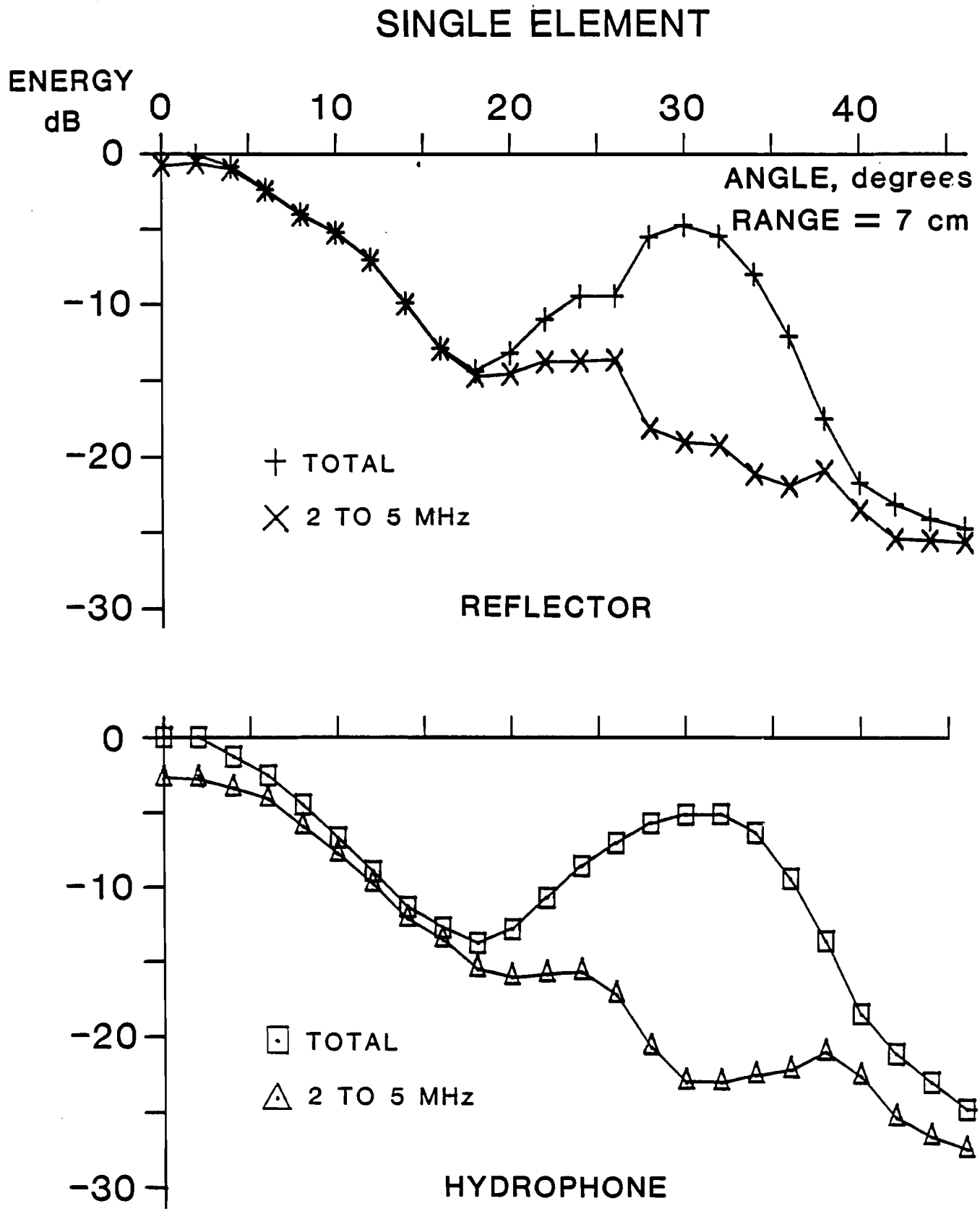

Figure 1. Energy delivered by a single element of a 32-element array with a center frequency of 3.5 MHz.

X-Z Sector Scan

Y-Z Sector Scan

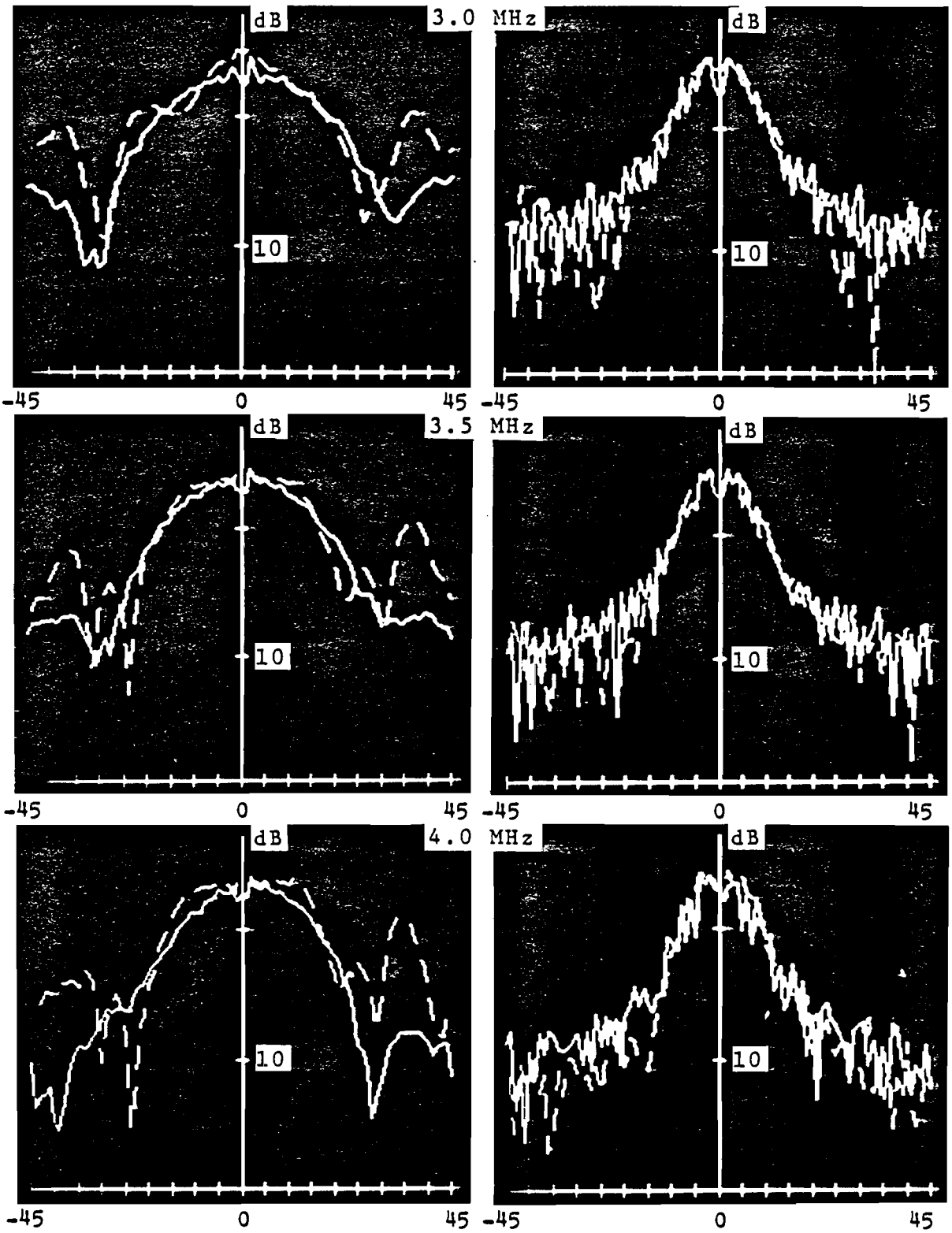

Figure 2. Comparison of pressure magnitudes generated by a single element of a 3.5 MHz, 32-element array (dashed lines) and a 16-facet transducer model (solid lines).

B-9. Adaptive Beamforming for Quantitative Imaging of Soft Tissue

Personnel: R. M. Arthur, BCL
S. R. Broadstone, BCL

Support: RR 01362

Conventional ultrasonic imaging systems combine signals received by phase-sensitive linear arrays as if tissue were homogeneous. Estimates of attenuation coefficient from such a beamformer are corrupted by the pertubation of wavefronts across the array caused by tissue inhomogeneities. Previously we proposed adaptive beamforming schemes in both the time and frequency domains which reduce phase cancellation across an array. The time-domain beamformer estimates the actual delay suffered at each element of the array by cross-correlating the received signal with, for example, the center frequency of the transmitted pulse. The frequency-domain beamformer sums the magnitudes of the Fourier transforms of each element signal, after the signals have been aligned by a homogeneous-medium beamformer. As long as all the element signals are within the transform window, then any mismatch between the homogeneous-medium beamformer delays and the actual delays can be ignored.

Both the time- and frequency-domain beamformers were tested in simulations on simple laminar geometries. The slope of attenuation versus frequency of a model consisting of two 5-cm layers, whose attenuation coefficients differed by a factor of 5, was estimated with a linear array composed of 21 point-like elements separated by 1 mm. Attenuation estimates were calculated for insonified volumes from 0 to 45 degrees off axis of the array. The homogeneous- medium beamformer error increased monotonically from 0 on axis to more than 80% at 45 degrees. Both adaptive beamformer estimates were within 1.6% of the value throughout the 45 degree viewing angle. This small error occurred because path length was found assuming that phase velocity was constant.

We are now completing circuitry to test beamforming algorithms with our processing environment. This circuitry is a simple extension of that used to test single elements of an array. It uses a single transmit channel and a single receive channel, each composed of commercially available components. These channels are switched in turn by relays under computer control to each of the elements of the array. A single element is pulsed and the signal received by that element or any other element in the array is recorded. The receiver circuitry is moved to the another element and the original element is pulsed again. This procedure is repeated until recordings have been made from all elements of the array. At this point the transmit circuitry is switched to the next element and the whole protocol repeated. Thus if there are N elements in the array, we record N^2 single-element signals. This approach permits us to perform all preprocessing steps off-line digitally. Thus we can precisely compare homogeneous and adaptive beamforming algorithms and test any other algorithms on tissue phantoms or tissue samples without buidling new acquisition circuitry.

Storage for the element signals from a 32-element array requires 2 to 4 megabytes. Beamforming these signals to a 256 x 256 image reduces storage to 64 kilobytes. Beamforming and other preprocessing steps, such

as correction for the angular response of the array elements takes place in the acquistion system based on a DEC LSI-11/23. After preprocessing, raw images are sent via serial line to our Masscomp workstation for further manipulation, quantitative assessment, comparison, and display.

B-10. The Processing Environment for Ultrasonic Tissue Characterization

Personnel: R. M. Arthur, BCL
S. R. Broadstone, BCL
P. H. Johnston, BCL
J. G. Miller, BCL
J. G. Mottley, BCL
L. J. Thomas, Jr., BCL

Support: RR 01362

In the past year we added a Masscomp MCS-537 workstation to our processing environment (PR 20, B-7). It is a multiuser system for generating and manipulating images (see Figure 1). Previously the heart of our processing environment was a DEC LSI-11/23 microcomputer whose total memory and user partitions within memory (56 kilobytes) are far too small to hold, much less manipulate, typical ultrasonic images (256 kilobytes). The workstation contains 2 megabytes of memory, special floating-point hardware, and an integral graphics processor with a high-resolution color display. It has significantly enhanced our ability to develop algorithms for extracting quantitative measures from ultrasonic signals and to display the resulting quantitative images.

The DEC LSI-11/23 is now dedicated to the acquisition of ultrasonic signals. Its main peripherals include: 1) a 111-megabyte Winchester drive, which this year replaced much smaller, obsolete drives; 2) an FPS 100E array processor; 3) a 9-track, industry compatible tape drive for backup storage; and 4) an IEEE-488 bus for communication with the instrumentation that controls our ultrasonic transducers and collects their signals. The array processor serves the function of the beamforming or other preprocessing hardware in conventional ultrasonic systems, but is much more flexible. We can tailor the processing, for example, such that beamforming delays are specific to the sample under insonification.

We also interfaced the acquisition system to a medium-resolution, gray-scale graphics system called digivision, which was designed and built in our laboratory. During the past year we streamlined the command structure and added a character generator to digivision. Although this unit is slow (90 seconds to fill the screen) it does permit display of raw images, so that we can see whether or not ultrasonic signals were acquired properly. Generation of quantitative images is done at the Masscomp workstation.

We added an Epson LQ-1500 dot-matrix printer, which serves both our acquisition system and the Masscomp workstation. It replaced a Versatec

printer/plotter, which was needed elsewhere in the Resource, and a 10-year-old line printer which could generate only upper-case fonts and which has no graphics capability. The LQ-1500 has both draft and letter-quality modes plus graphics capability. It permits us to generate finished papers and reports plus gray-scale representations of ultrasonic images.

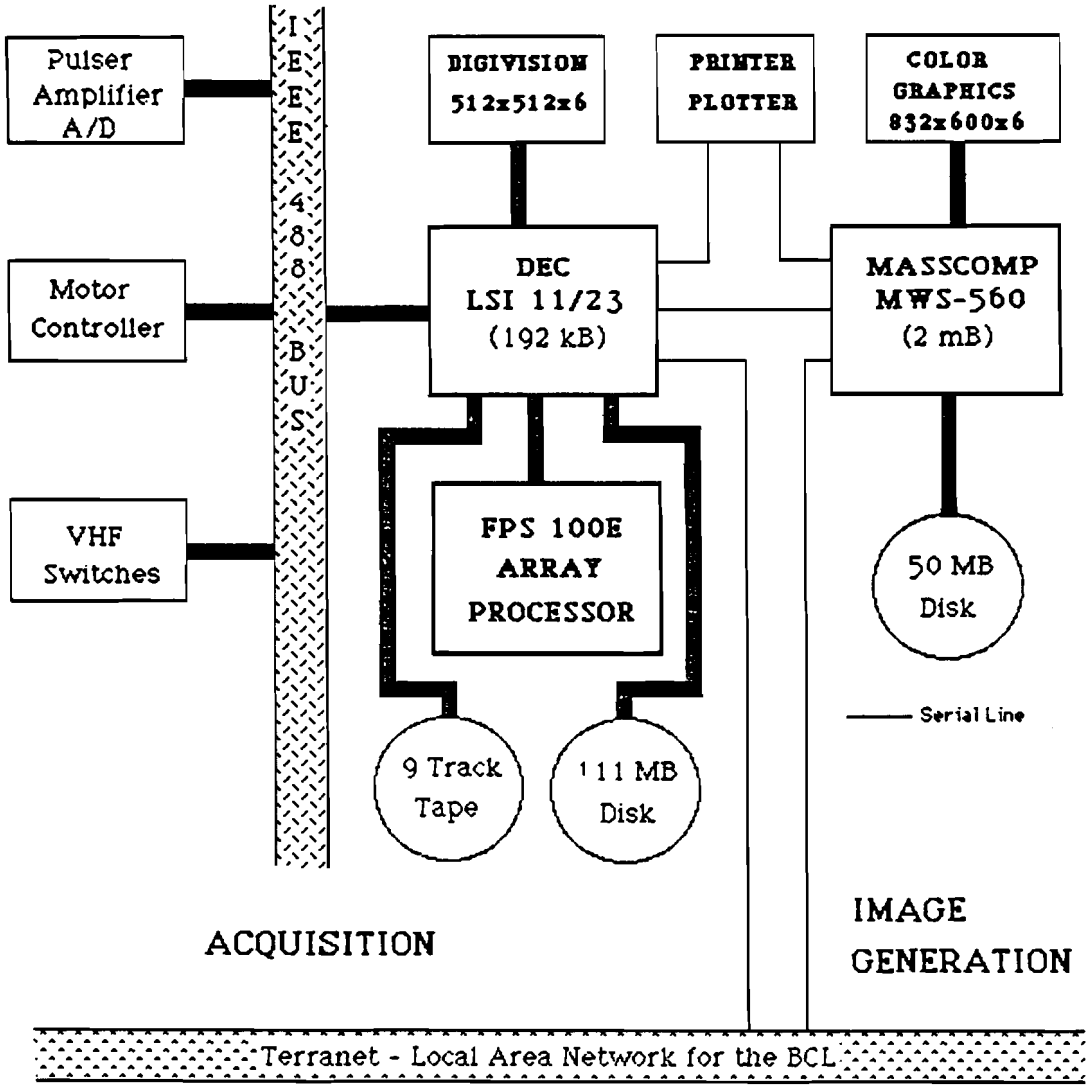

Figure 1. Processing Environment for Ultrasonic Tissue Characterization.

C. Quantitative Imaging: Radiation-Treatment Planning

The delta-volume method reported on previously (PR 19, PR 20) is now being implemented on a Modulex treatment planning system for use in a contract for evaluation of three-dimensional treatment planning. As a first step to extending dose calculation algorithms from Co-60 to higher energy treatment beams, a series of experimental studies and measurements has been initiated. This work is being done under the auspices of MIR (Mallinckrodt Institute of Radiology) and is to provide the experimental groundwork for dose calculations with high energy treatment beams.

C-1. Dose Calculation for Co-60

Personnel: J. W. Wong, Ph.D., Radiology
W. B. Harms, B.S., Radiology
J. A. Purdy, Ph.D., Radiology
F. U. Rosenberger, BCL and Computer Systems Laboratory

Support: RR 01380
RR 01379
CM 47696
Mallinckrodt Institute of Radiology

The delta-volume dose calculation algorithm reported on last year (PR 20) is being implemented on a Modulex treatment planning system for use in a contract for evaluating three-D dose-calculation algorithms. The BCL MMS-X high-performance display system has been moved to the Radiation Physics Department in MIR and connected to a Modulex treatment planning system. The MMS-X will be used to display outlines of patient anatomical features extracted from CT scans, to display treatment beam outlines, and to manipulate planned treatment beam positions, collimators, and blocks. After satisfactory beam specification, the beam parameters will be transmitted to the Modulex system for dose calculation. The three-D display with real time control of viewing position and beam parameters is expected to prove very useful in beam placement by allowing direct viewing and control of beam parameters.

C-2. Physics of High Energy Photon Dose Deposition in Heterogeneous Medium

Personnel: J. W. Wong, Ph.D., Radiology
J. A. Purdy, Ph.D., Radiology
F. U. Rosenberger, BCL and Computer Systems Laboratory
C. Y. Yu, M.S., Radiology

Support: RR 01380
RR 01379
Mallinckrodt Institute of Radiology

A major goal in Radiation Treatment Planning (RTP) is to develop an accurate method of photon dose calculations that can be applied to the wide range of photon energies and geometries encountered in radiotherapy. As mentioned in the last progress report, we had successfully completed the evaluation of our prototype delta-volume algorithm for photon-transport calculations as tested with cobalt-60 experiments.

Our present objective is to extend the delta-volume algorithm to higher energy bremsstrahlung beams as generated by medical accelerators. Dose deposition at these energies can no longer be assumed to be local (as is the case with cobalt-60) since the ejected secondary electrons travel several cm from the site of photon interactions. Consequently, the presence of heterogeneities of human anatomies affect both photon- and electron-transport. Furthermore, high energy photon pair-production interactions which can account for more than 10% of the dose deposited must be considered for more accurate dose calculations. Pair-productions are not accounted for in existing methods of dose calculations.

During the last year, we have concentrated our effort in the important initial phase of understanding the physics of the problem. Such knowledge is imperative in the development of an appropriate model that forms the basis of a practical and accurate algorithm. Germane to the architecture of the delta-volume algorithm in terms of boundary conditions is the measurement of minute dose perturbation due to the presence of a small inhomogeneity in the medium. These measurements have been made with the arrangements schematically shown in Figure 1 as small ring inhomogeneities of various materials were cycled up and down about the detector axis.

Figure 2 shows the plot of the measured perturbation in fractional change of dose per volume of water displaced vs. the depth-position of the ring inhomogeneity for a 4-MV x-ray beam. The chamber is at a depth of 15 cm on the central axis. The styrofoam and aluminum rings have identical dimensions, with a radius of 2.75 cm, height of 2.0 cm and a thickness of 0.5 cm. Their presence results in an increase or decrease in dose depending on their positions. Their effects are reversed in polarity but similar in magnitude. The quantitative difference is due to the non-linear nature of the perturbation as compounded by the unequal change in density with respect to water for styrofoam and aluminum. The effects can be explained by photon-transport calculations, with the assumption of local energy deposition, as were made in our earlier cobalt-60 studies.

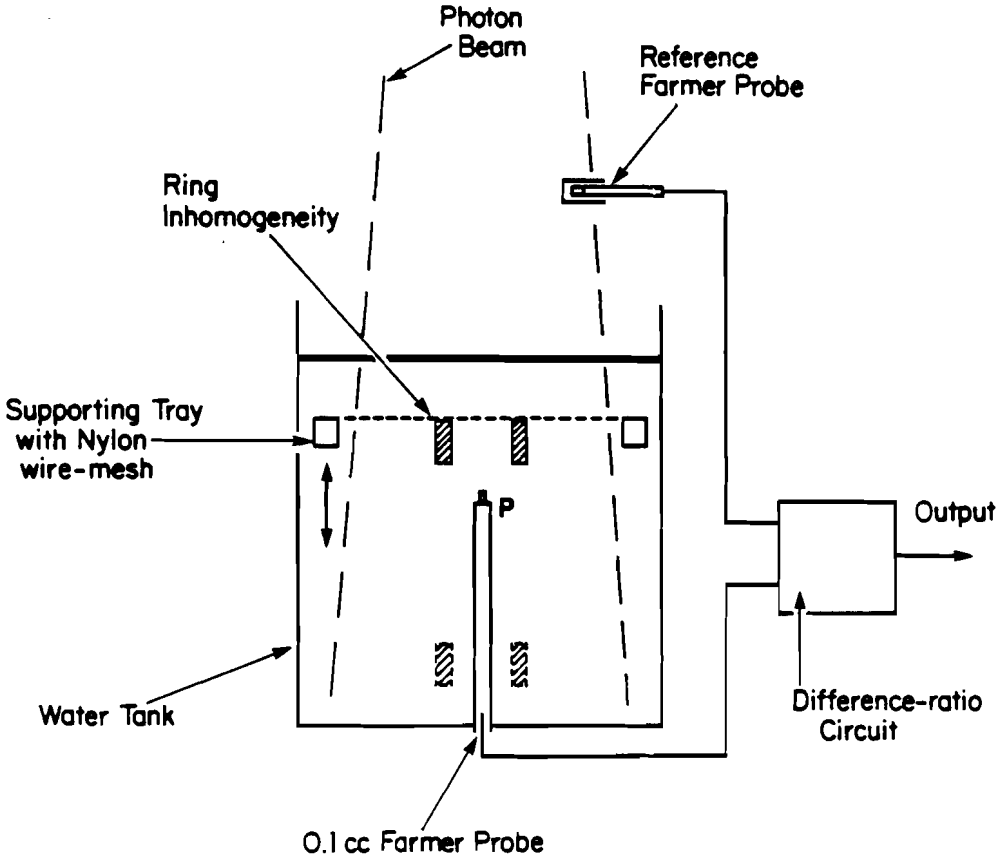

Figure 1. Dose perturbation measurement system.

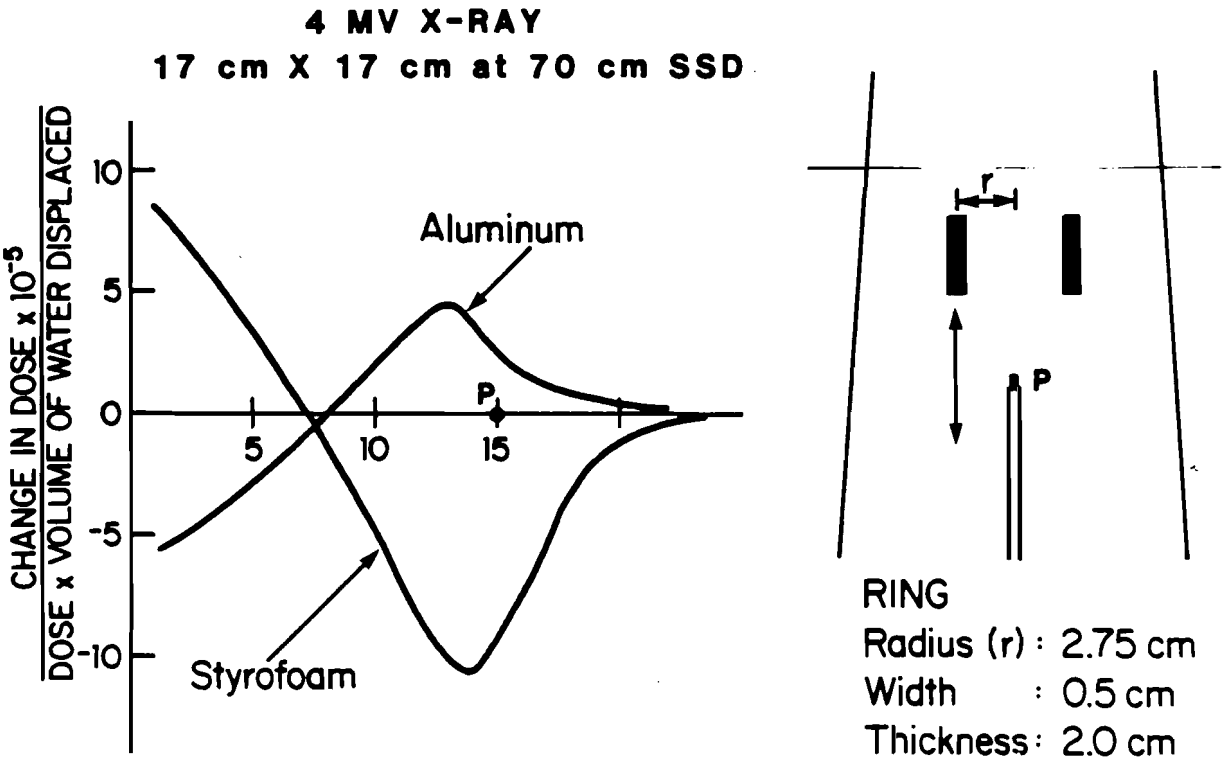

Figure 2. Measured dose perturbation due to aluminum and styrofoam in 4-MV X-ray beam.

Surprising results were observed for the higher energy 18-MV x-ray beam as shown in Figure 3. The ring inhomogeneities now have a radius of 1.75 cm, height of 2 cm and thickness of 0.5 cm. The differences between aluminum, carbon and styrofoam are dramatic. At the position of peak perturbation, the aluminum effect is about 30 times larger than that of styrofoam. This peak position is lateral to the detector and does not vary much with other ring configurations. Expectedly, this effect is primarily due to perturbation in electron transport. However, comparing the results for aluminum and graphite (which has roughly the same electron density as aluminum but roughly the same atomic number as water), led us to believe that this "local" effect related directly to pair-production interactions.

Using styrofoam rings of various radii for measurements, we were able to construct iso-effect maps to provide a clearer picture of the dose perturbations with respect to the position of the inhomogeneity in the medium. These are shown in Figure 4 for the photon energies of cobalt-60, 4-MV, 6-MV and 18-MV x-rays. With the exception of the 4-MV x-ray results, the shapes of the iso-effect maps demonstrate the dominance of small angle interactions as photon energy increases. The exception of the 4-MV results may be due to the increased contribution of multiple photon scattering due to the substantial low energy component of the bremsstrahlung beam spectrum. Figure 5 shows the iso-effect for the 18-MV x-rays with aluminum. Besides the expected reversal in polarity of the dose perturbations as compared to styrofoam, the large and yet very local pair-production contributions are clearly shown.

Results from these studies are new findings which illustrate the complexities of the effect of inhomogeneity on bremsstrahlung beam dosimetry. Models for pair-production are not readily available for the range of therapy photon energies, although it is shown here that pair-production interactions are significant and play a major role in the problem of electron transport.

We believe that elucidation of the many contributing factors to the overall dose perturbation is most important in the development of any model for dose calculation. For the next year we intend to:

(1) theoretically calculate these perturbation data by considering first-order, second-order photon transport and various electron transport models;

(2) deduce the importance of the many characteristics associated with therapy beams on dose calculations such as beam spectra and non-uniformity of the beam intensities;

(3) to continue our experimental measurements of dose perturbation with single and multiple inhomogeneities in order to obtain better models for pair-production phenomena and to examine whether empirical solutions such as that given by Rossi for photon energies >50 MV can be modified to provide an adequate model for the interactions; and finally

(4) identify the more important components in dose perturbation in terms of photon- and electron-transport such that they can be treated appropriately in the development of a practical algorithm.

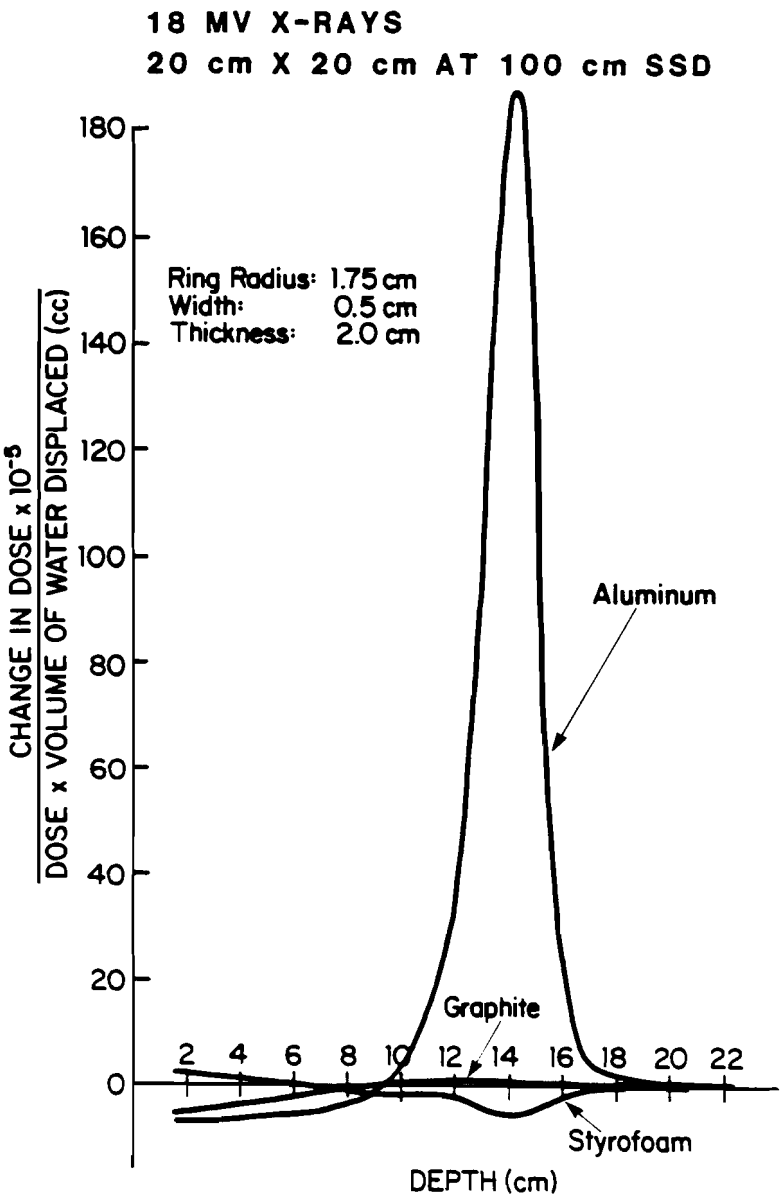

Figure 3. Measured dose perturbation due to aluminum and styrofoam in 18-MV X-ray beam.

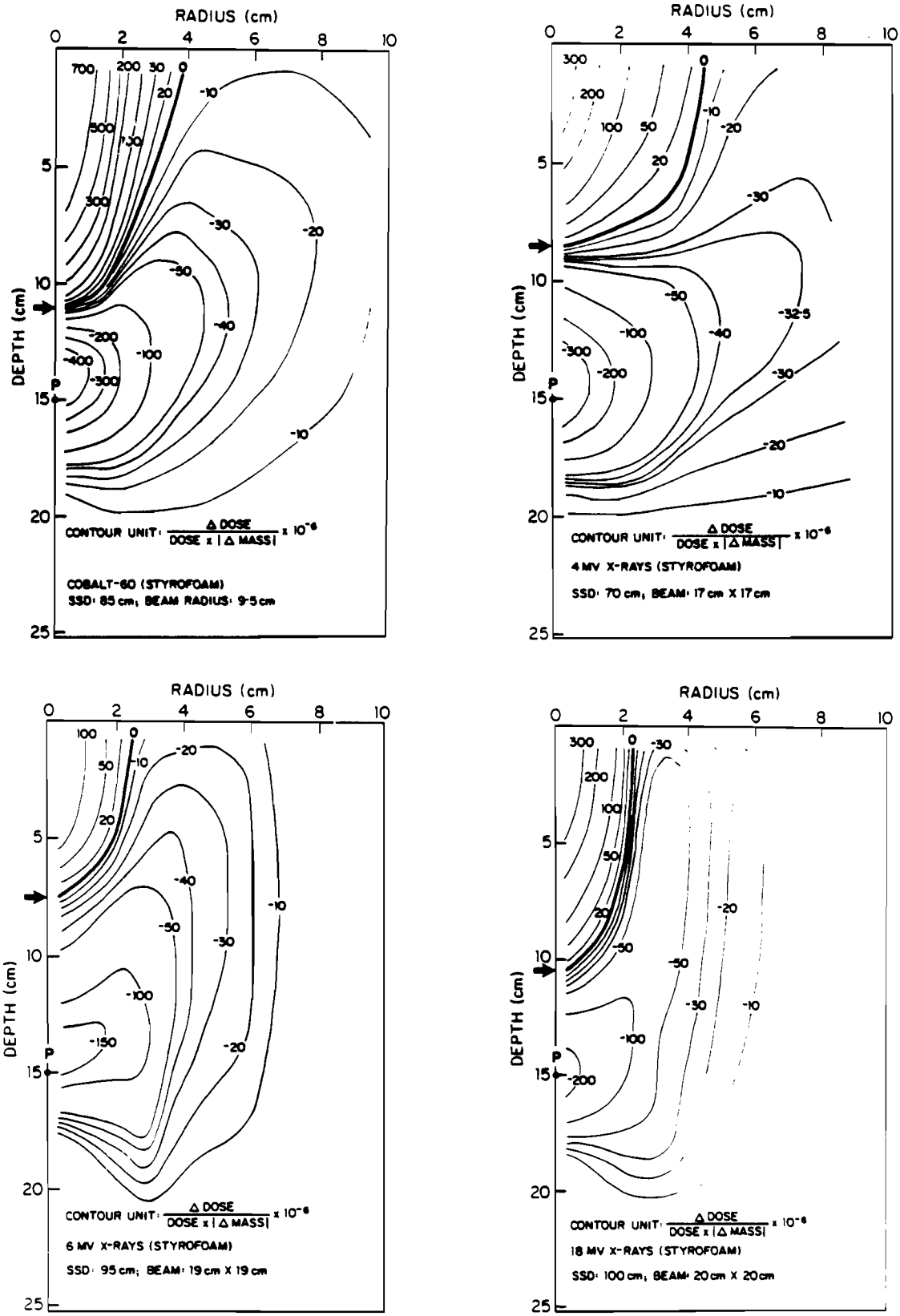

Figure 4. Iso-effect contours for styrofoam in Co-60, 4-MV, 6-MV, and 18-MV beams.

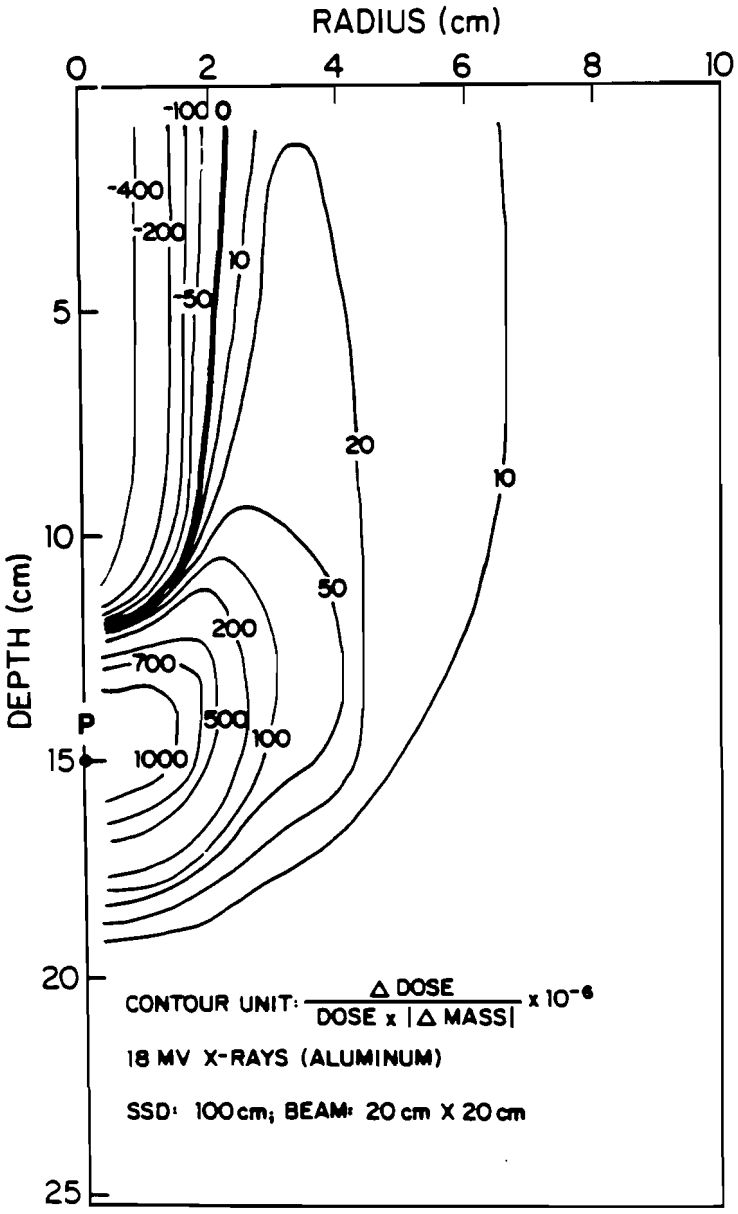

Figure 5. Iso-effect contours for aluminum in 18-MV X-ray beam.

D. Quantitative Imaging: Positron-Emission Tomography

Stimulated by the clinical impact of the EMI transmission tomographic scanner in 1973, experimental studies were initiated in collaboration with the Division of Radiation Sciences to evaluate positron coincidence-detection as a method for emission reconstruction tomography. This collaborative activity resulted in a prototype scanner called PETT (Positron-Emission Transaxial Tomograph). Extensive studies in patients and animals were conducted with the PETT III scanner in collaboration with the divisions of Neurology and Cardiology. A subsequent scanner, PETT IV, utilized concepts developed with its predecessor but incorporated a novel technique for the simultaneous collection of four tomographic slices from a single set of detectors. Until its decommissioning this past year, PETT IV was located in the Cardiac Care Unit for use in the SCOR project for the quantification of regions of myocardial ischemia and infarction (D-1, D-2). Subsequent scanners have been developed that permit more rapid data collection and improved spatial resolution. One of these, PETT V, was used in experimental studies in dog hearts. PETT VI became operational during the summer of 1980 and employs fast detectors and an entirely circular motion for rapid data acquisition. Further experimental and clinical studies with this system occurred over this past year (D-3, D-4). One of the most exciting recent developments for emission tomography results because of new developments in crystal technology and high-speed electronics. These now permit the propagation time of each of the two photons created in an annihilation to be measured. Theoretical and experimental studies of tomography systems that utilize this new information continued, and the software and hardware needed to realize the predicted benefits were developed. Super PETT-I, the first operational system utilizing time-of-flight information, has now been moved to the Cardiac Care Unit to replace PETT IV for use in the SCOR project (D-1, D-2). Studies to improve data acquisition and processing algorithms for Super PETT-I continued during the year (D-5 to D-9). Work continued on a new approach for estimating parameters in dynamic studies using list-mode data (D-10). A new time-of-flight instrument for neurological studies is under development (D-11, D-12). A reconstruction algorithm for single-photon tomography is being studied for use with data collected with a multiview gamma camera (D-13).

D-1. PETT Experimental Studies

Personnel: S. R. Bergmann, M.D., Ph.D., Medicine
K. A. A. Fox, M.B., Ch.B., Medicine
R. M. Knabb, Ph.D., Medicine
J. Markham, BCL
B. E. Sobel, M.D., Medicine
M. M. Ter-Pogossian, Ph.D., Radiology
M. J. Welch, Ph.D., Radiology

Support: HL 13851
HL 17646

The overall goal of this project is to implement and evaluate procedures required to translate into intact animals the results obtained with selected positron-emitting tracers used to characterize myocardial metabolism and perfusion in isolated hearts and anesthetized, open-chest dog studies performed with Isolated Probe Data Acquisition System (A-6). Utilizing positron-emission tomography with PETT VI, the distribution of tracer and the time course of its uptake and clearance from myocardium can be quantified. Such studies are intimately related to the clinical studies using positron-emission tomography (D-2).

During the past year, using $H_2{}^{15}O$ ($t_{1/2}$ = 2.1 min) we demonstrated that a modification of the tissue autoradiographic approach[1] permitted quantification of myocardial blood flow in open-chest dogs by direct assay of myocardium and subsequently extended that study to non-invasive estimation with positron-emission tomography in intact dogs.[1] In open-chest anesthetized dogs, the single pass extraction fraction of $H_2{}^{15}O$ averaged 96 ± 5% at flows of 80-100 ml/100/min. This high extraction fraction did not differ over the range 12-328 ml/100 gm/min. Flow calculated after 60 sec of intravenous infusion of $H_2{}^{15}O$ and direct analysis of tissue correlated well with results obtained with microspheres (r = .94, n = 9 dogs). Subsequently, the technique was adapted for use with PET by estimation of the myocardial content of radiolabeled $H_2{}^{15}O$ after intravenous infusion of 20-30 ml i.v. The activity in the myocardium was corrected for vascular activity with the use of tomographic data obtained after the administration of $C^{15}O$ by inhalation to label red blood cells. Tomograms obtained in vivo in 6 dogs with either normal or reduced regional blood flow correlated closely with tomographically detectable distribution of ^{68}Ga-microspheres (r = .93) with post-mortem microsphere distribution (r = .95). The use of this technique with PET should permit rapid subsequential non-invasive estimation of relative regional myocardial blood flow and should permit objective assessment of nutritional blood flow in patients in response to medical and surgical interventions designed to augment perfusion.

In an extension of the use of this technique, we performed an additional study to determine whether the method developed permits detection of the differences in blood flow in a dog preparation of sub-critical coronary stenosis. Coronary stenoses were induced with a small Teflon cylinder placed in the left anterior descending coronary artery of closed-chest dogs.[1] Regional myocardial blood flow was assessed tomographically with $H_2{}^{15}O$ given intravenously and $C^{15}O$ given by inhalation. Blood flow distal to the stenosis was normal under conditions of rest. However, significant reductions in the hyperemic response to

dipyridimole were detected consistently in regions distal to 50-70% diameter stenoses. Flow distal to the stenosis more than doubled in absolute terms (quantitatively determined with microspheres) in response to dipyridmole, but was only 43 ± 9% of the increase in flow in normal regions in the same dogs. Relative myocardial blood flow measured non-invasively with PET correlated closely with the distribution of radiolabeled microspheres in vitro (r = .88). Thus assessment of myocardial blood flow $H_2{}^{15}O$ and PET in dogs at rest and with vasodilator-induced stress permits detection of physiologically significant coronary stenosis. The procedure developed, therefore, should prove useful diagnostically for the detection of coronary insufficiency in patients, as well as for the assessment of clinical interventions designed to augment regional perfusion such as coronary thrombolysis or coronary artery bypass grafts.

We previously demonstrated that PET can be used to estimate the salutary response to coronary thrombolysis. These studies have continued during the current project year. To determine whether calcium blockage enhances salvage achieved in myocardium after coronary thrombolysis, thrombi were induced in 26 dogs with an intracoronary copper coil. Ten dogs had permanent occlusions. Thrombi were lysed in eight dogs with intracoronary streptokinase two hours after occlusion. The remaining eight dogs were given i.v. diltiazem (15μg/kg/hr) for 24 hours beginning 30 min before streptokinase. Regional myocardial blood flow was quantified with microspheres during occlusion, one hour after thrombolysis, and 24 hours later. Infarct size (% LV) was quantified by assay of myocardial CK depletion. Myocardial fatty-acid metabolism was assessed tomographically with ^{11}C-palmitate. Infarct size was maximal in controls (28 ± 12%, mean ± SD) and diminished by thrombolysis alone (18 ± 13%). Addition of diltiazem further reduced infarct size (9 ± 10%, $P < .05$ for each comparison). Myocardial blood flow was comparable in the three groups during occlusion, and diltiazem did not influence myocardial blood flow with reperfusion. Augmented salvage with diltiazem was documented by increased ^{11}C uptake at 24 hours (56% of normal vs. 40% for reperfusion alone). Thus the salvage of myocardium by thrombolysis is enhanced by calcium blockade with diltiazem by a mechanism other than increased perfusion, and can be documented with sequential analysis of myocardial perfusion and metabolism using positron tomography.

Although coronary thrombolysis restores macrovascular patency, as we have shown in open-chest dogs (A-6), even brief periods of ischemia followed by reperfusion impair myocardium metabolism. The prolonged effects of reperfusion on regional metabolism and nutritional perfusion, potentially compromised by the "no reflow" phenomenon, are unclear. Accordingly, we used positron emission tomography with $H_2{}^{15}O$ and ^{11}C-palmitate to sequentially assess myocardial perfusion and metabolism before and after angiographically documented lysis of occlusive coronary thrombi (occlusion interval of 2.5 hrs) and again at 24 hours, one week, two weeks, and four weeks after reperfusion. Myocardial blood flow (percentage normal) decreased to 18 ± 4% (mean ± SD) during ischemia. It averaged 82 ± 25% one hour after thrombolysis, but was reduced again to 37 ± 16% 24 hours later. Flow one week after lysis was 70 ± 5%, and persisted unchanged for two-four weeks (62 ± 7% and 60 ± 18%). During ischemia, ^{11}C activity varied from 14-50% of normal despite comparable ischemic flows. High ^{11}C-uptake one hour after reperfusion presaged greater perfusion and palmitate uptake at four weeks (r = .75 and .87 respectively). Thus positron emission tomography permits non-invasive characterization of the

long-term effects of coronary thrombolysis on myocardium. Early assessment with $H_2{}^{15}O$ and ^{11}C-palmitate provides useful predictors of the subsequent fate of myocardium after recanalization and should be useful for studies of experimental adjunctive therapy with reperfusion, as well as sequential evaluation of the efficacy of thrombolysis in patients.

The studies completed during the past year have demonstrated the utility of PET for evaluation of myocardial metabolism and perfusion, especially in sequentially evaluating the efficacy of interventions designed to improve myocardial metabolism and perfusion after coronary ischemia. The techniques developed in the project are currently being implemented in patient studies designed to evaluate the efficacy of coronary thrombolysis utilizing Super PETT-I.

During the coming year, we plan to continue our evaluation of the effects of coronary thrombolysis on the restoration of myocardium perfusion and metabolism with PET to better characterize the response of this promising intervention. Furthermore, we plan to evaluate algorithms for correction of the effects of partial volume and count spillover as well as institution of the evaluation of the EM algorithm for cardiac studies. This should enable measurements of perfusion in absolute terms.

1. S. R. Bergmann, K. A. A. Fox, A. L. Rand, K. D. McElvany, M. J. Welch, J. Markham, and B. E. Sobel, "Quantification of Regional Myocardial Blood Flow in Vivo with $H_2{}^{15}O$," Circulation, vol. 70, pp. 724-733, 1984.

2. R. M. Knabb, K. A. A. Fox, B. E. Sobel, and S. R. Bergmann, "Characterization of the Functional Significance of Subcritical Coronary Stenoses with $H_2{}^{15}O$ and Positron Emission Tomography," Circulation, vol. 71, pp. 1271-1278, 1985.

3. R. M. Knabb, K. A. A. Fox, B. E. Sobel, and S. R. Bergmann, "Sequential Tomographic Assessment of Myocardial Perfusion and Metabolism after Coronary Thrombolysis," Circulation, in press.

4. S. R. Bergmann, K. A. A. Fox, E. M. Geltman, and B. E. Sobel, "Positron Emission Tomography of the Heart," Progressive Cardiovascular Diseases, in press.

D-2. Super PETT I Cardiac Studies

Personnel: E. M. Geltman, M.D., Medicine
H. D. Ambos, Medicine
T. R. Baird, Medicine
D. E. Beecher, BCL
A. S. Jaffe, M.D., Medicine
J. Markham, BCL
B. E. Sobel, M.D., Medicine
M. M. Ter-Pogossian, Ph.D., Radiology
M. J. Welch, Ph.D., Radiology

Support: RR 01380
HL 13851
HL 17646

This project was designed to assess regional myocardial metabolism and perfusion quantitatively with positron-emission tomography (PET) in normal subjects and patients with coronary artery disease at rest and with stress induced with vasodilators or dynamic exercise. These studies were also designed to employ PET to assess the efficacy of reperfusion induced by thrombolysis, balloon angioplasty, surgical revascularization or their combination.

Studies in this project have been performed with Super PETT I, a positron-emission tomograph which incorporates time-of-flight information to provide seven simultaneous axial high resolution (7.5 mm FWHM) reconstructions throughout the heart with data collections as brief as 30 seconds, permitting dynamic acquisition in list mode. Dynamic cardiac studies were performed after the i.v. injection of 20 mCi of ^{11}C-palmitate in 11 normal subjects and eight patients with cardiac disease. During 30-minute data collections, data density was sufficient to reconstruct images at 30-second time intervals during the first two minutes, one-minute time frames through 10 minutes, and two- to four-minute time frames thereafter providing high-time activity curves with high temporal resolution. Myocardial accumulation of ^{11}C-palmitate was homogeneous in controls, and depressed in zones of infarction. In some cases, depressed metabolism was evident in zones with persistent perfusion (assessed with the intravenous infusion of $H_2{}^{15}O$ and the inhalation of $C^{15}O$ as validated in dogs). Peak radioactivity generally occurred between the fourth and sixth minutes and turnover of ^{11}C-palmitate was monoexponential from peak activity through 12-15 minutes after injection, after which the time-activity curves (corrected for physical decay of the isotope) demonstrated a very long half-time. Regions of infarction demonstrated decreased content of palmitate and slightly longer disappearance times.

Assessment of myocardial perfusion was performed in nine normal subjects and 19 patients with cardiac disease. Patients were studied after the bolus injection of 30-100 mCi of $H_2{}^{15}O$. Data collection began immediately upon injection of $H_2{}^{15}O$ and continued for at least 120 seconds. Data were reconstructed from multiple time intervals to determine the optimum period for data collection and analysis. After a delay of 10 minutes to allow decay of the initial tracer, patients were studied again after the inhalation of 50-75 mCi of $C^{15}O$ to label the cardiac blood pool. Data collection commenced approximately 30 seconds after the inhalation of

$C^{15}O$ and continued for five minutes. After reconstruction of axial matrices a pixel-by-pixel subtraction was performed of the tomograms acquired with $C^{15}O$ from the tomograms reconstructed from the data collected after the infusion of $H_2{}^{15}O$. The distribution of $H_2{}^{15}O$ (corrected for blood pool activity) was apparently homogeneous throughout ventricular myocardium in normal subjects, closely matching the distribution of radioactivity observed after administration of ^{11}C-palmitate. Among patients with transmural infarction and a persistently occluded vessel, defects in accumulation of $H_2{}^{15}O$ were observed in regions corresponding to the ECG locus of infarction and zones of decreased accumulation of ^{11}C-palmitate. However, in some patients in whom the infarct related artery had recanalized (spontaneously or with thrombolysis) $H_2{}^{15}O$ was evident in the zone of prior myocardial infarction, with an apparent mismatch between depressed accumulation of palmitate and restoration of myocardial perfusion.

Positron-emission tomography continues to be employed in the analysis of interventions designed to salvage ischemic myocardium. It is being used as an endpoint for studies of the efficacy of nifedipine, a calcium channel blocker, and for the salvage of ischemic myocardium in the setting of acute myocardial infarction. The enrollment of patients in this study has now been completed with a total of over 50 patients studied. Data analysis is currently underway and should be completed shortly. Interim analyses have shown a tendency towards salvage of ischemic myocardium with nifedipine. Patient studies continue with thrombolysis induced by tissue plasminogen activator or streptokinase administered within the first hours after infarction. At the present time the number of patients studied is too small to permit definitive conclusions concerning the ultimate extent of salvage of ischemic myocardium provided by these interventions.

To determine the relative sensitivity of PET and magnetic resonance imaging (MRI) for the detection and characterization of cardiomyopathy, and to determine the impact of wall thickness and attendant partial volume effects on PET images, 11 patients (six males and five females) aged 20 to 75 years with congestive cardiomyopathy were studied with both modalities. All were studied with multi-planar ECG gated proton MRI employing a superconductive 0.35 Tessla magnet and spin echo technique (echo-delays of 30 and 60 msec) and PET performed with ^{11}C-palmitate. PET revealed marked spatial heterogeneity of the accumulation of palmitate manifested by an increased number of discrete isocount zones during multiple threshold analysis (17.3 ± 0.8) regions vs 11.8 ± 0.7 in normal controls, $p < .01$) indicative of heterogeneous accumulation of a tracer of metabolism not accounted for by regional wall thinning or partial-volume effects. In contrast, although MRI delineated cardiac dilation with considerably higher spatial resolution, myocardial walls were of uniform thickness and myocardial signal intensity with MRI was visually relatively homogeneous with slight speckling. The standard deviation of the frequency distribution of signal intensity within myocardial reconstructions was extremely narrow, averaging only $6.3 \pm 1.1\%$ of mean myocardial signal intensity. Thus, magnetic resonance imaging and positron emission tomographic delineation of metabolism provide complementary information which, in concert, more thoroughly define the nature of underlying pathophysiology.

Clinical studies in progress are concerned with the further characterization of dynamic fatty acid metabolism in myocardium of normal subjects, patients with ischemic heart disease with and without reperfusion induced by coronary thrombolysis with rT-PA and patients with cardiomyopathies. Studies of the distribution of myocardial perfusion with $H_2{}^{15}O/C^{15}O$ are being continued to acquire a larger data base of normal subjects and patients with single or multi-vessel coronary artery disease. These patients are to be studied both at rest and after vasodilator stress with dipyridamole. Initial results are encouraging with myocardial perfusion remaining homogeneous in normal subjects during vasodilator stress, but demonstrating stress induced perfusion defects in patients with obstructive coronary lesions, even in the absence of infarction.

D-3. In Vivo Measurements of Regional Blood Flow and Metabolism in Brain

Personnel: M. E. Raichle, M.D., Neurology and Radiology
D. C. Ficke, B.S., Radiology
P. T. Fox, M.D., Neurology and Radiology
M. H. Gado, M.D., Radiology
R. L. Grubb, Jr., M.D., Neurological Surgery
P. Herscovitch, M.D., Neurology and Radiology
M. R. Kilbourn, Ph.D., Radiology
K. B. Larson, BCL
J. L. Lauter, Ph.D., Central Institute for the Deaf
J. Markham, BCL
M. A. Mintun, M.D., Neurology
J. S. Perlmutter, M.D., Neurology
W. J. Powers, M.D., Neurology and Radiology
D. L. Snyder, BCL
A. G. Swift, M.A., Radiology
M. M. Ter-Pogossian, Ph.D., Radiology
M. J. Welch, Ph.D., Radiology

Support: RR 01380
HL 13851
HL 25944
NS 06833
ECS 8215181
Washington University

Because of the previously noted (PR 20, D-3) deficiencies of compartmental models for estimating cerebral blood flow with PET using radioactive water as a tracer, we have been led to the formulation and testing of distributed models for this purpose. The distributed models we have investigated take into account longitudinal gradients of tracer concentration along the capillaries but assume that transverse gradients are zero. The resulting conservation conditions take the form of sets of partial differential equations in the concentrations, with axial distance and time as independent variables and with capillary and cellular permeabilities, surface areas, volumes, and thermodynamic activity coefficients as parameters.

Using an analytical solution of these equations, we have compared the predictions of our model unit-impulse response with our data for the uptake and clearance of radiolabeled water in rhesus monkey brain following bolus injection of the tracer into an internal carotid artery of the animal. The data are in the form of count-rate histograms obtained with a single scintillation detector collimated over the animal's head. The durations of the histogram data-collection intervals were made short enough to ensure proper temporal resolution for the residual histories. Typically, a data set consisted of 70 points collected over 180 sec. Data were collected in four experiments for which cerebral blood flow, determined by an independent method, was varied from 0.53 to 1.33 ml $min^{-1} g^{-1}$. Also measured independently were values of blood-brain-barrier permeability-surface-area product; these were varied between 1.33 and 1.72 ml $min^{-1} g^{-1}$. Since our data are for dose-normalized intracarotid injections, they and the model unit-impulse responses are directly comparable. To quantify our comparisons, we devised a statistical parameter-estimation procedure for fitting the model to the data. We obtained estimates of the parameter values using weighted nonlinear least-squares approximation. The minimization we employed was a suitably modified version of that of Marquardt.[1] In fitting our model, the final parameter estimates differed only slightly when different initial estimates were used. Although a systematic search of the parameter space was not undertaken, each case was run with at least three different initial estimates. The low values attained for the standard deviation of the estimates also suggest that the solutions are unique. Fractional deviations between parameters estimated from the data on the basis of the model varied from 3% to 11% for flow and from 2% to 32% for permeability-surface-area product.

Encouraged by these results, we plan to investigate the possibility of applying our model for measuring cerebral blood flow using positron-emission tomography (PET) in a clinical setting. New difficulties are anticipated for this undertaking. Clinical practice precludes use of intracarotid injections; instead tracer can be only administered intravenously, resulting in temporal dispersion of tracer inflow to the cerebral vasculature. Moreover, the limited temporal resolution achievable by current PET devices results in accumulation of only a few (typically ~ 12) data points representing the history of the cumulative number of detected decay events. In practice, this limits the number of parameters that can be estimated from the data to one, or at most, two. In preparation for clinical trials of our model, we have devised algorithms for simulating response of an external detector following i.v. injections. For this, we have convolved simulated arterial radioactivity histories with integrals of our model unit-impulse responses. We plan to study the performance of the resulting dispersed integrated residue curves as objective functions for parameter estimation in simulations and in further animal experiments in which we employ i.v. tracer administration and record real arterial radioactivity histories. Through use of sensitivity functions for the convolved and integrated model functions, we plan to identify optimum times for data collection such that one or two desired parameters (blood flow and perhaps blood-brain-barrier permeability) can be estimated from the relatively small data sets, with the remaining parameters set to average values.

A specialized parameter estimation technique, designed to estimate kinetic parameters for PET studies of brain receptors, was implemented for

routine use. This technique utilizes a three-compartment model, describing the kinetics of spiperone in brain tissue, to evaluate time-activity curves of regions of brain after injection of ^{18}F-spiperone in baboons and patients. Parameters estimated from the model include the blood-brain-barrier permeability for spiperone and brain receptor density.

The parameter estimation method uses a specialized algorithm for the first few iterations, then switches to a nonlinear least-squares approximation routine. Sensitivity analysis was employed to develop relationships between variations in the values of the parameters and variations in the tissue-activity curves. These relationships can be expressed by a simple mathematical function, resulting in very rapid convergence.

D-4. Maximum-Likelihood Image Reconstruction for PETT VI

Personnel: J. D. Gorman, BCL
M. I. Miller, BCL
M. A. Mintun, M.D., Neurology and Radiology
D. L. Snyder, BCL
A. G. Swift, M.A., Radiology

Support: RR 01380
RR 01379
HL 13851
ECS 8215181

Recent important results obtained with the expectation-maximization (EM) algorithm solution to the maximum-likelihood equation for real PETT VI studies (PR 20, D-4) have prompted a series of simulation studies to quantify algorithm performance. Software was developed to simulate PETT VI data collections and two simulation phantoms were created for use in simulation studies: a calibration pie phantom containing six regions of uniform activity, and a brain phantom, having a grey to white ratio of 4:1. Additional software was developed to evaluate PETT VI images. Metrics used to gauge algorithm performance were resolution, signal-to-noise ratio (SNR), contrast, and squared error.[1] With these software tools, several maximum-likelihood reconstruction techniques were investigated. The unconstrained maximum-likelihood algorithm[2] and the constrained algorithm employing the "method of sieves"[3] were of particular interest.

Initial studies were conducted to investigate and document the behavior of iterates obtained with the EM algorithm for unconstrained maximum-likelihood. The unconstrained maximum-likelihood images were shown to have superior resolution and contrast, and less squared error than images obtained with filtered backprojection.[1] In fact, the measured resolution of brain-phantom reconstructions was 6.8 mm after 500 iterations. This should be compared with a measured resolution of 12 to 17 mm for filtered backprojection reconstructions. Moreover, unconstrained maximum-likelihood reconstructions of brain phantom data contained 94% of

the original contrast between grey and white matter regions, whereas the corresponding contrast in filtered backprojection images was only 50-63%.

The expectation-maximization algorithm is iterative; the maximum-likelihood estimate is defined as the limit of the sequence of iterates obtained from the EM algorithm. Thus, although the iterative process eventually results in a maximum-likelihood estimate, intermediate iterations may contain biases associated with the convergence of the estimator. One indication of the presence of such biases is the fact that the resolution of images obtained by EM iteration changes with iteration. The measured resolution of pie phantom reconstructions was 9.4 mm after 50 iterations and 5.9 mm after 1000 iterations. In regions of the reconstructions where there are discontinuities, we observe overshoot artifacts which diminish as the iteration process continues. These overshoot artifacts appear, for example, in pie-wedge corners in the reconstruction of simulated and real pie-phantom data after 100 iterations and are approximately 120% of the underlying intensity. Moreover, the EM algorithm is a gradient-based algorithm, implying a linear convergence rate. Pixel values in the pie phantom change by less than 0.1% per iteration after 100 iterations. Thus, these artifacts may still be present after several hundred iterations. We have chosen to iterate until pixel changes fall below 0.05%; this requires between 500 and 1000 iterations for both the brain and pie phantoms.

Also present in the unconstrained maximum-likelihood images is a noise artifact. In both real and simulated data, estimates of uniform regions of activity are speckled, or contain peaks and valleys. This artifact results in decreased SNR and appears to be related to the intensity of the phantom. In one study we varied the number of counts collected in a simulated data collection. At an average intensity of 5340 counts/pixel the SNR of the resulting reconstruction was 21 dB after 1000 iterations, whereas for an intensity of 53.4 counts/pixel, the SNR fell to 6 dB. The effect of the convolution-kernel sieve constraint employed in the algorithm derived by Snyder and Miller[3] is to reduce the noise artifact present in the reconstructions.

We examined the reconstructions of several simulated pie phantom data collections subject to kernel sieves which had kernel widths[3] equal to 75, 100, 125, and 150 percent of the full-width at half maximum (FWHM) of the PETT VI detector resolution (1.17 cm). As the sieve parameter increased, the SNR of the reconstructions also increased, while the resolution decreased. The table below lists values of SNR, resolution, and sieve parameter for the pie phantom simulation containing 53.4 counts per pixel after 1000 iterations. This simulation corresponded to a 20 cm pie phantom having an average of 100k counts.

SNR and Resolution vs Sieve Parameter
for Pie Phantom Simulation

Sieve Parameter	SNR (dB)	Resolution (mm)
0.0 FWHM	5.1	5.8
0.75 FWHM	13.0	7.5
1.0 FWHM	15.2	9.3
1.25 FWHM	16.7	10.5
1.5 FWHM	17.8	13.6

1. J. D. Gorman, "Quantitative Evaluation of the Maximum-Likelihood Reconstruction Algorithm for PETT VI," Biomedical Computer Laboratory Working Note No. 73, September 1985.

2. Y. Vardi, L. A. Shepp, and L. Kaufman, "A Statistical Model for Positron Emission Tomography," Journal of the American Statistical Association, vol. 80, no. 389, pp. 8-37, March 1985.

3. D. L. Snyder and M. I. Miller, "The Use of Sieves to Stabilize Images Produced with the EM Algorithm for Emission Tomography," to appear in the IEEE Transactions on Nuclear Science, 1985.

D-5. Time-of-Flight Data Acquisition System Development for Super PETT I

Personnel: D. C. Ficke, B.S., Radiology
D. E. Beecher, BCL
G. R. Hoffman, B.A., Radiology
T. J. Holmes, D.Sc., Radiology
D. G. Politte, M.S., Radiology
M. M. Ter-Pogossian, Ph.D., Radiology

Support: RR 01380
HL 13851

Super PETT I has been relocated to the Coronary Care Unit and is routinely used for cardiac studies (D-2).

The gantry and custom electronics (PR 20, D-6) have been interfaced to a newly acquired Perkin Elmer 3230 host computer for system operation. The host configuration includes 4 Mbytes of main memory, floating-point hardware, writable control store, cache memory, and six selector channels for high-speed communications. System peripherals include an 80-Mbyte fixed-media disk, two 300-Mbyte removable-media disks for list-mode data collection, and a Ramtek 9400 display system for image viewing.

The addition of the second list-mode data disk and the upgrade to high-speed protocol on the gantry interface now support a maximum continuous event transfer rate in excess of 400,000 events per second.

Single-pass list-mode processing for seven slices with a reduced angle reconstruction algorithm (D-6) is now possible with the available memory. Retrospective processing with respect to the constraints of gating and time segmenting is optional, requiring a preliminary pass on the list-mode data for parameter selection.

D-6. A Reduced-Angle Reconstruction Algorithm for Super PETT I

Personnel: D. G. Politte, M.S., Radiology
D. E. Beecher, BCL
D. C. Ficke, B.S., Radiology
G. R. Hoffman, B.A., Radiology

Support: RR 01380
HL 13851
HL 17646

A software system which executes an algorithm similar to confidence-weighting, but with the "reduced-angle" technique, has been in use for routine image-reconstructions during the past year.

The motivations for use of this technique are that the required memory size and the reconstruction time are lessened. The required memory size is diminished because the measurement array now has 16 (angle) x 128 (distance) x 40 (time-of-flight) elements, whereas it formerly had 96 (angle) x 128 (distance) x 40 (time-of-flight) elements. Thus, the measurement array for several slices may be built and stored in memory simultaneously, without additional passes through the list-mode data, as had been required previously. The reconstruction time is further reduced because the angle-dependent portions of the processing are performed only 16 times instead of 96 times.

Developments during the past year include:

- The memory of the Perkin-Elmer 3230 host computer has been augmented so that only one pass through the list-mode data is necessary for most studies. The time to process seven slices of emission data with approximately one million counts per slice has been reduced from forty-five minutes to thirty minutes, assuming that the processing of the blank and transmission scans (used for calibration and data correction) has already been done. The corresponding time when the reduced-angle technique is not used is two and one-half hours.

- The weighting function used has been found to be suboptimal. The advantage of the suboptimal weighting function is that the two-dimensional convolution which performs the weighting step may be implemented as two one-dimensional convolutions, with a resulting computational efficiency. The optimal weight, which has not been implemented, does not possess this property. Optimal weighting corresponds to true confidence-weighting when the measured angle is

not known exactly, but is known to be uniformly distributed over a known range.

- The final filters which compute an image from a pre-image (when either optimal or suboptimal weighting functions have been used) have been derived. The latter has been implemented.

A systematic simulation study has been undertaken to measure the effect of the suboptimal or the optimal reduced-angle techniques on image signal-to-noise ratio and resolution, as a function of the number of angles and the reconstructed resolution of the image. It should be emphasized that the reduced-angle technique will not perform better than true confidence-weighting;[1] the motivation for its use is its relative computational efficiency .

1. D. L. Snyder, "Preimage Selection in Time-of-Flight Emission Tomography," IEEE Transactions on Nuclear Science, vol. NS-30, no. 1, pp. 701-702, February 1983.

D-7. The Use of Sieves to Stabilize Images Produced with the EM Algorithm for Emission Tomography

Personnel: D. L. Snyder, BCL
M. I. Miller, BCL

Support: RR 01380
RR 01379
HL 13851
ECS 8215181

Images produced in emission tomography with the expectation-maximization (EM) algorithm have been observed to become more 'noisy' as the algorithm converges towards the maximum-likelihood estimate. We argue that there is an instability which is fundamental to maximum-likelihood estimation as it is usually applied and, therefore, is not a result of using the EM algorithm, which is but one numerical implementation for producing maximum-likelihood estimates.[1] We show how Grenader's method of sieves can be used with the EM algorithm to remove the instability and thereby decrease the 'noise' artifact introduced into the images with little or no increase in computational complexity.

1. D. L. Snyder and M. I. Miller, "The Use of Sieves to Stabilize Images Produced with the EM Algorithm for Emission Tomography," Biomedical Computer Laboratory Monograph No. 464, April 1985.

D-8. Design Studies of Computational Alternatives for TOF-Based PET Reconstructions

Personnel: S. M. Moore, BCL
T. J. Holmes, D.Sc., Radiology

Support: RR 01380
HL 13851

Use of the maximum-likelihood (ML) algorithm for time-of-flight-based image reconstruction[1,2] is currently not feasible in a clinical setting due to excessive computational requirements. Phantom studies for algorithm evaluation performed on VAX-class computers require on the order of one to three days to perform fifty iterations of the ML algorithm. Methods for reducing computation time include restructuring the algorithm to take advantage of the geometrical properties of the detection process and computing the estimates on high-performance or specialized processors rather than on general purpose computers.

The most time-consuming step in the present implementation of the algorithm is the application of a two-dimensional Gaussian filter to the current estimate of the radioactivity distribution and to the count data for each of the detector angles. By performing the filtering step in the data collection space (radial distance, TOF) rather than in the image viewing space (x,y), it is possible to reduce the number of computations by a factor of 10.

Even with this reduction, image reconstruction cannot be performed on a super minicomputer system in a clinically acceptable time. Benchmark studies indicate that an array processor coupled to a supermini can reduce the time needed to reconstruct one slice to one hour. Special purpose processors will be needed to achieve reconstruction times on the order of one minute for a single slice. Custom-designed VLSI circuits can be used to perform coordinate transformations which will allow the filtering steps to be performed in the <distance, TOF> space. Multiple processors can be used to process data collected at each angle in parallel rather than serially. With the appropriate architecture and taking advantage of custom VLSI designs, a clinical study consisting of seven slices can be reconstructed using the ML algorithm in less than five minutes.[3]

1. L. A. Shepp and Y. Vardi, "Maximum-Likelihood Reconstruction for Emission Tomography," IEEE Transactions in Medical Imaging, vol. MI-1, no. 2, pp. 113-121, October 1982.

2. D. L. Snyder and D. G. Politte, "Image Reconstruction from List-Mode Data in an Emission Tomography System Having Time-of-Flight Measurements," IEEE Transactions on Nuclear Science, vol. NS-30, pp. 1843-1849, 1983.

3. S. M. Moore and T. J. Holmes, "M-L Algorithm: Computation Time Estimates for Custom Processor-Based Implementations," BCL Working Note No. 61, 1984.

D-9. Effects of Positron-Emission Tomography Scintillation Detectors on Resolution and Sensitivity

Personnel: D. C. Ficke, B.S., Radiology
T. J. Holmes, D.Sc., Radiology
M. M. Ter-Pogossian, Ph.D., Radiology

Support: RR 01380
HL 13851

The analytic studies initiated in PR 20, D-11 have been continued and reported,[1] including experimental results for a particular detector geometry which tend to validate the model used. In particular, the normalized resolution uniformity of detectors being developed for Super PETT II (D-12) has been accurately predicted, thereby encouraging the application of the model to other detector geometries.

The findings indicate that a triangular face added to the present Super PETT II detector should improve the system sensitivity, while reducing the total length of the detector should improve the resolution uniformity at the expense of reduced sensitivity. In conjunction, these modifications might yield an improved performance over the present design.

It should be noted that the analytic model used considers only the first interaction of each photon, hence the absolute values obtained do not coincide with the measured results which include multiple interactions. Therefore, experimental verification is required. In addition, there may be technological problems in constructing a module with the triangular faced detectors.

1. T. J. Holmes and D. C. Ficke, "Analysis of Positron-Emission Tomography Scintillation Detectors with Wedge Faces and Inter-Crystal Septa," IEEE Transactions on Nuclear Science, vol. NS-32, no. 1, pp. 826-830.

D-10. Maximum-Likelihood Estimation of Parameters in Dynamic Tracer Studies

Personnel: J. M. Ollinger, BCL
D. L. Snyder, BCL

Support: RR 01380
RR 01379
ECS 8215181

The advent of positron-emission tomography (PET) made possible for the first time non-invasive, regionally localized parameter estimation in dynamic tracer studies. Despite the hope that multicompartment models developed for single-probe experiments could be readily adapted for use with PET, investigators find that this is often not the case due to the poor time resolution of the data available to them. Data are currently collected by reconstructing a series of images over the time course of the study, spatially integrating each image over a region of interest to form a histogram of activity levels versus time, and then estimating parameters from this histogram. Since each image must span a time subinterval containing enough counts to yield an adequate image, the total number of subintervals in the histogram is limited. Since the compartmental models used for dynamic tracer studies frequently require that data be collected over a short time interval, and that parameters with short time constants be estimated, this limitation results in either degraded estimation accuracy or in inability to perform the experiment.

Snyder[1] proposed a method that solves this problem by using the EM algorithm of Dempster, Laird, and Rubin[2] to compute the maximum-likelihood parameter estimates from list-mode data, that is, from data which contain a record of each detected annihilation. The method can be decomposed into two algorithms, a weighting algorithm, which estimates a histogram of activity levels from list-mode data, and an estimation algorithm, which computes parameter estimates from this histogram. The research effort during the past year has been directed at evaluating this method.

The weighting algorithm computes an approximate minimum-mean-square error estimate of the histogram based on the Poisson statistics of the list-mode data. This estimate cannot be computed exactly, since it depends on the tracer concentration, which, being both unknown and non-stationary, must be approximated by a series of reconstructed images. The algorithm consists of first reconstructing images over each of a number of time intervals, identifying a region of interest in each image, if this is not already known, computing probability arrays for each interval, weighting each detected event with the probability that it occurred in the region of interest and, finally, summing the weighted events into a histogram. Since the number of subintervals in the histogram is limited only by the time resolution of the list-mode data, the output histogram can have the same number of subintervals as if it were collected with a single probe. These high-resolution histograms can be used with either the maximum-likelihood estimation algorithm discussed here or with any of the commonly used weighted least-squares algorithms. Initial results of the evaluation of this algorithm indicate that the final parameter estimates are significantly more accurate than those obtained by conventional methods when compared in terms of their bias and the standard deviation of their error.

The parameter-estimation algorithm is an iterative method of computing maximum-likelihood estimates. An evaluation of this algorithm[3] indicates that its estimates are unbiased, that the variance of the error is near the theoretical minimum as given by the Cramer-Rao bound, and that the algorithm converges even for very poor starting values. Furthermore, in every simulation, the algorithm converged either to a unique maximum close to the true value, or to an easily recognized local maximum where two or more parameter values were equal. The major drawback to the algorithm is its linear convergence rate, which can be quite slow. Our first approach to resolving this problem was to implement a line-search along the ascent direction given by the EM algorithm. Initial results are promising, showing a speed improvement of a factor of two.

In the next year we plan to complete the evaluation of the weighting algorithm, extend it to include the effects of randoms and attenuation, and to evaluate it using real data. We intend to further investigate the uniqueness of the estimation algorithm and to try other methods for accelerating convergence.

1. D. L. Snyder, "Parameter Estimation for Dynamic Studies in Emission Tomography Systems Having List-Mode Data," IEEE Transactions on Nuclear Science, no. 2, pp. 925-932, April 1984.

2. A. P. Dempster, N. M. Laird, and D. B. Rubin, "Maximum Likelihood from Incomplete Data via the EM Algorithm," J. R. Statistical Society, vol. 39, pp. 1-38, 1977.

3. J. M. Ollinger and D. L. Snyder, "A Preliminary Evaluation of the Use of the EM Algorithm for Estimating Parameters in Dynamic Tracer Studies," IEEE Trans. on Nuclear Science, no. 1, pp. 848-854, February 1985.

D-11. Slice Processor Selection for Super PETT II

Personnel: D. E. Beecher, BCL
D. C. Ficke, B.S., Radiology
D. G. Politte, M.S., Radiology

Support: RR 01380
HL 13851

Careful analysis of the collection and processing requirements for Super PETT II have demonstrated the need for fast, distributed processors for each slice in the new generation machine called Super PETT II. Selection of the processor to fulfill these needs was based on the price/performance of several commercially available products. The final selection was the Perkin-Elmer 3205 processor with one to two megabytes of main memory, depending on the scanner it will support (i.e. a head or a body unit). Each slice of the scanner is supported by a single 3205

processor capable of collecting up to one million counts per second for that particular slice.

We have successfully implemented a multi-processor system to support Super PETT II. The configuration is as shown in PR 20, D-16, Figure 2. We expect this system to be fully operational by the beginning of calendar year 1986.

D-12. Super PETT II Detector Design

Personnel: D. C. Ficke, B.S., Radiology
G. L. Engel, BCL
R. O. Gregory, BCL
T. J. Holmes, D.Sc., Radiology
J. T. Hood, Sr., B.S., Radiology
M. M. Ter-Pogossian, Ph.D., Radiology

Support: RR 01380
HL 13851

The detector module described in PR 20, D-17 has been refined and targeted for use in Super PETT II, which is now under development. The critical components of the module consist of eight barium fluoride scintillation detectors (7x24x45mm) which are grown, cut, and polished on all surfaces by Harshaw Chemical; and five Hamamatsu R2076 photomultiplier tubes with associated divider networks. Reflection of the scintillation is achieved with 0.1 mm centered Teflon and inter-crystal scattering is reduced with the use of 1.25 mm tungsten septa. The critical components are assembled into an aluminum housing with light-tight adhesives to form the finished module. Approximately 20% of the required 285 modules for two instruments have been assembled and tested.

Previous work on a novel detector employing a micro-channel plate and a special high-gain amplifier has been discontinued. Local facilities at Washington University and at commercial firms were found to be inadequate for achieving reliable photocathode deposition. The primary difficulty was deterioration of the photoemissive characteristic with time. It became clear that with other stringent requirements for detector fabrication, the expense would be prohibitive if pursued with commercial firms elsewhere.

D-13. Maximum-Likelihood Reconstruction for Single-Photon Emission Computed-Tomography

Personnel: M. I. Miller, BCL
D. L. Snyder, BCL

Support: RR 01380
RR 01379
HL 17646
ECS 8215181

A mathematical model is formulated for a gamma camera used to observe single-photon emissions from multiple view angles. The model accounts for the statistics of radioactive decays, nonuniform attenuation, and a depth-dependent point-spread function. The maximum-likelihood method of statistics is used with the model to derive an algorithm for estimating the distribution of radioactivity.

The approach we take differs in three fundamental ways from classical methods of SPECT reconstruction. It is not based on modifications of the conventional filtered back-projection algorithm or on linear, least-squares theory; rather it is based upon a Poisson process model that accurately describes both the emission process as well as the detection process. Maximum-likelihood estimation is then subsequently used with this model to derive the reconstruction algorithm. The algorithm we proposed permits the depth-dependent point-spread function to be included in the reconstruction which conventional methods can not do. Finally, the algorithm we propose accounts for the attenuation of photons due to absorption and scattering in tissues; we make no assumptions about the physical medium or geometry of attenuation.

E. Systems for Specialized Biomedical Studies

The reports in this section are, in general, applications of fundamental technology developed at BCL. Inevitably they have only one common factor; - each is emerging from the laboratory and awaiting entry to the clinic.

The use of modeling techniques to describe the blood acid-base relationships in vivo should encourage greater quantification and account for significant discrepancies that occur in the theory and practice of the management of acid-base abnormalities.

Work continues on a device that should increase our understanding of EEGs and special hardware and software has been devised to aid in other areas of neurology, especially the evoked response potentials in relation to rapid eye movements.

The use of computers to obtain an overall genetic description of certain yeasts continues to be pursued and offers exciting prospects.

The ability of computers to perform complex statistical calculation is being exploited in the analysis of autoradiographs of materials made in electron microscopy.

Finally, the study of peripheral vision by means of color perimetry is continuing on a limited clinical basis.

E-1. Further Development of a Toposcope System for Electroencephalograms

Personnel: H. W. Shipton, BCL and Electrical Engineering

Support: RR 07054

The frequency and phase indicating toposcope (described in PR 18, C-7) has been used on a variety of EEG data, mostly recorded off-line. The object was not to establish a meaningful experimental protocol but rather to get a "feel" for the instrument. It became clear that the problems noted in PR 18 section C-7 seriously limited the use of the method especially when using photic stimulation.

A major upgrade of the system is now in hand: Memory size has been increased to 2K x 8 bits per channel, the A/D converters have been replaced and a "spongy lock" between the clocks has been devised to overcome problems of stimulus synchronization. As an interesting side-light on this project there is an on-going controversy over the basic instrumental technology. The P.I. believes that this is one of the few cases where a hard-wired hybrid system has a considerable edge over a software (general purpose computer) approach.

There has been a world-wide resurgence of interest in toposcopic displays, most of which are applications of computer graphics technology. Most of these systems are probably not capable of posing or solving basic physiological questions although they may well have clinical utility. Use of this system should clarify and refine questions about the nature and function of what have been called the "intrinsic rhythms of the brain."

E-2. DNA Restriction-Mapping

Personnel: J. R. Cox, Jr., BCL and Computer Science
M. V. Olson, Ph.D., Genetics
J. S. Turner, Ph.D., Computer Science

Support: RR 01380
GM 28232
Washington University

The DNA-mapping project, under the direction of M. V. Olson of the Department of Genetics is directed towards global physical mapping of the DNA in the yeast Saccharomyces cerevisiae. This goal is of immediate practical value, since yeast has become a major experimental model in molecular biology, and also is of methodological interest since the most complex DNA's that have yet been successfully mapped are only a few percent as complex as yeast DNA.

The basic approach involves generating 15-kb (1 kb = 1000 base pairs) segments of yeast DNA by random breakage, and then cloning these segments by recombinant-DNA techniques. Each cloned segment is digested with restriction enzymes to obtain a set of approximately 8 sub-fragments whose sizes are characteristic of the DNA sequences present in the particular clone analyzed. The sizes of the sub-fragments are measured by electrophoresis and entered into a computerized data base. The original plan called for analyzing 5000 random clones, which corresponds to a sampling redundancy of 5. It is expected that this redundancy will allow the ordering of most of the sub-fragments in the source DNA; this ordering information is obtained by inferring the way in which the clones must overlap in order to produce the lists of sub-fragment sizes that are associate with them.

Experimental progress during the past year has involved completion of the electrophoretic measurements and creation of the 5000-clone database. Preliminary examination of the database indicates that overlaps between clones are readily detected and that the sampling redundancy indeed appears to be approximately 5 (i.e. a particular sub-fragment can generally be found in approx. 5 clones, which are non-identical but can be ordered to produce a topologically consistent map for the sub-fragment order in the source DNA).

Collaborative effort with the BCL has shifted from a past emphasis on the quantification of the electrophoretic measurements to an analysis of algorithms for global analysis of the data set. Two aspects of the problem have received emphasis. On the one hand, local-searching strategies have

been developed and implemented that allow the data for sets of approximately 3-50 clones from a local region of the source DNA to be analyzed. The key to these strategies is a tree-searching algorithm with judicious pruning that allows the most plausible pairing schemes between the sub-fragment lists for two clones to be recovered without elaboration of all conceivable schemes. Extensive experience with a FORTRAN implementation of this algorithm has validated its suitability for analyzing data of the quality present in the data set. However, a more difficult problem concerns the optimum way of pre-selecting sets of clones that are appropriate for analysis by the local-searching programs. A number of laboratory methods have been developed that are contributing to our ability to carry out this pre-selection with the use of supplementary data, but we have also been pursuing computational approaches that do not require supplementary data.

The problem of global analysis of the data is intrinsically difficult. We have developed a formal proof that the computational problem is NP-complete, implying that there is unlikely to be an efficient algorithm that is assured of finding a solution if one exists. Given the scale of the problem (5000 clones, 40000 sub-fragments), algorithms that require more than "0"(n^2) in computing time, where n is the number of clones, are unlikely to be practical. For this reason, work has focused on a greedy algorithm, whose dominant characteristic is that it builds up the source map starting with the clone overlaps that are the least likely to be fortuitous and moves towards overlaps with progressively decreasing statistical significance. Analysis of the computational complexity of the approach suggests that it should be feasible to implement, but its accuracy cannot be reliably predicted without actual experience analyzing real data. We plan to develop and test an implementation during the next year. Major emphasis will be on developing a productive interplay between the computational activities and the experimental program so that a variety of laboratory resources will be available to test the accuracy of maps that are predicted by the data analysis.

E-3. A Quantitative Model for In Vivo Acid-Base Relations

Personnel: L. J. Thomas, Jr., BCL

Support: Washington University

Work is in progress on a new model to represent the acid-base relations of the blood in vivo. The model will account for steady-state equilibrium between the blood and interstitial fluid (plus lymph), the transition from mixed-venous to arterial blood,[1] and for intracellular buffering as well as acid production. The object is to achieve a precise representation of the composition of arterial blood in vivo. Earlier work[2] had modeled the in vitro behavior of arterial blood in order to quantify acid-base abnormalities. Subsequently, improved estimations of the reaction constants for carbamino formation and revised estimates for the upper portion of the oxyhemoglobin dissociation curve have been added to the extensive information available about the physicochemical behavior of

blood. Also, major advances have been made in understanding the factors affecting the relations between intracellular and extracelluar pH. More importantly, classical methods for quantifying acid-base abnormalities have fallen into disfavor because they were based on the in vitro behavior of blood and more precise clinical methods have shown discrepancies with actual in vivo behavior. As a result, clinical applications in recent years have reverted to semiquantitative empirical methods that in many cases lead to errors at least as large as those of the classical methods.

In order to evaluate its potential, a preliminary version of the new model has been programmed on the IBC VAX 11/750. Even though neither the transition from mixed-venous to arterial blood nor the release of acids from the intracellular space were included, the preliminary model compared very favorably with data from the literature for acute in vivo titration with carbon dioxide. Discrepancies in base excess from several milliequivalents/liter (based on in vitro methods) were reduced an order of magnitude to a few tenths of a meq/liter for hypercapnea up to CO_2 tensions of 90 mmHg. In hypocapnea, the preliminary model deviated from in vivo titration results almost exactly in accordance with the demonstrated release of lactic acid from the intracellular space during hyperventilation by awake subjects. These results encourage further work to complete and evaluate the model. If it proves to be satisfactory, it will provide the basis for reinstating truly quantitative methods for evaluating acid-base abnormalities.

1. A. Roos and L. J. Thomas, Jr., "The In-Vitro and In-Vivo Carbon Dioxide Dissociation Curves of True Plasma: A Theoretical Analysis," Anesthesiology, vol. 28, pp. 1048-1063, 1967.

2. L. J. Thomas, Jr., "Algorithms for Selected Blood Acid-Base and Blood Gas Calculations," Journal of Applied Physiology, vol. 33, pp. 154-158, 1972.

E-4. Isolated-Scintillation-Probe Data Acquisition System

Personnel: D. E. Beecher, BCL
H. D. Ambos, Medicine
R. E. Hermes, BCL

Support: RR 01380
HL 13851
HL 17646

Software development for the Probe Data Acquisition System (PR 19, E-8, PR 20, E-6) is now in the final stages of testing. Six major modules have been designed, written, and are either fully operational or in final testing. The modules are:

File Setup: completed and fully tested.
File Update: completed and fully tested.
Collection: completed and fully tested.
Report Generation: completed and fully tested.
Curve Analysis I: in final testing stage.
Curve Analysis II: in final testing stage.

The major new features of this system are the addition of user-definable protocols and the ability to interactively manipulate the uptake curves in the Curve Analysis portions of the system. The final system should be installed for routine service shortly.

E-5. Software Development for Neurological Sciences

Personnel: D. E. Beecher, BCL
D. G. Barr, Radiation Sciences
P. T. Fox, M.D., Neurology and Radiology
M. A. Mintun, M.D., Neurology

Support: RR 01380
NS 06833
McDonnell Center for Studies of Higher Brain Function

Work continues on the alteration of existing software and the creation of new software for visual evoked potentials measured by PET scanners. There are now three major visual stimulus programs.

The existing checkerboard and moving box stimulus software underwent minor modifications to make them more user-definable and tailored to specific investigator's needs. A Ramtek 9400 display is used as the stimulus generator.

A third random-box stimulus was developed to study rapid eye movement. The software is very flexible and stimulates by alternating boxes at a fixed or random rate.

Altered versions of the above three programs were developed utilizing high task priority to minimize interference from other users. All three are currently being used in research projects, involving visual evoked potentials.

E-6. Maximum-Likelihood Estimation Applied to Electron-Microscopic Autoradiography

Personnel: M. I. Miller, BCL
D. R. Fuhrmann, BCL
K. B. Larson, BCL
B. Roysam, BCL
J. E. Saffitz, M.D., Pathology and Medicine
D. L. Snyder, BCL and Electrical Engineering
L. J. Thomas, Jr., BCL

Support: RR 01380
HL 17646

A new method for analysis of electron microscope autoradiographs has been described which is based on the maximum-likelihood method of statistics for estimating the intensities of radioactivity in organelle structures. A Poisson statistical model describing the autoradiographic grain distributions is adopted, which we prove results from the underlying Poisson nature of the radioactive decays as well as the additive errors introduced during the formation of grains. Within the model, an iterative procedure derived from the expectation-maximization algorithm of mathematical statistics is used to generate the maximum-likelihood estimates. The algorithm has the properties that at every stage of the iteration process the likelihood of the data increases; and for all initial non-zero starting points the algorithm converges to the maximum-likelihood estimates of the organelle intensities.

The maximum-likelihood approach differs from the mast-analysis method, and other published quantitative algorithms in the following ways:

1) In deriving estimates of the radioactivity intensities the maximum-likelihood algorithm requires the actual locations of the grains as well as the micrograph geometries; each micrograph is digitized so that both the grain locations as well as the geometries of the organelle structures can be used.

2) The maximum-likelihood algorithm iteratively computes the minimum-mean-squared-error estimate of the underlying emission locations that resulted in the observed grain distributions, from which intensity estimates are generated; this algorithm does not minimize a Chi-squared-error statistic.

3) The maximum-likelihood approach is based on a Poisson model and is therefore valid for low-count experiments; there are no minimum constraints on data collection for any single organelle compartment.

4) The maximum-likelihood algorithm requires the form of the point-spread function describing the emission spread, a probability matrix based on the use of overlay masks is not required.

5) The maximum-likelihood algorithm does not change for different organelle geometries; arbitrary geometries are incorporated by maximizing the likelihood-function subject to the geometry constraints.

We have performed a preliminary evaluation of the quantitative accuracy of the maximum-likelihood and mask-analysis algorithms. Based on two different phantoms in which we compared the squared-error resulting from the two algorithms, we find that the new maximum-likelihood approach provides substantially improved estimates of the radioactivity intensities of the phantoms.

E-7. Color Perimetry Studies

Personnel: W. M. Hart, Jr., M.D., Ph.D., Ophthalmology

Support: RR 01380
EY 03703
Washington University

The microcomputer-based color perimetry system was used during the last project year for ongoing clinical studies of patients with glaucoma and diseases of the retina and optic nerve. Unexpected results were obtained, demonstrating that visual field defects in these diseases can be mapped by color contrast perimetry in the visual field at locations exactly matching those for defects detected by conventional luminance increment perimetry. While use of the color contrast technique seems to have failed to produce any greater sensitivity or specificity for the detection and diagnosis of disease, the results have nevertheless provided interesting insights into the pathogenesis of the types of color vision defects that occur in patients with ocular diseases. In addition, the possibility remains that a form of testing may yet be devised with the use of the color technique that would provide a higher level of sensitivity. For this purpose, software changes will need to be made in the system during the next project year to allow variations in test parameters that cannot now be achieved.

F. Resource Development Activities

Resource development activities are those which contribute to the goals of more than one major program of the laboratory, address the needs of individual users who can benefit from the expertise of the BCL staff and the inventory of computing and specialized test equipment, or identify new technologies which may become appropriate foundations for new experimental tools. Service to users does not follow the usual computation-center pattern with an established fee schedule and a highly centralized facility. Rather, senior laboratory staff members consider requests for assistance from investigators who must address a particular biomedical computing problem. If an appropriate technology exists, investigators may be referred to commercial vendors or fee-for-service organizations when these are available. In other cases, problems may be approached by the laboratory provided that the effort complements other activities of the laboratory. Many times the project can be assigned to a staff member with appropriate experience and completed in a short time. The investigator then has his or her results, and a short note describing the work will appear in the annual report and perhaps the open literature. A few projects, however, may develop into major initiatives within the laboratory. Most of the major projects began in this fashion and the opportunities that supporting activities provide are valued.

A goal of the IPAQ activity (F-1) is to provide a software development environment which promotes portability to our local and national collaborators. Continuing studies and measurements on broadband cable transmission (F-3) support both local and campus-wide networking projects. System development aids primarily benefit BCL staff, but may also be used by others (F-2, F-5, F-6, F-7).

Many digital hardware designs are one-time, special purpose projects. Others may have wide appeal and construction of multiple copies may result, as in the case of the TERRANET local network.

F-1. A Distributed Facility for Image Presentation, Analysis and Quantification (IPAQ)

Personnel: G. J. Blaine, BCL
D. E. Beecher, BCL
K. W. Clark, BCL
J. R. Cox, Jr., BCL
R. E. Hermes, BCL
S. M. Moore, BCL
F. U. Rosenberger, BCL and Computer Systems Laboratory

Support: RR 01380
RR 01379
Washington University

Decentralized computing organized along departmental and research laboratory lines characterizes the environment which continues to evolve at most major medical research institutions. This is particularly true in quantitative imaging where many projects have diverse image-data sources (modalities), different data-acquisition requirements, and dissimilar methods for the extraction of quantitative information. Rather naturally, diverse computing styles and equipment choices have evolved. For example, our major collaborative research groups support installations tailored to their specific measurement and picture transformation needs, for which display peripherals from a variety of manufacturers (DeAnza, Ramtek, and Lexidata) are tightly coupled to different computers (DEC 730, 750, 780, PE 3230, 3242). Commonality is limited to little more than the popularity of Vax-class computers and a FORTRAN programming environment. Furthermore, the lack of common program-development tools and display-support software has minimized the opportunities for sharing developments across research programs and has necessitated large host-specific investments by those Resource researchers and collaborators who participate in modeling and algorithm development.

Algorithm, development is often characterized by computationally demanding and memory-intensive tasks which must compete with concurrent usage of the existing computing resources for data acquisition and analysis activities. The limited computational capacity available for algorithm development and pressures for expediting the research process biases the investigator's attention toward ad hoc approaches to improvements in execution performance, often at the expense of fundamental algorithm studies which are more likely to yield long term benefits.

The broad goal of this core research and development activity is to create an environment for biomedical image presentation, analysis and quantification (IPAQ)[1] which:

1) is focused on fundamental algorithm developments that individual biological scientists may not have the time, patience or resources to pursue;

2) provides an integrated approach to expedite the development and export to the local and national communities of new algorithms for improved quantification of biological information;

3) improves access for purposes of algorithm development to data from the diverse imaging modalities to encourage modality integration; and,

4) protects existing investments in decentralized and specialized biomedical research systems.

A series of study efforts led to the definition of an architecture and system components capable of addressing the needs of quantative imaging. The components of the distributed IPAQ facility are to include: 1) acquisition nodes consisting of the specialized imaging resources at the sites of the collaborations; 2) a computation-oriented node to support development and initial evaluation of algorithms within the Resource; 3) high-performance computation/display nodes which are tailored to export specialized computation and/or picture presentation; and 4) a high-bandwidth network to interconnect our development activities with the collaborative research, (F-3).

Software

We have chosen the UNIX operating system for supporting our software development activities. The choice of this system was motivated by several factors:

a) UNIX runs on a variety of machines, and software-development tools can be easily moved among those machines running UNIX;

b) many software-development and maintenance tools already exist on the UNIX system;

c) workstation development trends strongly support the choice of UNIX as the operating system; and

d) software portability to other operating environments, VMS, RSX, and OS/32, can be achieved by recompilation of appropriately constrained module implementations.

The widespread use and availability of FORTRAN and C compilers suggests application and support of both these languages. The "C" programming language will be used both in the development of tools and in the implementation of support routines. Creation of consistent, structured picture-presentation techniques within the IPAQ facility will require special attention to the data types produced at any given node on the network. Further review of existing standards both nationally and within Washington University will provide the basis for our work in this area.

Computation-Oriented Node

The computation and memory-intensive tasks associated with algorithm research and development necessitate availability of a computing system of adequate power whose management is sensitive and responsive to the research requirements. Our approach is to establish this computation-oriented node within the Resource.

The node must supply adequate primary memory, secondary storage and processing speed to allow computation-intensive tasks (as those

characterizing emission tomography algorithms, D-7) to be conducted in a time-frame deemed reasonable to accomplish the research goals. Benchmark studies[2], providing both frequency and time domain computation time-estimates, indicate the adequacy of a VAX-750 class processor augmented by a floating point accelerator and an array processor. General-purpose interactive usage will be severely limited on the computation-node in order to maintain flexibility for dedicating the whole computation capability of the node to its designated task of algorithm research. A responsive environment for program development, documentation, and image presentation will be supported on our MASSCOMP workstations and appropriately connected to the computation-node via the picture-based local area network.

Efforts in the next reporting period will focus on a review, selection and purchase of a general purpose processor(s) and an array processor to form the hardware base of the computation-oriented node. System integration, software importation/installation and system evaluation will be given substantial attention.

1. L. J. Thomas, Jr., Principal Investigator, "A Resource for Biomedical Computing," Biomedical Research Technology Program Renewal Proposal, Washington University Institute for Biomedical Computing, St. Louis, MO, December 1984.

2. S. M. Moore and T. J. Holmes, "M-L Algorithm: Computation Time Estimates for Array Processor-Based Implementation," BCL Working Note No. 60, September 1984.

F-2. MASSCOMP Workstations

Personnel: R. E. Hermes, BCL
G. J. Blaine, BCL
S. R. Phillips, BCL

Support: RR 01380

The laboratory has utilized a MASSCOMP MCS-500 for about a year now (PR 20, F-10). The system is Motorola 68010 based, uses UNIX as an operating system and supports a modest number of simultaneous users.

The system has been upgraded significantly during the past year with the addition of the MASSCOMP array processor and floating point units, an SMD disk controller with an 80 megabyte CDC Storage Module drive, a 52 megabyte Winchester disk, an additional megabyte of memory, and eight additional serial communication ports. The increased disk capacity was required for storage of large data sets used for algorithm evaluation. The array processor and floating point units have helped reduce computation times.

System performance has been good for computationally demanding tasks, offering comparable performance to the Institutes multiuser VAX 11/750. Frequently, tasks requiring hours or days of compute time (D-7, D-10) have been run on the system with little impact on other system users.

The tightly coupled MASSCOMP graphics processor has aided in algorithm evaluation and development studies by providing for quick display of algorithm results. MASSCOMP windowing software for the graphics processor provides a valuable mechanism by which results from different algorithm implementations may be viewed simultaneously for comparison.

A second MASSCOMP workstation was recently acquired to support text processing requirements of the laboratory. This includes support for the MUSE word-processing system as well as NROFF and TROFF support for technical document preparation. The system includes two megabytes of memory, a 52 megabyte Winchester, and eleven serial communication lines. In addition to text processing, programs can be developed and tested and later executed on the larger MASSCOMP configuration.

The systems currently communicate via serial lines using UUCP, users use either directly connected terminals or terminals connected via TERRANET. Intersystem communiation between these systems and the local VAX installation is over TERRANET. The VAX is a central node providing access to other systems outside the laboratory as well as a connection to a laser printer for high quality text output.

F-3. A Picture Communication System for Radiology

Personnel:
G. J. Blaine, BCL
J. C. Chabut, BCL
J. R. Cox, Jr., BCL and Computer Science
R. L. Hill, BCL and Radiology
R. G. Jost, M.D., Radiology
A. Kumar, B.Tech., Radiology
S. R. Phillips, BCL
A. P. Rueter, B.S., Radiology

Support:
RR 01380
RR 01379
Mallinckrodt Institute of Radiology
Washington University

A pilot cable system to transport analog and digital radiology pictures and support terminal-to-computer digital data transmission has been designed and installed (PR 20, F-6, PR 19, F-7, F-8). A dual-cable 400 MHz system utilizes "off-the-shelf" cable television components to provide approximately 50 channels, achieved by frequency multiplexing channels of 6 MHz each. The system provides a workbench environment for the evaluation of commercial digital transmission equipment in addition to supporting experiments related to digital picture networking and archiving studies.

Studies and subsequent designs have been directed at communicating radiological images using channels based on frequency division of the 400 MHz channel. Multiple shared-transmit/receive channels were shown to have favorable cost-delay characteristics.[1] Most of the MIR efforts have been directed at accessing and displaying images related to an on-line clinical database containing both picture and text information.

Characteristics of the cable TV medium for communicating digital pictures were reviewed, and nominal values were tabulated.[2] A method for evaluating the impact of white Gaussian noise, burst noise, and sinusoidal interference was developed and the design and implementation of a low cost (parts cost <$500) bit error tester was completed. Measurements were conducted for noncoherent FSK broadband modems (1 Mb/s rate) used either independently or in conjunction with the MIR cable TV network. Experimental results indicate that digital pictures can be successfully communicated with the modems at signal-to-noise ratios in excess of 29 dB.

Development of a low-cost frame-buffer (512 x 512 x 8 bits/pixel) continued. A 1 MHz serial synchronous interface was designed and implemented. A second prototype was constructed and initial experiments were conducted using a parallel load from a VAX 11/750 - DR 750 DMA interface into one unit, and 1 MHz serial transmission over the broadband network to the second. Effort is currently directed to improving robustness of the transfer.

1. C. D. Shum, J. R. Cox, and G. J. Blaine, "Design Analysis of a Wide-Band Picture Communication System," IEEE 1984 International Symposium on Medical Images and Icons - ISMII '84, Arlington, VA, pp. 66-77, July 1984.

2. J. C. Chabut, "An Examination of FSK-Based Digital Picture Communication Over the CATV Medium," Master of Science thesis, Department of Electrical Engineering, Washington University, St. Louis, MO, August 1985.

F-4. An Experimental Local-Area Network: TERRANET

Personnel: S. M. Moore, BCL
G. J. Blaine, BCL
R. E. Hermes, BCL
S. R. Phillips, BCL
D. A. Schwab, BCL

Support: RR 01380
Washington University

TERRANET is now an integral part of the day-to-day operations of BCL. TERRANET provides terminal-to-computer and computer-to-computer communications for most multiuser computer systems in the laboratory.

Nearly every office is equipped with a terminal tied to a TERRANET port; in addition, several public ports are available within BCL. Intersystem communication via TERRANET is used to transfer text and data files. The initial TERRANET network (30 ports) has been augmented by a second parallel network. Communication between networks is accomplished through the use of 3 gateway ports on each network. Current resources on the two networks include 22 terminals, 13 ports to 4 distinct computer systems, and 9 modem or other network gateway connections.

The hardware design of both tap and insert units has remained unchanged over the last year. Software updates were made to all terminal units during the installation of the second network to bring each unit up to the most current revision level. Software in gateway units was also updated to reflect changes made to software in terminal units during the past two years. Additional changes to software and hardware have been identified which will better facilitate networking machines and will be implemented as time permits.

F-5. Systems Support for Programming and Image Processing

Personnel: R. E. Hermes, BCL
S. Husodo, BCL
S. M. Moore, BCL
R. J. Paisley, BCL
S. R. Phillips, BCL
T. D. Scholz, BCL

Support: RR 01380

Systems support (both hardware and software) is a critical component of the the overall research environment. Until very recently, scientific programming support was supplied by a pair of Digital PDP 11/34's running RSX11M. These systems are configured with disk and tape storage devices which provide common data interchange media with other systems within the university. In addition, one system hosts a Lexidata 3400 color display system, for which a general purpose image display utility package was recently completed. The package allows for display of images of arbitrary size, interactive manipulation of color tables, and supplies a simple windowing system for display of multiple images simultaneously. Several investigators have found this package to be a valuable aid to their research activities.

Recently, emphasis has been placed on software development for the MASSCOMP systems (F-2). MASSCOMP supplies a vast number of data manipulation and display libraries. Effort has been devoted to utilizing these libraries to provide a set of data display utilities which are easy to use. In addition, work continues toward the definition of an image and data storage format and the importation of image and data manipulation packages (F-1). These include the acquisition of the CORE graphics system from Precision Visuals and the importation of the University of North

Carolina V-Shell, the Cornell PDS system, and the Brigham Young University MOVIE.BYU display package.

Data communication has become a critical part of the local computing environment. Investigators often do program development on different machines, require a variety of hardware resources, and require data from many different sources. Software has been developed and is supported for intersystem data communication and data type conversion for systems with dissimilar data storage formats (F-6).

F-6. Data Formats for Inter-Machine Transfer

Personnel: S. M. Moore, BCL
D. E. Beecher, BCL
R. E. Hermes, BCL

RR 01380

Transferring data between computer systems requires not only a communications channel (physical connection, magnetic tape) but also a common data format. Simple data formats such as text files, program source code and integer data are easily handled. Studying biomedical images acquired on a foreign machine requires additional effort as the floating point format is usually machine dependent.

Studies for evaluating the ML algorithm were moved from a Perkin Elmer system at the Division of Radiation Sciences to a Masscomp system at BCL. Images and programs used in the evaluation were written to magnetic tape by the PE machine, read by a VAX 750 using standard UNIX utilities, and transferred via TERRANET to the Masscomp system. A floating point number on a PE machine is represented by a 24 bit fraction, a 7 bit exponent and a sign bit. The fraction is interpreted as 6 hexadecimal digits with a radix point to the left of the most significant digit. The exponent is stored in "excess-64" format; the value stored is the true value of the exponent plus 64. The magnitude of a floating point number is:

$$\text{FRACTION} \times 16^{(\text{EXPONENT} - 64)}$$

The sign bit is 0 for a positive number and 1 for a negative number. A program written in "C" on the Masscomp interpreted this format and created numbers consistent with Masscomp floating point format.

Floating point numbers on a Masscomp follow the IEEE standard which is based on a binary rather than a hexadecimal system. Any positive number x can be represented by a unique pair of values, an integer e and a real number g, where $1 \leq g < 2$. The relationship between x, e, and g is:

$$x = 2^e \times g$$

On the Masscomp, the values stored on the exponent (E) and significant (F) fields are (e + 127) and (g - 1), respectively. The exponent is a biased value and the significant is a fraction between 0 and 1. The sign bit gives the sign of the number as described above. A zero value is encoded by setting both the exponent and significant to 0.

As the communications network connectivity is established with our collaborators, similar interpretation programs will be written for each node. Efforts are now in progress to establish a standard file structure which will facilitate data transfer, manipulation and display within the IPAQ environment (F-1).

F-7. A Fortran Interface for the H-P 745A Plotter

Personnel: T. O. Videen, BCL
D. E. Beecher, BCL

Support: RR 01380

A software library was developed to handle most of the primitive plotting functions available in HP Graphics Language through FORTRAN subroutines. This library, consisting of over 60 subroutines, will speed the development of programs which use the HP 7475A plotter for graphic display of data.

A general purpose plotting program has been written which allows users to plot data in custom-designed plots. The program is interactive and allows each user to select nearly all of the characteristics of a plot. Each user may save default parameters so as to rapidly recreate a particular format on future plots. This program allows any user to create publication-quality plots of his own data, complete with centered titles, labeled axes, error bars, and legends.

VI. INDUSTRIAL COLLABORATION

Industrial collaboration provides a mechanism for the deployment of laboratory developments. In addition, it benefits our staff by keeping us abreast of the practical considerations of reliability, maintainability, and cost. During the past year, our collaboration was quite diversified, involving: (1) foreign corporations, (2) a small American biotech start-up company, and (3) a major American pharmaceutical corporation.

1. The TERRANET system, which provides a simple, low-cost interconnect to support terminal-to-computer and computer-to-computer communications at modest speeds (up to 9600 bps), is currently being produced and marketed in Japan under a licensing agreement with Computer Services Corporation (CSK), a major facilities management consulting firm headquartered in Tokyo (PR 20, VI). Recently, BCL loaned a six-unit demonstration unit to the Biodata Informatica and Technologia, Ltd., of Brazil for display at the Brazilia Informatics Conference and Exhibit. Washington University is now negotiating a licensing agreement which would allow production and sale in Brazil.

2. BCL personnel have continued to work closely with Biosensor Corporation (Brooklyn Center, Minnesota) to complete the transfer, implementation and refinement of the entire set of frequency-domain-based Argus algorithms (A-1) into a microprocessor-based real-time ambulatory patient ECG monitoring device (PR 20, VI). Within the past year, algorithm refinements for enhanced PVC couplet and run detection, atrial fibrillation detection, and signal-quality assurance testing were developed by BCL and implemented by Biosensor.

As each ECG complex is detected, analyzed, and classified, the patient monitor records beat counts and digital sample data for significant events. Information saved by the monitor is sent to a "central station" computer which prints ECG strips and tables of beat counts. The patient devices are capable of monitoring for up to 120 continuous hours. Data in the monitor may be "dumped" directly to the central station or transmitted transtelephonically, typically at 8-hour intervals.

Biosensor markets three embodiments of their Argus-based device: (1) the Multiday System, featuring a central station supporting up to eight monitors and designed for transtelephonic transmission and monitoring periods up to five days; (2) the Uniday System, featuring simplified central station software for monitoring periods up to 24 hours for which a monitor's data are dumped directly to the central station; and (3) the Multiscan System, for which monitor data are transmitted to a Biosensor-owned central station.

3. For a year and a half, BCL has analyzed long-term ECG recordings for a Mead-Johnson (Evansville, Indiana) sponsored "Multicenter Placebo-Controlled Study of Trazadone's Effects in Depressed Cardiac Patients." The study was described last year (PR 20, VI). BCL's contract to analyze these recordings expires in October 1985.

VII. TRAINING ACTIVITIES AND SEMINARS

Training activities of the Biomedical Computer Laboratory are directed toward the goals of informing the local and national scientific communities about resource projects and facilities and of instructing a broad spectrum of people in the application of advanced computer-techniques to problems in clinical medicine and biological research. Training activities include the teaching of formal courses at the School of Medicine and the School of Engineering as well as supervision of graduate students by Laboratory staff. Both individual and small-group training about resource facilities are made available to the biomedical scientist. National workshops and symposia on topics of interest and importance to the resource and community are supported.

The bringing together of biomedical scientists, engineers, and computer scientists provides important cross-fertilization between disciplines. In these settings, students and staff find the need and opportunity to test the relevance of theory and the usefulness of technology in applications to real problems. Also, the biomedical scientists are aided in learning new techniques for acquiring useful information. To this end, some of the courses offered are addressed to biologists without strong technical backgrounds who want and need a below-the-surface appreciation of biomedical computing. Laboratory personnel also participate in regularly scheduled conferences in the clinical departments where both the biological and technological issues are examined.

Seminars and presentations relating to resource projects and applications are conducted by Laboratory staff as well as scientists and engineers from the national community. During the year the following activities were supported:

Seminars

"Regional Metabolism and Blood-Flow Studies" July 12, 1984	Joanne Markham Biomedical Computer Laboratory Washington University St. Louis, Missouri
"3D Image Display" July 12, 1984	David E. Beecher Biomedical Computer Laboratory Washington University St. Louis, Missouri
"TERRANET Update" July 19, 1984	Steven M. Moore Biomedical Computer Laboratory Washington University St. Louis, Missouri

"Image Presentation, Analysis and Quantification: Plans for July 19, 1984	G. James Blaine Biomedical Computer Laboratory Washington University St. Louis, Missouri
"Radiation Treatment Planning" August 2, 1984	Lewis J. Thomas, Jr. F. U. Rosenberger John Wong
"Data Acquisition for Neurophysiology" August 9, 1984	Harold W. Shipton Biomedical Computer Laboratory Washington University St. Louis, Missouri
"Design Considerations for Positron Emission and Transmission Tomographs Used for Industrial Applications" November 5, 1984	Hannu H. Heusala University of Oulu Oulu, Finland
"Reflections on the Nuclear Science Symposium" November 7, 1984	David C. Ficke Department of Radiology John D. Gorman Michael I. Miller John M. Ollinger Donald L. Snyder Biomedical Computer Laboratory Washington University St. Louis, Missouri
"Some Current Thoughts About the Use of Maximum-Likelihood Estimation in PET, SPECT, and EMA" January 7, 1985	Donald L. Snyder Michael I. Miller Biomedical Computer Laboratory Washington University St. Louis, Missouri
"MCF: A Technical View" February 13, 1985	Simon Igielnik Medical Computing Facilities Washington University St. Louis, Missouri

"Maximum Entropy, Minimum Cross Entropy and Maximum-Likelihood Estimation: Their Relationship to Tomographic Imaging and Other Problems"

February 20, 1985

Michael I. Miller
Donald L. Snyder
Biomedical Computer Laboratory
Washington University
St. Louis, Missouri

"CONVEX Computer Presentation"

March 20, 1985

William Ott
CONVEX Computers
Dallas, Texas

"Effects of Electrical Stimulation of Efferent Fibers Projecting to the Cochlea: Auditory-Nerve Fiber Response Properties"

March 27, 1985

Raimond L. Winslow
The Johns Hopkins University
Baltimore, Maryland

"Data Collection and Preprocessing Considerations in Time-of-Flight Positron-Emission Tomography"

March 27, 1985

Timothy J. Holmes
Department of Radiology
Washington University
St. Louis, Missouri

"Quantitative Analysis of Rate-Place Coding in the Auditory-Nerve"

March 28, 1985

Raimond L. Winslow
The Johns Hopkins University
Baltimore, Maryland

"An Examination of FSK-Based Digital Picture Communication Over the Cable TV Medium"

June 19, 1985

John Chabut
Biomedical Computer Laboratory
Washington University
St. Louis, Missouri

- - - - - - - - - - - - -

Other Activities

A Lecture Series in support of Biomedical Engineering 3/2 Intensive Course
Sponsored by the Program in Biomedical Engineering
Sever Institute of Technology
Washington University

"An Engineer Looks at the Brain" and a film - "The Brain" January 1, 1985	Harold W. Shipton Biomedical Computer Laboratory Washington University St. Louis, Missouri
"Biomedical Instrumentation and Transducers" January 2, 1985	R. Martin Arthur Department of Electrical Engineering Biomedical Computer Laboratory Washington University St. Louis, Missouri
"Computers, Cardiologists and Cardiograms" January 3, 1985	Lewis J. Thomas, Jr. Biomedical Computer Laboratory Washington University St. Louis, Missouri
"Biophysical Measurements" January 9, 1985	Harold W. Shipton Biomedical Computer Laboratory Washington University St. Louis, Missouri
"Computers: Communication and Storage" January 12, 1985	G. James Blaine Biomedical Computer Laboratory Washington University St. Louis, Missouri

VIII. PUBLICATIONS AND ORAL PRESENTATIONS

Abendschein, D. R., Fox, K. A. A., Knabb, R. M., Ambos, H. D. Elmaleh, D. R., and Bergmann, S. R., "The Metabolic Fate of ^{11}C-Beta Methyl Heptadecanoic Acid (MHA) in Myocardium Subjected to Ischemia," Circulation, vol. 70, supplement II, p. II-148, 1984 (abstract).

Ambos, H. D., Markham, J., and Cain, M. E., "Use of Fast Fourier Transform Analysis to Detect Patients Prone to Sustained Ventricular Arrhythmias," Proceedings of the IEEE Conference on Computers in Cardiology, IEEE Catalog No. 84CH2078-4, Park City, UT, pp. 181-184, September 18-21, 1984.

Arthur, R. M., and Gurumurthy, K. V., "A Single-Pole Model for the Propagation of Ultrasound in Soft Tissue," Journal of the Acoustical Society of America, vol. 77, pp. 1589-1597, 1985.

Arthur, R. M., Sieger, M. L., and Stein, Jr., D. W., "Assessing Ultrasonic Arrays for Imaging Tissue Properties," Ultrasonic Imaging, vol. 6, p. 209, 1984 (abstract).

Barzilai, B., Madaras, E. I., Sobel, B. E., Miller, J. G., and Perez, J. E., "Effects of Myocardial Contraction on Ultrasonic Backscatter Before and After Ischemia," American Journal of Physiology, vol. 247, p. H478, 1984.

Beecher, D. E., Cox, Jr., J. R., and Thomas, Jr., L. J., "A New Voxel-Model Approach for 3-Dimensional View Generation," Proceedings of the Eighth Conference on Computer Applications in Radiology, St. Louis, MO, pp. 214-231, May 23-25, 1984.

Bergmann, S. R., Fox, K. A. A., Rand, A. L., McElvany, K. D., Welch, M. J., Markham, J., and Sobel, B. E., "Quantification of Regional Myocardial Blood Flow in vivo with $H_2{}^{15}O$," Circulation, vol. 70, no. 4, pp. 724-733, October 1984.

Bergmann, S. R., Fox, K. A. A., Rand, A. L., Welch, M. J., Ter-Pogossian, M. M., and Sobel, B. E., "Assessment of Restoration of Myocardial Perfusion and Metabolism with Positron Emission Tomography after Coronary Thrombolysis," Journal of Nuclear Medicine, vol. 24, no. 5, p. 5, 1984 (abstract).

Bergmann, S. R., Ter-Pogossian, M. M., and Sobel, B. E., "Biomedical Applications of Positron Emission Tomography," in Cardiovascular Instrumentation: Applicability of New Technology to Biobehavioral Research, J. A. Herd, A. Gotto, P. J. Kaufmann, and S. M. Weiss, eds., National Institutes of Health Monograph 84-1654, Bethesda, MD, 1984.

Blodgett, E. D., Johnston, P. H., and Miller, J. G., "Estimating Attenuation in Composite Laminates Using Backscattered Ultrasound," Proceedings of the IEEE Ultrasonics Symposium, 84 CH 2112-1, pp. 748-753, 1984.

Cain, M. E., Ambos, H. D., Fischer, A. E., Markham, J., and Schechtman, K. B., "Non-Invasive Prediction of Antiarrhythmic Drug Efficacy in Patients with Sustained Ventricular Tachycardia from Frequency Analysis of Signal Averaged ECGS," Circulation, vol. 70, supplement II, p. II-252, 1984 (abstract).

Cain, M. E., Cox, J. L., Kramer, J. B., Witkowski, F. X., and Corr, P. B., "Simultaneous Intraoperative Computer Mapping from Multiple Sites to Facilitate Localization of Accessory Pathways," Journal of American College of Cardiology, vol. 5, p. 399, 1985 (abstract).

Corr, P. B., Gross, R. W., and Sobel, B. E., Amphipathic Metabolites and Membrane Dysfunction in Ischemic Myocardium," invited review for Circulation Research, vol. 55, pp. 135-154, 1984.

Corr, P. B., and Witkowski, F. X., "Arrhythmias Associated with Reperfusion: Basic Insights and Clinical Relevance," Journal of Cardiovascular Pharmacology, vol. 6, pp. S903-S909, 1984.

Corr, P. B., and Yamada, K. A., "Pathophysiological Mechanisms of Alpha-Adrenoceptor Stimulation in Ischemic Heart," in Methods in Clinical Pharmacology, N. Rietbrock and B. G. Woodcock, eds., Vieweg Publishers, Wiesbaden, West Germany, vol. 5, p. 161-168, 1984.

Creer, M. H., Pastor, C., Corr, P. B., Gross, R. W., and Sobel, B. E., "Quantification of Choline and Ethanolamine Phospholipids in Rabbit Myocardium," Analytical Biochemistry, vol. 144, pp. 65-74, 1985.

Croft, C. H., Rude, R. E., Gustafson, N., Stone, P., Poole, W. K., Roberts, R., Strauss, H. W., Raabe, D., Thomas, L. J., Jaffe, A., Sobel, B., Passamani, E., Willerson, J., and the MILIS Study Group, "Beta Blockade Withdrawal in Acute Myocardial Infarction," Journal of the American College of Cardiology, vol. 5, p. 448, 1985 (abstract).

Eisenberg, P. R., and Jaffe, A. S., "New Uses for Nitroglycerin: Intravenous Applications," Drugs Today, vol. 20, pp. 91-95, 1984.

Eisenberg, P. R., Lee, R. G., Biello, D. R., Geltman, E. M., and Jaffe, A. S., "The Absence of Coronary Vasospasm after Non-Transmural Myocardial Infarction," American Heart Journal, in press.

Eisenberg, P. R., Sherman, L. A., Schechtman, K. B., Perez, J. E., Sobel, B. E., and Jaffe, A. S., "Fibrinopeptide A: A Marker of Acute Coronary Thrombosis," Circulation, vol. 71, pp. 912-918, 1985.

Eisenberg, P. R., Sherman, L., Schwartz, D., Reich, M., Sobel, B. E., and Jaffe, A. S., "Unmasking Continuing Thrombin Activation and Rethrombosis As a Determinant of Clinical Failure of Coronary Thrombolysis," Journal of the American College of Cardiology, vol. 5, p. 398, 1985 (abstract).

Elnahas, S. E., Jost, R. G., and Dunham, J. G., "Compression of Digital Diagnostic Images in Radiology," Proceedings of the 8th Conference on Computer Applications in Radiology, St. Louis, MO, pp. 388-409, 1984.

Ficke, D. C., "Time-of-Flight Positron Emission Tomography," invited tutorial as part of a short course on Timing Spectroscopy, presented at the IEEE Nuclear Science Symposium, Orlando, FL, October 31 - November 2, 1984.

Fox, K. A. A., Abendschein, D. R., Ambos, H. D., Sobel, B. E., and Bergmann, S. R., "Efflux of Metabolized and Non-Metabolized Fatty Acid from Canine Myocardium: Implications for Quantifying Myocardial Metabolism Tomographically," Circulation Research, in press.

Fox, K. A. A., Abendschein, D. R., Sobel, B. E., and Bergmann, S. R., "Persistent Impairment of Myocardial Metabolism and Clearance of Labeled Fatty Acid after Brief Ischemia: Implications for Positron Emission Tomography (PET)," Journal of the American College of Cardiology, vol. 5, no. 2, p. 451, 1985 (abstract).

Fox, K. A. A., Bergmann, S. R., and Sobel, B. E., "Coronary Thrombolysis: Pharmacological Considerations with Emphasis on Tissue-Type Plasminogen Activator (t-PA)", Biochemical Pharmacology, vol. 33, p. 1831, 1984.

Geltman, E. M., Bergmann, S. R., and Sobel, B. E., "Cardiac Positron Emission Tomography," in Positron Emission Tomography," M. Reivich, ed., Alan R. Liss, Inc., New York, in press.

Geltman, E. M., Bergmann, S. R., and Sobel, B. E., "PET Studies of the Heart," in Positron Emission Tomography, M. Reivich, ed., Alan R. Liss, Inc., New York, in press.

Glueck, R. M., Mottley, J. G., Miller, J. G., Sobel, B. E., and Perez, J. E., "Effects of Coronary Artery Occlusion and Reperfusion on Cardiac Cycle-Dependent Variation of Myocardial Ultrasonic Backscatter," Circulation Research, in press.

Glueck, R. M., Mottley, J. G., Sobel, B. E., Miller, J. G., and Perez, J. E., "Systematic Changes in Ultrasonic Attenuation and Backscatter of Muscle," Ultrasound in Medicine and Biology, in press.

Glueck, R. M., Mottley, J. G., Perez, J. E., Miller, J. G., and Sobel, B. E., "Systematic Changes in Quantitative Ultrasonic Indexes Caused by the Contractile State of Muscle," Clinical Research, vol. 32, p. 169-A, 1984 (abstract).

Goldring, S., "Epilepsy Surgery," in Clinical Neurosurgery, M. H. Weiss, ed., vol. 31, pp. 369-388, 1984.

Hackel, D. B., Reimer, K. A., Ideker, R. E., Mikat, E. M., Hartwell, T. D., Parker, C. B., Braunwald, E. B., Gold, H. K., Jaffe, A. S. Raabe, D. S., Rude, R. E., Sobel, B. E., Stone, P. H., Buja, M., Muller, J. E., Roberts, R., and the MILIS Study Group, "Comparison of Enzymatic and Anatomic Estimates of Myocardial Infarct Size in Man," Circulation, vol. 70, pp. 824-835, 1984.

Hart, Jr., W. M., and Burde, R. M., "Color Contrast Perimetry: The Spatial Distribution of Color Defects in Optic Nerve and Retinal Diseases," Ophthalmology, vol. 92, pp. 768-776, 1985.

Hart, Jr., W. M., Kosmorsky, G., and Burde, R. M., "Color Perimetry of Central Scotomas in Diseases of the Macula and Optic Nerve," Documente Ophthalmologica, in press.

Hoagland, P., Stone, R., Turi, Z., Muller, J., Croft, C., Parker, C., Gold, H., Jaffe, A., Raabe, D., Rude, R., and the MILIS Study Group, "Tolerance to Propranolol in Patient with Acute Myocardial Infarction," Circulation, vol. 70, p. II-257, 1984 (abstract).

Holmes, T. J., "Data Collection and Preprocessing Considerations in Time-of-Flight Positron-Emission Tomography," Department of Electrical Engineering, Washington University, St. Louis, MO, May 1985 (D.Sc. Dissertation).

Holmes, T. J., and Ficke, D. C., "Analysis of Positron-Emission Tomography Scintillation-Detectors with Wedge Faces and Inter-Crystal Septa," IEEE Transactions on Nuclear Science, vol. NS-32, no. 1, pp. 826-830, February 1985.

Holmes, T. J., Snyder, D. L., and Ficke, D. C., "The Effect of Accidental Coincidences in Time-of-Flight Positron-Emission Tomography," IEEE Transactions on Medical Imaging, vol. MI-3, no. 2, pp. 68-79, 1984.

Jaffe, A. S. for the MILIS Study Investigators, "The Administration of Hyaluronidase to Patients with Acute Myocardial Infarction: Results of the MILIS Study," Journal of the American College of Cardiology, vol. 5, p. 447, 1985.

Jaffe, A. S., Lee, R., Perez, J., Geltman, E. M., Wilner, G., and Sobel, B. E., "Lack of Elevation of Platelet Factor IV in Plasma from Patients with Myocardial Infarction," Journal of the American College of Cardiology, vol. 4, pp. 653-659, 1984.

Jaffe, A. S., Ritter, C., Meltzer, V., Harter, H., and Roberts, R., "Unmasking Artifactural Increases in Creatine Kinase Isoenzymes in Patients with Renal Failure," Journal of Laboratory Clinical Medicine, vol. 104, pp. 193-202, 1984.

Jansen, D., Corbett, J., Lewis S., Wolfe, C., Gabliani, G., Jaffe, A., Sobel, B., Filipchuk, N., Redish, G., Parkey, R., Buja, L. M., and Willerson, J., "Measurement of Myocardial Infarction Size: A Comparison of Single Photon Emission Computed Tomography with Pyrophosphate and Serial CK-MB Measurements," Circulation, vol. 70, p. II-311, 1984.

Jost, R. G., "A Radiology Networking System," presented at Conference and Workshop on Radiology Networking and Interactive Computer Graphics, Kansas City, MO, October 28-30, 1984.

Jost, R. G., "Computer Applications in Radiology," presented at the Conjoint Meeting of the Radiologic Technologists of Missouri and Illinois, St. Louis, MO, October 3-6, 1984.

Knabb, R. M., Fox, K. A. A., and Bergmann, S. R. "Detection of Coronary Stenoses by Positron Emission Tomography with $H_2{}^{15}O$," Circulation, vol. 70, supplement II, p. II-340, 1984 (abstract).

Knabb, R. M., Fox, K. A. A., Sobel, B. E., and Bergmann, S. R., "Characterization of the Functional Significance of Subcritical Coronary Stenoses with $H_2{}^{15}O$ and Positron Emission Tomography," Circulation, in press.

Kramer, J. B., and Corr, P. B., "Mechanisms Contributing to Arrhythmias During Ischaemia and Infarction," European Heart Journal, vol. 5, pp. 11-18, 1984.

Kramer, J. B., Corr, P. B., Cox, J. L., Witkowski, F. X., and Cain, M. E., "Simultaneous Computer Mapping to Facilitate Intra-Operative Localization of Accessory Pathways," American Journal of Cardiology, in press.

Kramer, J. B., Davis, A. G., Dean, R., McCluskey, E. R., Needleman, P., and Corr, P. B., "Thromboxane A_1 Does Not Contribute to Arrhythmogenesis During Evolving Canine Myocardial Infarction," Journal of Cardiovascular Pharmacology, in press.

Kramer, J. B., Saffitz, J. E., Witkowski, F. X., and Corr, P. B., "Intramural Reentry As a Mechanism of Ventricular Tachycardia During Evolving Canine Myocardial Infarction," Circulation Research, in press.

Kramer, J. B., Witkowski, F. X., and Corr, P. B., "Intramural Reentry: A Mechanism for Ventricular Tachycardia with Evolving Myocardial Infarction," Circulation, vol. 70, supplement II, p. II-222, 1984 (abstract).

Lamas, G., Muller, J., Turi, Z., Stone, P., Rude, R., Jaffe, A., Raabe, D., Settergren, S., Poole, W. K., Passamani, E., Braunwald, E., and the MILIS Study Group, "A Simplified Method to Predict the Occurrence of Complete Heart Block During Myocardial Infarction," Circulation, vol. 70, p. II-310, 1984 (abstract).

Mead, C. N., Clark, K. W., Platt, J. C., and Thomas, Jr., L. J., "Argus Algorithm Development: A Decade of Progress - Results of Final System Evaluation and Implementation in a CMOS Environment," Proceedings of the IEEE Conference on Computers in Cardiology, IEEE Catalog No. 84CH2078-4, Park City, UT, pp. 197-200, September 18-21, 1984.

Miller, M. I., "Algorithms for Removing Recovery Related-Distortion from Auditory-Nerve Discharge Patterns," Journal of the Acoustical Society of America, vol. 77, no. 4, pp. 1452-1464, April 1985.

Miller, M. I., "Statistical Coding of Tones and Tones in Noise in Auditory Nerve Discharge Patterns," presented at the Eighth Midwinter Research Meeting for the Association for Research in Otolaryngology, Clearwater Beach, FL, February 2, 1985.

Miller, M. I., Larson, K. B., Saffitz, J. E., Snyder, D. L., and Thomas, Jr., L. J., "Maximum Likelihood Estimation Applied to Electron-Microscopic Autoradiography," in press.

Miller, M. I., Snyder, D. L., and Miller, T. R., "Maximum-Likelihood Reconstruction for Single-Photon Emission Computer-Tomography," IEEE Transactions on Nuclear Science, vol. NS-32, no. 1, pp. 769-778, February 1985.

Mintun, M. A., Gorman, J., Swift, A. G., and Snyder, D. L., "Evaluation of the Maximum-Likelihood Method for Reconstruction Images in Positron Emission Tomography," presented at the 32nd Annual Meeting of the Society of Nuclear Medicine, Houston, TX, June 2-5, 1985.

Mottley, J. G., "Physical Properties of the Ultrasonic Attenuation and Backscatter of Soft Tissues: Dependence on the Angle of Propagation and the Physiological State," Department of Physics, Washington University, St. Louis, Missouri, May 1985 (D.Sc. Dissertation).

Mottley, J. G., Glueck, R. M., Perez, J. E., Sobel, B. E., and Miller, J. G., "Changes in Attenuation and Backscatter of Frog Skeletal Muscle Between Rest and Tetanic Contraction," Ultrasonic Imaging, vol. 6, p. 221, 1984 (abstract).

Mottley, J. G., Glueck, R. M., Perez, J. E., Sobel, B. E., and Miller, J. G., "Regional Differences in the Cyclic Variation of Myocardial Backscatter that Parallel Regional Differences in Contractile Function," Journal of the Acoustical Society of America, vol. 76, pp. 1617-1623, 1984.

Mukarji, J., Rude, R. E., Poole, W. K., Gustafson, N., Thomas, Jr., L. J., Strauss, H. W., Jaffe, A. S., Muller, J. E., Roberts, R., Raabe, D. S., Croft, C. H., Passamani, E., Braunwald, E., Willerson, J. T., and the MILIS Study Group," Risk Factors for Sudden Death Following Acute Myocardial Infarction: Two Year Follow-Up," American Journal of Cardiology, vol. 54, pp. 31-36, July 1984.

Ollinger, J. M., and Snyder, D. L., "An Evaluation of an Improved Method for Computing Histograms in Dynamic Tracer Studies Using Positron Emission Tomography," accepted for presentation at the 1985 IEEE Nuclear Science Symposium, San Francisco, CA, October 23-25, 1985.

Ollinger, J. M., and Snyder, D. L., "A Preliminary Evaluation of the Use of the EM Algorithm for Estimating Parameters in Dynamic Tracer-Studies," IEEE Transactions on Nuclear Science, vol. NS-32, no. 1, pp. 848-854, February 1985.

Onufer, J. R., Kramer, J. B., Sobel, B. E., and Corr, P. B., "Lysophosphatide Induced Delayed After-Depolarizations and Triggered Activity," Circulation, vol. 70, supplement II, p. II-22, 1984 (abstract).

Perez, J. E., Barzilai, B., Madaras, E. I., Glueck, R. M., Saffitz, J. E., Johnston, P. H., Miller, J. G., and Sobel, B. E., "Applicability of Ultrasonic Tissue Characterization for Longitudinal Assessment and Differentiation of Calcification and Fibrosis in Cardiomyopathy," Journal of the American College of Cardiology, vol. 4, pp. 88-95, 1984.

Perez, J. E., Madaras, E. I., Sobel, B. E., and Miller, J. G., "Quantitative Myocardial Characterization with Ultrasound," Automedica, vol. 5, p. 201, 1984.

Roberts, R., Croft, C., Gold, H. K., Tyler, D. H., Jaffe, A. S., Muller, J. E., Mullin, S. M., Parker, C., Passamani, E. R., Poole, W. K., Raabe, D. S., Rude, R. E. Stone, P. H., Turi, Z. G., Sobel, B. E., Willerson, J. T., Braunwald, E., and the MILIS Study Group, "Effect of Propranolol on Myocardial Infarct Size in a Randomized, Blinded, Multicenter Trial," New England Journal of Medicine, vol. 311, pp. 218-225, 1984.

Rosenberger, F. U., Krippner, K., Stein, Jr., D. W., and Wong, J. W., "Implementation of the Delta-Wave Dose Calculation Algorithm," Proceedings of the IEEE 8th International Conference on the Use of Computers in Radiation Therapy, Toronto, Canada, pp. 78-82, July 1984.

Saffitz, J. E., and Corr, P. B., "Autoradiographic Detection of Alterations of Myocardial Adrenergic Receptors Induced by Ischemia," European Heart Journal, in press.

Sharma, A. D., and Corr, P. B., "Alpha-Adrenergic Mediated Effects of Catecholamine in the Ischemic and Reperfused Heart," in Role of Alpha-Adrenoreceptors in Cardiovascular Disease, Churchill Livingstone, in press.

Sheffield, L. T., Berson, A., Bragg-Remschel, D., Gillette, P. C., Hermes, R. E., Hinkel, L., Kennedy, H., Mirvis, D. M., and Oliver, C., "Recommendations for Standards of Instrumentation and Practice in the Use of Ambulatory Electrocardiography: The Task Force of the Committee on Electrocardiography and Cardiac Electrophysiology of the Council on Clinical Cardiology," AHA Special Report, Circulation, vol. 71, no. 3, pp. 626-636A, 1985.

Shipton, H. W., "From Entertainment to Education; from Education to Enlightment," in Topographic Mapping of the Brain, F. H., Duffy, ed., in press.

Shipton, H. W., guest faculty at conference, "Progress in Mapping Neurophysiological Data," Harvard Medical School and Boston Children's Hospital, October 1984.

Shipton, H. W., "Topography," in Encyclopedia of Neuroscience, G. Adelman, ed., in press.

Shum, C. D., Cox, J. R., and Blaine, G. J., "Design Analysis of a Wide-Band Picture Communication System," IEEE 1984 International Symposium on Medical Images and Icons - ISMII '84, Arlington, VA, pp. 66-77, July 24-27, 1984.

Snyder, D. L., "Algorithms and Architectures for Statistical Image Processing in Emission Tomography," Proceedings of the 28th Annual Symposium, Society of Photo-Optical Instrumentation Engineers, San Diego, CA, vol. 495, pp. 109-111, August 1984.

Snyder, D. L., "Algorithms and Architecture for Statistical Image Processing in Positron Emission Tomography," presented at the Johns Hopkins University School of Medicine, Baltimore, MD, December 1984.

Snyder, D. L., "Algorithms and Architecture for Statistical Image Processing in Positron Emission Tomography," presented at the University of Illinois, Urbana, IL, November 1984.

Snyder, D. L., "Estimating the Intensity Function of a Poisson Process When Each of Its Points is Observed after a Random Translation," Proceedings of the Twenty-Second Annual Allerton Conference on Communication, Control, and Computing, University of Illinois, Urbana, IL, p. 343, October 3, 1984.

Snyder, D. L., and Miller, M. I., "An Evaluation of the Use of Sieves for Producing Estimates of Radioactivity Distributions with the EM Algorithm for Positron Emission Tomography," accepted for presentation at the 1985 IEEE Nuclear Science Symposium, San Francisco, CA, October 23-25, 1985.

Snyder, D. L., and Miller, M. I., "Estimating the Intensity of a Poisson Process When Each of Its Points Is Observed with Insertions, Deletions, and Random Translations," 1985 IEEE International Symposium on Information Theory (ISIT), Brighton, England, p. 171, June 1985 (abstract).

Sobel, B. E., and Bergmann, S. R., "The Impact of Coronary Thrombolysis and Tissue-Type Plasminogen Activator (t-PA) on Acute Myocardial Infarction," in Thrombolysis, D. Collen and M. Verstraete, eds., Churchill Livingstone, Edinburgh, in press.

Sobel, B. E., Gross, R. G., and Robison, A. K., "Thrombolysis, Clot Selectivity, and Kinetics," Circulation, vol. 70, p. 160, 1984.

Stone, P., Turi, Z., Jaffe, A., Gold, H., Raabe, D., Rude, R., Parker, C., Hartwell, T., Muller, J., and the MILIS Study Group: Prognostic Significance of and Exercise Treadmill Test 6 Months Post Myocardial Infarction," Circulation, vol. 70, p. II-60, 1984 (abstract).

Ter-Pogossian, M. M., Geltman, E. M., Sobel, B. E., and Ficke, D. C., "Dynamic Cardiac Studies with Super PETT I," Journal of Nuclear Medicine, vol. 24, no. 5, p. 61, 1984 (abstract).

Thomas, III, L. J, Wickline, S. A., Perez, J. E., Sobel, B. E., and Miller, J. G., "A Model for the Change in Backscatter Accompanying the Contraction of Muscle," Ultrasonic Imaging, in press (abstract).

Tilton, R. G., Cole, P. A., Larson, K. B., Kilo, C., and Williamson, J. R., "Hyaluronidase Does Not Prevent Deterioration of Vascular Functional Integrity During Reprefusion after No-Flow Ischemia in Isolated Rabbit Hearts," in press.

Toga, A. W., Goo, R. L., Murphy, R., and Collins, R. C., "Neuroscience Application of Interactive Image Analysis," Optical Engineering, vol. 23, no. 3, pp. 279-282, 1984.

Turi, Z. G., Rutherford, J. D., Roberts, R., Muller, J. E., Jaffe, A. S., Rude, R. E., Parker, C., Raabe, D. S., Stone, P. H., Hartwell, T. D., Lewis S. E., Parker, R. W., Gold, H. K., Robertson, T. L., Sobel, B. E., Willerson, J. T., Braunwald, E., and the Multicenter Investigation for the Limitation of Infarct Size (MILIS), "Electrocardiographic, Enzymatic and Scintigraphic Criteria of Acute Myocardial Infarction As Determined from Study of 726 Patients," in press.

Yu, C. X., Wong, J. W., and Purdy, J. A., "Photon Dose Perturbations Due to Small Inhomogeneities," accepted for presentation in the Young Investigator's Symposium, Twenty-Seventh Annual Meeting of the American Association of Physicists in Medicine, Seattle, WA, August 11-15, 1985.

Witkowski, F. X., and Corr, P. B., "An Automated Simultaneous Transmural Cardiac Mapping System," American Journal of Physiology, vol. 247 (Heart and Circulatory Physiology), p. H661-H668, 1984.

Witkowski, F. X., and Corr, P. B., "Mechanisms Responsible for Arrhythmias Associated with Reperfusion of Ischemic Myocardium," in Clinical Aspects of Life-Threatening Arrhythmias, H. M. Greenberg, H. E. Kulbertus, A. J. Moss and P. J. Schwartz, eds., New York Academy of Sciences, New York, pp. 187-198, 1984.

Wong, J. W., Slessinger, E. D., Rosenberger, F. U., Krippner, K., and Purdy, J. A., "The Delta-Volume Method for 3-Dimensional Photon Dose Calculations," Proceedings of the IEEE 8th International Conference on the Use of Computers in Radiation Therapy, Toronto, Canada, pp. 26-30, July 1984.

Yamada, K. A., Saffitz, J. E., and Corr, P. B., Sympathetic Influences on Arrhythmogenesis in the Ischemic Heart," European Heart Journal, in press.

IX. MONOGRAPHS AND WORKING NOTES

The Biomedical Computer Laboratory's Monograph Series was established to systematize the many reports, reprints, program descriptions and other documents written at BCL or supported in part by the Laboratory's facilities or staff.

A forum, much less formal than our monograph series, has been instituted to serve as a repository for materials such as: research notes, system and component documentation, technical survey notes and prepublication drafts. A Working Note File is maintained for access by anyone associated with the Washington University Computer Labs. Distribution for outside use can be made available with the consent of the contributing author.

Monographs

Following is a list of the monographs published by BCL during the past year. Copies of the complete index to the Monograph Series are available on request.

Monograph Number	Author(s)	Title	Date
456	Miller, M. I. Larson, K. B. Saffitz, J. E. Snyder, D. L. Thomas, Jr., L. J.	Maximum-Likelihood Estimation Applied to Electron-Microscopic Autoradiography	11/84
457	Miller, M. I. Snyder, D. L. Miller, T. R.	Maximum-Likelihood Reconstruction for Single-Photon Emission Computed-Tomography	9/84
458	Holmes, T. J. Snyder, D. L. Ficke, D. C.	The Effect of Accidental Coincidences in Time-of-Flight Positron Emission Tomography	6/84
459	Ollinger, J. M. Snyder, D. L.	A Preliminary Evaluation of the Use of the EM Algorithm for Estimating Parameters in Dynamic Tracer-Studies	10/84
460	Holmes, T. J. Ficke, D. C.	Analysis of Positron-Emission Tomography Scintillation-Detectors with Wedge Faces and Inter-Crystal Septa	11/84
461	Bergmann, S. R. Fox, K. A. A. Rand, A. L. McElvany, K. D. Welch, M. J. Markham, J. Sobel, B. E.	Quantification of Regional Myocardial Blood Flow in Vivo with $H_2{}^{15}O$	10/84

Monograph Number	Author(s)	Title	Date
462	Mottley, J. G. Glueck, R. M. Perez, J. E. Sobel, B. E. Miller, J. G.	Regional Differences in the Cyclic Variation of Myocardial Backscatter that Parallel Regional Differences in Contractile Performance	1/85
463	Fuhrmann, D. R.	Use of Linear Constraints to Reduce Computation in the EM Algorithm	2/85
464	Snyder, D. L. Miller, M. I.	The Use of Sieves to Stabilize Images Produced with the EM Algorithm for Emission Tomography	4/85
465	Holmes, T. J.	Data Collection and Preprocessing Considerations in Time-of-Flight Positron-Emission Tomography	5/85
466	Arthur, R. M. Gurumurthy, K. V.	A Single Pole Model for the Propagation of Ultrasound in Soft Tissue	4/85
467	Mottley, J. G.	Physical Principles of the Ultrasonic Attenuation and Back-scatter of Soft Tissues: Dependence on the Angle of Propagation and the Physiologic State	5/85
468	Ambos, H. D. Markham, J. Cain, M. E.	Use of Fast Fourier Transform Analysis to Detect Patients Prone to Sustained Ventricular Arrhythmia	9/84

Working Notes

Following is an index of notes submitted during the current reporting period.

Working Note Number	Author(s)	Title	Date
59	Chabut, J. C.	Bit Error Tester	8/84
60	Moore, S. M. Holmes, T. J.	M-L Algorithm: Computation Time Estimates for Array Processor-Based Implementations	9/84
61	Moore, S. M. Holmes, T. J.	M-L Algorithm: Computation Time Estimates for Custom Processor-Based Implementations	9/84

Working Note Number	Author(s)	Title	Date
62	Chabut, J. C.	Bandwidth Measurements of the Neuroanatomical Image Processing Facility	11/84
63	Chabut, J. C.	Pilot Demonstration of 1 MBPS Picture Communication	12/84
64	Markham, J.	Infarct Size Estimation	1/85
65	Videen, T. O.	A FORTRAN Library for the HP7475A Graphics Plotter	2/85
66	Videen, T. O.	System Manager's Manual for PLOT1	4/85
67	Videen, T. O.	User's Manual for PLOT1 Interactive Plotting Program for the HP7475A Graphics Plotter	4/85
68	Browder, M. W.	An MC6800 Based Serial-to-Parallel Interface: May 1978	6/85